Enabling Technologies for Internet of Things: Licensed and Unlicensed Techniques

Mahmoud Elsaadany

A Thesis

In the Department

of

Electrical and Computer Engineering

Presented in Partial Fulfillment of the Requirements

For the Degree of

Doctor of Philosophy (Electrical and Computer Engineering) at

Concordia University

Montréal, Québec, Canada

April, 2018

© Mahmoud Elsaadany, 2018

CONCORDIA UNIVERSITY

SCHOOL OF GRADUATE STUDIES

This is to certify that the thesis prepared

By: Mahmoud Elsaadany

Entitled: Enabling Technologies for Internet of Things:

              Licensed and Unlicensed Techniques

and submitted in partial fulfillment of the requirements for the degree of

Doctor of Philosophy (Electrical and Computer Engineering)

complies with the regulations of the University and meets the accepted standards with

respect to originality and quality.

Signed by the final examining committee:

	Chair
Dr. De Visscher	
	External Examiner
Dr. Claude D'Amours	
	External to Program
Dr. A. Stancu	
	Examiner
Dr. M.R. Soleymani	
	Examiner
Dr. Y.R. Shayan	
	Thesis Supervisor
Dr. W. Hamouda	

Approved by: _____

                Dr. W.-P. Zhu, Graduate Program Director

May 24, 2018

                _____

                Dr. A. Asif, Dean, Faculty of Engineering & Computer Science

ABSTRACT

Enabling Technologies for Internet of Things: Licensed and Unlicensed Techniques

Mahmoud Elsaadany, Ph.D.

Concordia University, 2018

The Internet of Things (IoT) is a novel paradigm which is shaping the evolution of the future Internet. According to the vision underlying the IoT, the next step in increasing the ubiquity of the Internet, after connecting people anytime and everywhere, is to connect inanimate objects. By providing objects with embedded communication capabilities and a common addressing scheme, a highly distributed and ubiquitous network of seamlessly connected heterogeneous devices is formed, which can be fully integrated into the current Internet and mobile networks, thus allowing for the development of new intelligent services available anytime, anywhere, by anyone and anything. Such a vision is also becoming known under the name of Machine-to-Machine (M2M), where the absence of human interaction in the system dynamics is further emphasized.

A massive number of wireless devices will have the ability to connect to the Internat through the IoT framework. With the accelerating pace of marketing such framework, the new wireless communications standards are studying/proposing solutions to incorporate the services needed for the IoT. However, with an estimate of 30 billion connected devices, a lot of challenges are facing the current wireless technology.

In our research, we address a variety of technology candidates for enabling such a massive framework. Mainly, we focus on the underlay cognitive radio networks as the unlicensed candidate for IoT. On the other hand, we look into the current efforts done by the standardization bodies to accommodate the requirements of the IoT into the current cellular networks. Specifically, we survey the new features and the new user equipment categories added to the physical layer of the LTE-A.

In particular, we study the performance of a dual-hop cognitive radio network sharing the spectrum of a primary network in an underlay fashion. In particular, the cognitive network consists of a source, a destination, and multiple nodes employed as amplify-and-forward relays. To improve the spectral efficiency, all relays are allowed to instantaneously transmit to the destination over the same frequency band. We present the optimal power allocation that maximizes the received signal-to-noise ratio (SNR) at the destination while satisfying the interference constrains of the primary network. The optimal power allocation is obtained through an eigen-solution of a channel-dependent matrix, and is shown to transform the transmission over the non-orthogonal relays into parallel channels. Furthermore, while the secondary destination is equipped with multiple antennas, we propose an antenna selection scheme to select the antenna with the highest SNR. To this end, we propose a clustering scheme to subgroup the available relays and use antenna selection at the receiver to extract the same diversity order. We show that random clustering causes the system to lose some of the available degrees of freedom. We provide analytical expression of the outage probability of the system for the random clustering and the proposed maximum-SNR clustering scheme with antenna selection. In addition, we adapt our design to increase the energy-efficiency of the overall network without significant loss in the data rate.

In the second part of this thesis, we will look into the current efforts done by the standardization bodies to accommodate the requirements of the IoT into the current cellular networks. Specifically, we present the new features and the new user equipment categories added to the physical layer of the LTE-A. We study some of the challenges facing the LTE-A when dealing with Machine Type communications (MTC). Specifically, the MTC Physical Downlink control channel (MPDCCH) is among the newly introduced features in the LTE-A that carries the downlink control information (DCI) for MTC devices. Correctly decoding the MPDCCH, mainly depends on the channel estimation used to compensate for the channel errors during transmission, and the choice of such technique will affect both the complexity and the performance of the user equipment. We propose and assess the performance of a simple channel estimation technique depends in essence on the Least Squares (LS) estimates of the pilots signal and linear interpolations for low-Doppler channels associated with the MTC application.

Acknowledgments

First and foremost, all praise and thanks are due to Allah for giving me the strength to keep trying, and for surrounding me with very supportive personals.

I would like to express my great gratitude to my supervisor Prof. Walaa Hamouda for being such a great advisor, and for all the support he provided me both technically and personally. His support and insightful advices were crucial to my academic achievement and my development as an independent researcher. Honestly, I consider Prof. Hamouda as an elder brother not only a supervisor or a teacher. Prof. Walaa, thank you for all the technical and ethical values I have learned from you.

I am also thankful to my friends, Shoukry Shams and Abdelmohsen Ali, for their help and support.

I am sincerely thankful to Concordia Graduate Student Support Program (GSSP) for partially funding my PhD's studies.

Finally, I would like to express my greatest and deepest appreciation to my family, specially my wife. She has been such a huge support for me and my small family while I was away. Marwa, thank you for being my co-pilot.

To my beloved wife, Marwa Abdelaziz,

To my kids Abdelrahman and Omar,

and to my parents

Contents

List of Figures

xiii

List of Tables

List of Symbols

S	Secondary source
D	Secondary destination
K	Number of secondary relays
N_D	Number of receive antennas at the secondary destination
$\mathbf{x}$	vector $\mathbf{x}$
$\mathbf{X}$	Matrix $\mathbf{X}$
$\mathbf{x}^T$	Transpose of vector $\mathbf{x}$
$\mathbf{X}^{-1}$	Matrix inverse of matrix $\mathbf{X}$
$x_{i,j}$	Matrix element of row i and column j
$Eigen\{\mathbf{X}\}$	Eigenvalues of the matrix $\mathbf{X}$
$\mathrm{Tr}\{\mathbf{X}\}$	The trace of the matrix $\mathbf{X}$
P_S	Transmission power of S
P_{R_i}	Transmission power of node R_i
P_{max}	Maximum transmission power of Secondary nodes
P_T	Total transmission power
ψ_{R_i}	Scaling gain at the node R_i
G_{R_i}	Phase correction at the node R_i
$\sigma_{R_i}^2$	Noise variance at the node R_i
$\mathcal{CN}$	Complex normal random variable
$\mathbb{E}[\cdot]$	The expected value
$g_{a,b}$	The channel coefficient from node a to node b
$\log_a$	The logarithmic function of base a
R	The secondary transmission rate
I_{max}	Interference temperature of the Primary network
$|a|$	The absolute value of a

max	The maximization problem
arg max	The maximization problem of the argument function
$\Gamma(a, x)$	The upper incomplete Gamma function
$\gamma(a, x)$	The lower incomplete Gamma function
$Q(x)$	Q-function
$F(x)$	Cumulative distribution function
$f(x)$	Probability density function
$\in$	Within the group
$\forall$	For all
$\approx$	Approximated as
$\mathbf{G}_{p,q}^{m,n}\left(\begin{array}{c} a_1,...,a_p \\ b_1,.....,b_q \end{array}\middle\vert z\right)$	The Meijer G-function
$\Gamma(x)$	The Gamma function
$aF_b(\alpha, \beta; \gamma, z)$	The Gauss-hypergeometric
$\Pr(a)$	Probability of event a
P_e	Error probability
P_{out}	Outage probability
γ^*	Optimal SNR of the secondary network
γ_S	Secondary source power relative to noise power
γ_i	The received SNR at the destination D through relay R_i
γ_{th}	The received SNR threshold at the destination D
γ_{e2e}	The end-to-end received SNR at the destination D
$\mathfrak{C}_j$	The jth cluster of secondary relays.
A_j	The size of the cluster $\mathfrak{C}_j$
$h(t, \tau)$	Baseband wireless channel impulse response
$S^j(l_p, k_p)$	The pilot signal at OFDM symbol l_p and subcarrier index k_p
$\hat{\mathbf{h}}_p^j$	Channel estimation at the pilot locations for antenna port j
$\hat{\mathbf{H}}^{MMSE}$	MMSE channel estimation
$\hat{B}_r^c$	The decoded control bits of the received rth repetition
Υ^{-1}	Receiver Processing

List of Acronyms

3GPP   3rd Generation Partnership Project

ACK   Acknowledge

AF   Amplify-and-Forward

AP   Access Point

AWGN   Additive White Gaussian Noise

BER   Bit Error Rate

BPSK   Binary Phase Shift Keying

BL/CE   Bandwidth-reduced Low-complexity and Coverage Extension

CAT-M   Category of Machine Type Communications

CAT-N   Category of Narrow Band

CF   Compress-and-Forward

CDF   Cumulative Distribution Function

CP   Cyclic Prefix

CR   Cognitive Radio

CRN   Cognitive Radio Networks

CSCGRV   Circularly Symmetric Complex Gaussian Random Variable

CSI   Channel State Information

DCI   Downlink Control Information

DRX	Discontinuous Reception
DSAN	Dynamic Spectrum Access Networks
DSP	Digital Signal Processor
DF	Decode-and-Forward
EPDCCH	Enhanced Physical Downlink Control Channel
FCC	Federal Communications Commission
FFT	Fast Fourier Transform
i.i.d.	independent, and identically distributed
ICI	Inter Carrier Interference
IFFT	Inverse Fast Fourier Transform
IoT	Internet of Things
LoRa	Long Range
LPWAN	Low Power Wide Area Networks
LS	Least Squares
LTE	Long Term Evolution
LTE-A	Long Term Evolution Advanced
M2M	Machine to Machine
MAC	Medium Access Control
MCL	Maximum Coupling Loss
MGF	Moments Generating Function
MIMO	Multiple Input Multiple Output

MMSE	Minimum Mean Squared Error
MSE	Mean Squared Error
MPDCCH	MTC Physical Downlink Control Channel
MTC	Machine Type Communication
NB	Narrow band
OFDM	Orthogonal Frequency Division Multiplexing
PBCH	Physical Broadcast Channel
PDCCH	Physical Downlink Control Channel
PDF	Probability Density Function
PDSCH	Physical Downlink Shared Channel
PSD	Power Spectral Density
PSS	Primary Synchronization Signal
PRB	Physical Resource Block
PU	Primary User
PUCCH	Physical Uplink Control Channel
PUSCH	Physical Uplink Shared Channel
QCQP	Quadratically Constrained Quadratic Problem
QoS	Quality-of-Service
SDR	Software Defined Radio
SNR	Signal-to-Noise Ratio
RB	Resource Block

RE	Resource Element
RF	Radio Frequency
RS	Reference Symbol
RSSI	Received Signal Strength Indicator
SC-FDMA	Single Carrier Frequency Division Multiple Access
SFBC	Space-Frequency Block Code
SFO	Sampling Frequency Offset
SIMO	Single Input Multiple Output
SISO	Single Input Single Output
SNR	Signal to Noise Ratio
SSS	Secondary Synchronization Signal
SU	Secondary User
UE	User Equipment

Chapter 1

Introduction

1.1 Machine Type Communications and Internet-of-Things

The Internet technology has undergone enormous changes since its early stages and it has become an important communication infrastructure targeting anywhere, anytime connectivity. Historically, human-to-human (H2H) communication, mainly voice communication, has been the center of importance. Therefore, the current network protocols and infrastructure are optimized for human-oriented traffic characteristics. Lately, an entirely different paradigm of communication has emerged with the inclusion of "machines" in the communications landscape. The exchange of any machine-generated traffic is known as Machine-to-Machine (M2M) communication [1]. As a result, the speculations about the number of devices expected to access the Internet in the near future is increasing every day. This is indeed supported by the Internet-of-Things (IoT) framework being promoted to allow a tremendous number of "Things" to generate and communicate information among each other without the need of human interaction [2]. The term "Things" can be used to refer to human services, machineries (or parts of machines), sensors in smart grids, monitoring devices in e-Health applications, smart motors/cars or any house hold device in a smart home or a smart city [3] [4].

In terms of M2M communications and IoT features, a new paradigm of networks has to respect the requirements of machines, such as power and cost [5]. For instance, a set-and-forget type of application in M2M devices, such as smart meters, require very long battery life where the device has to operate in an ultra low-power mode [6]. Moreover, the future network should allow for low complex and low data rate communication technologies which

1

provide low cost devices that encourages the large scale of the IoT. The network architecture, therefore, needs to be flexible enough to provide these requirements and more.

1.2   IoT Applications

The requirements as to be anticipated vary widely from application to application. However, there is an effort to categorize applications in a broader framework to provide the best possible support with an appropriate technical variant of the candidate technologies. A common list of requirements for IoT use cases can be broadly summarized as follows:

- General requirements of data speeds for both uplink and downlink.

- Relative speed of the IoT device where the application is used

- Tolerance limits on the latency response required for the application.

- Number of reports or readings that are required from the IoT device for the corresponding application.

- Battery requirements for IoT devices that are necessary for a given application.

- Type and extent of security required to preserve the content and communications to the IoT device.

For example, for applications in the domain of Fleet Management and Logistics, the typical data rates required are in the range of a few 100s of Kbps, mainly for the uplink. The IoT application that serves this category needs to ensure that the IoT devices will be moving at speeds ranging from 10 to 150 Kmph. For these applications, securing real time and accurate information is of key concern and therefore the tolerance on latency is very low. The number of reports generated by the IoT devices in this category range from 1 per hour to 1 per day. Table 1.1 provides a generic requirements for typical IoT applications.

Table 1.1: Generic requirements for typical IoT applications.

Application	Data Rate	Relative speed	Latency	Range
Fleet Management and Logistics	100s of Kbps	High-speed 10-150km/h	Low (Seconds)	few km
Automotive Telematics	10s of Mbps	Pedestrian: $\leq$ 5km/h	Low (Seconds)	few km
Automation and Monitoring	50-500kbps	Fixed	High (Hours)	few km
Security and Surveillance	0.5-8Mbps	Fixed	Milliseconds	few km
Health Monitoring	50-500kbps	Pedestrian: $\leq$5km/h	Low (Seconds)	10s of meters
Wearable (e.g. sports and data sharing)	10s of Mbps	Pedestrian: $\leq$5km/h	Low (Seconds)	10s of meters

1.3 Candidate Technologies for IoT

A considerable amount of research has been directed towards available network technologies such as ZigBee (IEEE 802.15.4), Bluetooth (IEEE 802.15.1), or WiFi (IEEE 802.11b) by interconnecting devices in a form of large heterogeneous network [7] [8]. Furthermore, solutions for the heterogeneous network architecture (connections, routing, congestion control, energy-efficient transmission, etc.) have been presented to suit the new requirements of M2M communications. However, it is still not clear whether these sophisticated solutions can be applied to M2M communications due to constraints on the hardware complexity, coverage, and coordination. Indeed, while WiFi, Bluetooth and ZigBee are widely used nowadays for -more or less- similar applications as M2M communication, the coverage range of these technologies is very short [9] [10] making them only candidates for some of the applications.

Also, operation on unlicensed spectrum forces such technologies to adopt spectrum sensing techniques (listen-before-talk) or controlled interference (Underlay networks) which affects the transmission duty cycle.

On the other hand, Low Power Wide Area (LPWA) networks present a good candidate to support the aforementioned diverse requirements of the IoT framework [11] [12] [13]. A variety of LPWA technology candidates can overcome the short range constraint of the LAN and still satisfy the power and latency constraints using either proprietor or cellular technologies (using licensed or unlicensed spectrum). It seems more efficient to take advantage of the currently well developed and mature radio access networks. With the large coverage and flexible data rates offered by cellular systems, research efforts from industry have recently been focused on optimizing the existing cellular networks considering M2M specifications [14]. Among the possible solutions, the famous proprietary technologies: Sigfox [15] and LoRa [16], along with the new developments of the current cellular technologies such as the new categories of LTE-A user equipments are considered.

Due to the radical change in the number of users, the network has to carefully utilize the available resources in order to maintain reasonable quality-of-service (QoS). Generally, one of the most important resources in wireless communications is the frequency spectrum. To support larger number of connected devices in the future IoT, it is likely to add more degrees of freedom represented in more operating frequency bands. However, the frequency spectrum is currently scarce and requiring additional frequency resources makes the problem of supporting this massive number of devices even harder to solve. In fact, this issue is extremely important especially for the cellular architecture since the spectrum scarcity problem directly influences the reliability and the QoS offered by the network.

1.3.1 Unlicensed Technologies

1.3.1.1 Sigfox

Sigfox is a French company works with network operators to offer an end-to-end LPWA connectivity solution based on its patented technologies. Sigfox Network Operators deploy the proprietary base stations equipped with cognitive software defined radios to operate as a

secondary system (unlicensed), and connect them to the back-end servers using an IP-based network. The connectivity to the base station is simplified and uses only Binary Phase Shift Keying (BPSK) modulation in an ultra narrow bandwidth (100Hz) in the 868 MHz or 915 MHz ISM band. This way, Sigfox utilizes bandwidth efficiently and promises ultra-low power consumption, and inexpensive radio frequency (RF) chain designs. However, Sigfox offers a throughput of only 100bps rendering it a candidate for low traffic applications. Further, a Sigfox downlink communication can only precede uplink communication after which the end device should wait to listen for a response from the base station. The number and size of messages over the uplink are limited to 140 12-byte messages per day to conform to the regional regulations on use of license-free spectrum.

1.3.1.2   LoRa/LORAWAN

A special interest group constituted from several commercial and industrial partners known as LoRa™ Alliance proposed LoRaWAN, as an open standard defining the network architecture and layers above the LoRa physical layer. LoRa (short for Long Range), originally developed and commercialized by Semtech Corporation [17], is a physical layer technology that modulates the signals in the industrial, scientific and medical (ISM) radio band. Using chirp spread spectrum (CSS) technique, a narrow band input signal spread over a wider channel bandwidth. The resulting signal has noise like properties, making it harder to detect or jam and hence, at the receiver, the signal enjoys an increased resilience to interference and noise. LoRa supports multiple spreading factors (between 7-12) to decide the tradeoff between range and data rate. Higher spreading factors deliver long range at an expense of lower data rates. Also the combination of Forward Error Correction (FEC) with the spread spectrum technique to increases the receiver sensitivity. The data rate ranges from 300bps to 37.5kbps depending on the spreading factor and channel bandwidth. Further, multiple transmissions using different spreading factors can be received simultaneously by a LoRa base station. The messages transmitted from end devices are received by multiple base stations, giving rise to "star-of-stars" topology, and hence improves the probability of successfully received messages. However, this increases the overhead of the network side as the resulting duplicate receptions are filtered out in the back-end. Some studies reported the performance

of LoRa for outdoor applications [18] [19] [20] and [21] focused on indoor applications.

1.3.1.3 INGENU RPMA

Unlike LoRa and Sigfox, INGENU (also known as On-Ramp Wireless) is a proprietary LPWA technology that operates in 2.4 GHz ISM band and takes advantage of more relaxed regulations on the unlicensed spectrum use across different regions [22]. INGENU leads efforts to standardize the physical layer specifications under IEEE 802.15.4k standard [23]. INGENU uses a patented physical access scheme named as Random Phase Multiple Access (RPMA) [24] Direct Sequence Spread Spectrum, which it employs for uplink communication only. Using Code Division Multiple Access (CDMA), RPMA enables multiple transmitters to share a single time slot. However, RPMA increases the duration of time slot of traditional CDMA and then distributes the channel access within this slot by adding a random offset delay for each transmitter. By asynchronous access grants, RPMA reduces overlapping between transmitted signals and thus increases signal to interference ratio for each individual link [25]. INGENU provides bidirectional communication, although with a slight link asymmetry. For downlink communication, base stations spread the signals for individual end devices and then broadcast them using CDMA. Further, the end devices can adjust their transmit power for reaching closest base station and limiting interference to nearby devices.

1.3.2 Licensed Technologies

Among licensed solutions to enable wireless infrastructure of M2M communications, scenarios defined by the 3rd Generation Partnership Project (3GPP) standardization body emerge as the most promising solutions [26]. Due to the M2M communication challenges and the wide range of supported device specifications, developing the features for M2M communication, also refers to machine-type-communication (MTC) in the context of Long Term Evolution (LTE), started as early as release 10 (R10) for the advanced LTE standard [27]. From the history of M2M communication (in the LTE convention) development, the first generation of a complete feature MTC device has emerged in R12. In this release, R12, the 3GPP committee has defined a new profile referred to as category 0 or CAT-0 for low-cost MTC operation [28]. Also a full coverage improvement is guaranteed for all LTE duplex modes. Indeed, the effort

continued to future releases including release 13 (R13) that was released late in 2016. In this front, two special categories, namely CAT-M for MTC and CAT-N for Narrowband-IoT (NB-IoT), have been incorporated by the 3GPP to LTE specifications to support complete M2M and IoT features, respectively. The new categories satisfy the general requirements of MTC and can support the wide range of IoT applications. For example, the capabilities of the new categories can support applications in the domain of fleet management and logistics, which require secured, wide range, real time and accurate information with typical data rate of hundreds of Kbps at speeds ranging from 10 to 150 Km/h. On the other hand, they can also support applications with very low moving speeds (or stationary) and moderate data rates with hours of latency, such as, automation and monitoring applications.

1.4 Unlicensed Access and Cognitive Radios

Fixed spectrum allocation is currently used for wireless network, in which a long term assignment of the spectrum is made to the license holders in large geographical regions. This assignment is regulated by governmental agencies. The federal communications commission (FCC) proved recently, by measurements, that the spectrum is not optimally utilized [29]. For instance, cellular networks are overloaded while TV spectrum is under-utilized. Therefore, the apparent scarcity of spectrum is in fact due to inefficient utilization rather than a shortage of this precious resource. This situation increased the interest in developing more flexible spectrum usage models rather than the exiting ones. In particular, new ideas emerged to allow non-licensed users (referred to as secondary users) to be able to utilize the spectrum allocated to the licence owners (referred to as primary users), as long as the primary communication is not disturbed.

The term *"Cognitive radio"* (CR), coined by J. Mitola [30], refers to the technology that improves the utilization of the spectrum by sharing the resources in an intelligent way. He proposed a new spectrum usage policy, namely *"Spectrum Pooling"*, to increase the spectrum efficiency. The idea of spectrum pooling suggests the license owners to create a pool of their spectra to bring their idle resources to market. A description of the main properties of CR, and the ways it may enhance the spectrum utilization are found in the landmark paper of

Haykin [31]:

"A cognitive radio is an intelligent wireless communication system that is aware of its surrounding environment, and uses the methodology of understanding-by-building to learn from the environment and adapt its internal states to statistical variations in the incoming radio frequency stimuli by making corresponding real time changes in certain operating parameters (e.g., transmit power, carrier frequency, and modulation strategy) with two primary objectives:

- Highly reliable communications whenever and wherever needed.

- Efficient utilization of the radio spectrum."

Cognitive radios support is a promising solution for supporting massive MTC devices. It can be argued that cognitive radio concept is a possible solution from the cost and performance perspectives. However, there are more practical challenges that need efforts from researchers in order to have a reliable and a mature solution. Future standards are encouraged to provide both options (i.e. the cognition concept and the heterogeneous/traditional network model).

1.5   Cognitive Networks

While the fixed spectrum allocation cannot hold for the increased number of services and devices associated with the IoT framework, it was necessary to find a new communication paradigm to exploit the existing wireless spectrum. Dynamic spectrum access is proposed to solve the current spectrum crisis. Dynamic Spectrum Access Networks (DSANs)- also known as cognitive radio networks- can offer spectrum usage to mobile users via heterogeneous wireless architectures and dynamic spectrum access techniques. The success in applying the cognitive radio concept is conditioned to find a way to merge the secondary signals with the primary ones such that the primary users are unaware of the presence of the secondary users. This merging may take one of these forms: overlay, underlay, or interweave [32]. We discuss briefly the properties of each approach.

1.5.1 Underlay Cognitive Networks

The underlay approach allows concurrent primary and secondary users transmissions by enforcing the secondary network power level to be below a certain level. This level ensures secondary network interference to be below the acceptable noise floor of the primary network. As a result, the underlay systems need to use more bandwidth to provide useful signal to noise ratio (SNR). Spread spectrum techniques and Ultra-Wide Band (UWB) communications are proposed to implement this approach [33].

1.5.2 Overlay Cognitive Networks

The overlay approach also allows concurrent primary and secondary transmissions but in a different way. The most common method of overlay systems allows the secondary users to assist the primary transmissions. This assistance may take the from of relaying while using combination of coding schemes such as the Han-Kobayashi coding scheme for the general interference channel and Costas dirty paper coding as in [34].

1.5.3 Interweave Cognitive Networks

The licensed spectrum bands might be unused for a specific time or at certain location. These bands are conceptually referred as spectrum holes or white spaces. These holes can be used for communication by secondary users based on the ability of these users to identify these holes. Consequently, the utilization of the spectrum is improved by opportunistic frequency reuse over the spectrum holes. Therefore, an opportunistic cognitive radio is an intelligent wireless communication system that periodically monitors the radio spectrum to detect occupancy in the different parts of the spectrum, and then opportunistically communicates over spectrum holes with minimal interference to the primary users. This type of opportunistic communications is the key idea behind the interweave approach.

1.6 Motivation

The key objectives of this thesis are to:

1. Study the challenges for the next generation MTC networks and provide an efficient solution based on cognitive radio concept for the massive interconnected devices in a scarce spectrum;

2. Address the practical implementation challenges for the LTE-A cellular support for MTC;

3. Develop analytical and simulation frameworks for the developed techniques.

The proposed work in this thesis is important in various ways. It certainly addresses a timely topic (cognitive radio systems in conjunction with cellular MTC and IoT), which is expected to play a major role in many of the future wireless communication systems. In fact, this technology is expected to revolutionize how wireless communication networks will be implemented or deployed in the future, with a focus on addressing the problems of spectrum under-utilization and supporting numerous number of interconnected MTC devices.

From the merge between the underlay cognitive radios and cooperative communications an interesting scenario rises, namely "The Underlay Cognitive Relay Networks". Such type of networks does not require the overhead of sensing the primary users existence and still offers a huge increase in the spectrum usage efficiency. However, the main challenge of this type of networks is how to choose the transmission power level of each and every node in the network, such that the generated interference due to its existence is not violating the primary users constraints. Hence, the problem of power allocation of different cognitive nodes in the relaying network is receiving an increased attention. A lot of effort has been put into the modeling and the formulation of the power allocation problem over the last decade. However, due to its complexity, not all of the parameters are included. For example, the focus of most of the existing work in literature is on single relay networks, although multiple relay networks offer better performance over single-relay networks for the same amount of feedback. However, when the multiple relay network problem is addressed, most of the studies focus on

subgroup selection and on-off (binary) power allocation. Also, the performance of such type of networks becomes mathematically intractable, due to the lack of closed form expression for the statistics of the important parameters in the system, such as the received SNR.

On the other hand, MTC devices are expected to work in environments characterized by low coverage, ultra low power consumption, and reduced complexity. This will impose a significant number of implementation challenges on cellular (licensed) networks to support such requirements. Fore example, the 3GPP standard for LTE-A recently included new categories of user equipment to support MTC. The new categories can provide low cost, low power, and extended coverage modes, but at the expense of changing some features in the physical layer. The introduction of these changes will affect the performance of the currently used algorithms, such as cell search and channel estimation techniques. New solutions have to be investigated to proved optimized solutions for the new systems.

1.7 Thesis Contributions

Given the motivating points in the last section, the contributions of this thesis can be summarized as follows.

- A study of the optimal power allocation of an underlay cognitive relay network in order to maximize the received SNR is provided. The system under consideration employs multiple amplify-and-forward relays that use the same frequency band simultaneously. Given an interference threshold on the primary network, we formulate a quadratically constrained quadratic optimization problem (QCQP). Using this novel formulation, we obtain the optimal power allocation at the different cognitive nodes. Our results show that the obtained power allocation transforms the non-orthogonal relaying channel into parallel channels. We also study the energy efficiency of the proposed power allocation, and provide new algorithms to enhance this efficiency.

- We assess the performance of the cognitive system while employing multiple antennas at the destination. We propose approximating the individual SNRs as exponential random variables using moment matching method. Hence, the received SNR is approximated as

a Gamma random variable. For this approximation, we provide closed-form expressions for the performance of the cognitive system in terms of the outage probability and bit error rate.

- Finally, we will look into the current efforts done by the standardization bodies to accommodate the requirements of the IoT into the current cellular networks. Specifically, we present the new features and the new user equipment categories added to the physical layer of the LTE-A. We study some of the challenges facing the LTE-A when dealing with Machine Type communications (MTC). Specifically, the MTC Physical Downlink control channel (MPDCCH) is among the newly introduced features in the LTE-A that carries the downlink control information (DCI) for MTC devices. Correctly decoding the MPDCCH, mainly depends on the channel estimation used to compensate for the channel errors during transmission, and the choice of such technique will affect both the complexity and the performance of the user equipment. Therefore, here, we propose and assess the performance of a simple channel estimation technique based on the Least Squares (LS) estimates of the pilots signal and linear interpolations for low-Doppler channels associated with the MTC application.

1.8   Thesis Organization

The rest of the thesis is organized as follows:

In Chapter 2, we present a background on the cognitive radio systems, a literature review about different types of cooperation among cognitive nodes, and the existing power allocation schemes in underlay cognitive relay networks. Then, we introduce the basic concepts of physical LTE systems and its relevant transmission technique, namely the Orthogonal Frequency Division Multiplexing (OFDM). The essential information about the MTC and NB-IoT categories are also covered. In the last part of this chapter, we provide the related works to this research in the literature. We also present the major challenges of future M2M cellular networks such as spectrum scarcity problem, support for low-power, low-cost, and numerous number of devices. As being an integral part of the future IoT, the true vision of M2M communications cannot be reached with conventional solutions that are typically cost

inefficient. To this extent, we present a complete fundamental understanding and engineering knowledge of cognitive radios, and power and cost challenges in the context of future M2M cellular networks.

In Chapter 3, we address the power allocation for non-orthogonal cognitive relay networks. We first introduce the system model and assumptions. Then, the formulation of the power allocation problem and the proposed solution are provided, along with the analysis of the statistics of the received SNR and the system performance. We also present assessment of the performance of the system through simulation and analytical expressions. Finally, we address an energy-efficient design for the proposed power allocation.

In Chapter 4, we study the underlay cognitive network while the secondary destination has multiple antennas. To reduce the overall system complexity, we propose using antenna selection and relay clustering. We introduce a novel criterion for antenna selection to maximize the received SNR at the secondary destination. We present the outage performance of the system while utilizing multiple non-orthogonal relays (forming a distributed antenna system) and antenna selection at the destination. While the optimal beamforming using all the available relays enhance the performance by allowing more degrees of freedom to the system designer, it suffers from increased complexity. As a solution, we propose a clustering scheme to subgroup the available relays and use antenna selection at the receiver to extract the same diversity order. We show that random clustering results in lose of some of the available degrees of freedom. Hence, we propose a new technique for clustering, namely Max-SNR clustering, to jointly associate subset of relays to one of the receive antennas and select the antenna that provides the maximum SNR. We provide a closed-form analytical expression of the outage probability of the system for the random clustering and the proposed Max-SNR clustering schemes with antenna selection.

In Chapter 5, we mainly address challenges for the practical implementation side of LTE-MTC systems. In particular, we study the concepts of MPDCCH compared to the legacy EPDCCH. This includes the resource allocation, the new involved downlink control information formatting, the concept of frequency hopping, the repetition, and others. We propose a channel estimation algorithm for the newly introduced MPDCCH in the specifications of the LTE-A CAT-M. The proposed technique aims at reducing the complexity of the channel

estimation of the MPDCCH as minimum as possible. In order to achieve this goal, we propose using the simple Least-Squares (LS) estimation to estimate the pilots signals, followed by two stage first-order polynomial interpolation (linear) to obtain the channel estimates at every point in the time-frequency grid. We also propose using the repeated transmissions (in case of coverage enhancement mode) to enhance the performance of the proposed technique.

In Chapter 6, we present a brief summery of our investigation and some important conclusions. We also suggest some potential topics for future research.

Chapter 2

Background and Literature Review

2.1 Introduction

In this chapter, a background for the main topics of this thesis is given. First, we present an overview of cognitive radio systems as a candidate enabling IoT through unlicensed access. We present the cognitive radio properties, the cognitive network setup and architecture, and a literature survey on cooperative cognitive radio networks is given. We also highlight the concept of cognitive relaying and summarize recent works relate to the problems studied in this thesis. Next, we give a background about one of the major candidates to support cellular connections for MTC and IoT applications, namely LTE-A. We start by introducing the basic concepts of legacy LTE systems and their physical layer transmission techniques for different channels. Then, the essential information related to the new MTC and NB-IoT user categories are covered. In the last part of this chapter, we discuss some of the implementation challenges that will be studied in this thesis.

2.2 Cognitive Radio Systems

A huge demand for bandwidth is expected to grow in the future triggered by the anticipated increased number of wireless devices through the IoT framework [32]. Spectrum licensing has been the traditional approach to ensure the coexistence of diverse wireless systems. An alternative technology, enabling new coexistence approaches, is receiving increased attention in recent wireless communication research literature, namely *"Cognitive Radios"*. The attractive feature in cognitive radios is its promise to increase the spectrum utilization. This

promise is driven mainly by the ability of the cognitive radios to coexist with traditional spectrum owners (primary or licensed users) and share the spectrum band in an opportunistic fashion. This ability is conditioned to not altering the operation of licensed users or negatively affecting their performance. The idea behind the cognitive radio concept was initiated by the ability to build a *"Software Defined Radio"* (SDR). In SDRs, a radio architecture uses powerful computational resources available in Digital Signal Processors (DSPs) and General Purpose Processors (GPPs) to implement the modulation and demodulation and all of the signaling protocols of a radio as a software function [35].

The term Cognitive radio was coined by J. Mitola [30]. The main focus was on the radio knowledge representation language (RKRL) and how the cognitive radio can enhance the flexibility of personal wireless services. One description of the main properties of CR, and the ways it may enhance the spectrum utilization is given in [36]:

"A Cognitive Radio is a radio that can change its transmitter parameters based on interaction with the environment in which it operates".

Cognition can be associated with machine learning [37], which uses any algorithm that improves the performance through experience gained over a period of time without complete information about the operation environment of the radio. Adaptive decision making algorithms can be used to give cognitive networks a wide scope of possible mechanisms to use for learning. Learning serves to complement the objective optimization part of the cognitive process by retaining the effectiveness of past decisions under a given set of conditions. Out of this description, we can obtain the two main properties of the cognitive radio as follows.

2.2.1 Cognitive Capability

Cognitive capability refers to the ability of the radio technology to collect information from its radio environment in a real time fashion. This capability may not be the simple monitoring of the power spectral density in the band of interest, but it might require more sophisticated techniques in order to avoid interference to other users as well as capturing the variations in the radio environment. Through this capability, the spectrum bands that are not used at a specific time or location can be identified. This concept is referred as spectrum hole or white space. Following spectrum holes identification, the node can select best spectrum

and appropriate operating parameters for the required service. The cognitive capability is divided into three main processes referred as the cognition cycle. These processes are spectrum sensing, spectrum analysis and spectrum decision [38]:

- Spectrum sensing: cognitive radio monitors the available spectrum bands and detect the spectrum holes.

- Spectrum analysis: The characteristics of the spectrum holes that are detected through spectrum sensing are estimated.

- Spectrum decision: Depending on the analysis, a cognitive radio determines the data rate, the transmission mode, and the bandwidth of the transmission.

2.2.2 Reconfigurability

Real time interaction with the environment is required as the spectrum holes locations change temporally and spatially. Reconfigurability is the ability of adjusting transmission parameters on real time basis without any modifications in the hardware components. This capability enables the cognitive radio to adapt easily to the dynamic radio environment. The operating frequency, modulation, transmission power and the communication technology may be incorporated into the reconfigurable parameters that cognitive radio can adapt to accommodate for the environmental changes.

2.2.3 Cognitive Networks Architecture

Developing the cognitive radio networks communication protocols requires a clear identification of network elements. The network architecture of the cognitive radio networks consists of two main components: the primary network and the secondary network. The primary network is licensed to use a certain spectrum band while the secondary network is the unlicensed network attempting to share the same spectrum with the primary network. The primary network users should not be affected by the presence of the secondary network users. On the other hand, the secondary network users should make use of cognitive radio abilities to perform all functions necessary to coexist with the primary network. They are

required to protect the primary network from interference that could happen due to the existence of the secondary network.

2.3 Cooperative Communication

Multiple-input multiple-output (MIMO) systems are able to significantly improve the performance of wireless systems (e.g., increase data rate, reduce interference, and improve link reliability) by means of diversity. However, due to cost, size or hardware limitations, multiple antennas might not be applicable for some network nodes. For such scenarios, user cooperation can create a virtual MIMO system and thus enabling a single-antenna user to gain the benefits of MIMO systems. Transmissions via cooperation can be typically modeled as a traditional relay channel. A literature survey on relay channels can be traced back to the seminar paper by Cover and El Gamal in [39], in which the capacity region was determined for the Gaussian single relay network case. Cooperative communications can be accomplished via a wireless network consisting of geographically separated nodes (relays) cooperating in order to improve system performance. The interest in relay networks has recently increased from several different perspectives. Modeling of link abstractions at higher layers in a communication system, coding, synchronization, and signal processing designs within a physical layer are the common research areas in this context. Different cooperative communications protocols have been proposed which can be found in [40]- [41], and in the references therein. In the following, we discuss briefly the most common strategies for cooperative communication.

2.3.1 Amplify-and-Forward

In amplify-and-forward (AF), the relay simply amplifies the received signal and forward the scaled signals to the destination [41]. This method is often used when the relays have limited resources, e.g. processing time or power. The idea behind AF relaying is simple. During the first interval, the transmitter sends it signal to the relays. Then each relay multiplies its received signal by a coefficient and during the second interval forwards it to the destination. In this process, noise at each relay is also amplified.

2.3.2 Decode-and-Forward

In decode-and-forward (DF), each relay decodes the entire received message, re-encodes it and sends the resulting sequence to the destination [42]. In this strategy, each relay should know the codebook used by the source in order to be able to decode and re-encode the received message. The output of each relay acts like an exact copy of the source message. The performance of DF outperforms AF (in case of error-free decoding), at the expense of increased complexity in the signaling communications to establish the knowledge about the used codes.

2.3.3 Compress-and-Forward

In compress-and-forward (CF), the relay transmits a quantized and compressed version of the received signal to the destination. The destination, then, decodes the desired signal by combining the received signal from the relay and the directly received signal from the source. Although the DF strategy is optimal for degraded relay channels [39], the CF strategy is more powerful when the channel between the relay and destination nodes is good enough [43]. For Gaussian relay channels, an achievable rate for the CF strategy is explicitly shown in [44].

2.4 Cooperation and Cognitive Radios

As the primary users have privileged access to the common channel, there are a lot of technical challenges facing the cognitive radios such as:

Spectrum sensing: In case of interweave cognitive radios, secondary users need to monitor the available spectrum or a portion of it in order to be able to detect the white spaces. A typical way to address the problem is to detect the primary transmissions by using a signal detector. The trade-off between probability of false alarm and missed detection is reflected in either: missing transmission opportunities or in increasing interference level to the primary [45]- [46]. The main issue is to enable quick and effective detection at all the secondary nodes that can potentially interfere with the primary transmission.

Also detecting or locating the primary receivers is a major problem [47]. The impact of practical limitations in spectrum sensing on the performance of cognitive radio from a system perspective have been investigated in [48].

Resources allocation: In case of underlay cognitive radios, secondary users need to exploit the transmission opportunity while satisfying two conflicting objectives:

- Making their activity transparent to the primary users (according to a defined criterion for transparency, such as keeping the interference level below a given threshold).

- Maximize their own performance in terms of the desired QoS (e.g., rate, delay, etc.).

Secondary users might be competing for the resource, or cooperating in order to improve efficiency and fairness of resource sharing. A solution for both problems illustrated above can greatly benefit from cooperation among different secondary terminals.

In the following, we present some of the possible scenarios where cognitive radios make use of cooperation to enhance their performance.

2.4.1 Cooperative Sensing

One of the major problems in the primary user activity detection is the low SNR of the received signal at the cognitive user. This low SNR leads to longer sensing times especially in energy detectors. Even with infinite sensing time, the detection may be impossible with the signal SNR is below a certain limit [49]. Enhancing the performance of primary detection requires a solution that can mitigate poor channel conditions, which is achieved through "Cooperation" [50]- [51]. The basic idea is to employ distributed detection at the secondary nodes with each node measuring the local received signal. Then local signals are exchanged to a central point and finally a global decision on the primary activity is achieved, as shown in figure 2.1. This approach is clearly robust to possible unbalance of the channel qualities of different secondary users and can achieve better detection performance. In [52], Ghasemi et al proposed the use of cooperative transmission to enhance the sensing process. The main
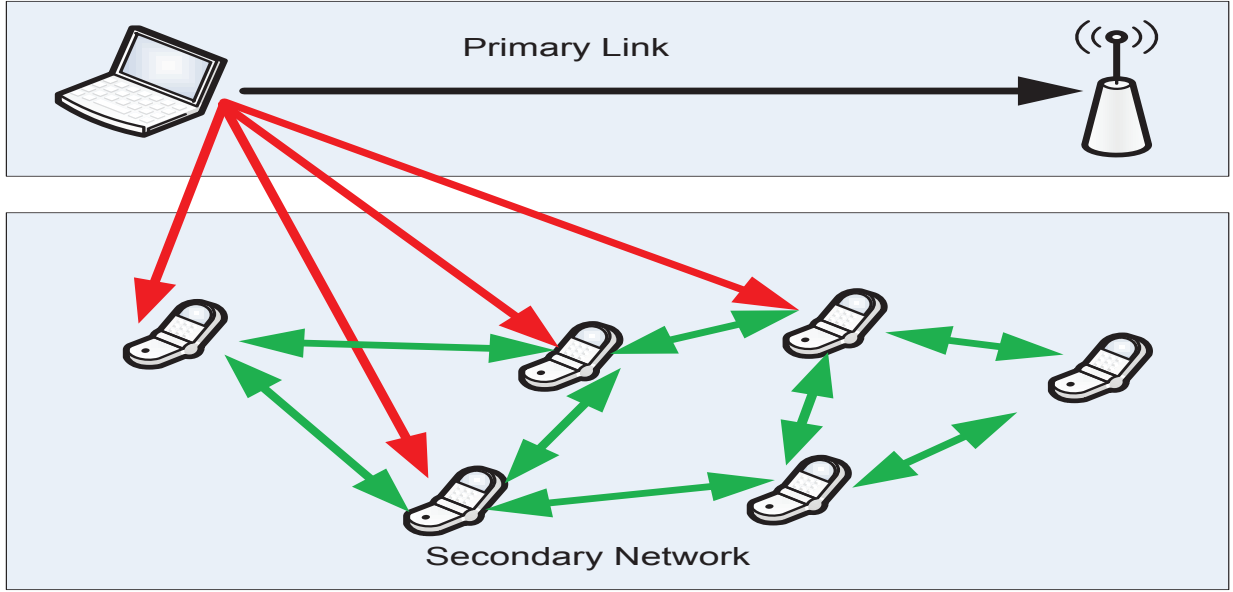
Figure 2.1: Wireless cognitive network with cooperative sensing for the primary activity.

idea is to let the secondary relay node amplify-and-forward the received signal as it contains not only the transmission from the secondary source, but also the signal from the primary. This relayed signal allows the secondary destination to improve the detection of the primary user if the relay is placed approximately halfway between the primary transmitter and the secondary destination.

2.4.2 Cognitive Relay Networks

Cooperative transmission in its basic forms refers to the information theoretic model of the *"Relay Channel"*, where one node (the relay) forwards the transmission of another node (the source) towards the intended destination. Performance advantages achievable from collaboration arise from:

- Power gains, that can be harnessed if the relay happens to be in a convenient location, typically halfway between source and destination.

- Diversity gains, that leverage the double path followed by the signal (direct source-destination and relay transmissions) [50]. In the context of cognitive radio, cooperative

transmission between the nodes gives rise to the cognitive relays networks.

In cognitive relay networks, single or multiple secondary users forward the transmission of another secondary terminal to the destination (see figure 2.2). All the secondary nodes should keep the interference to the primary network within allowed limits.

In [53], the outage performance of a cognitive wireless relay network is investigated. The model used consists of a source node, a destination node, and a group of network clusters each consisting of a number of cognitive (unlicensed) relay nodes and a primary (licensed) node. Cognitive nodes relay information from the source depending on their geographical proximity and their ability to acquire the spectrum hole successfully. Also, an investigation of the high SNR approximation of the outage probability of the dual-hop system to obtain the diversity order is performed. A full diversity gain is achieved only if each relay node successfully identifies the spectrum hole unoccupied by the corresponding primary node in the cluster. However, the imperfect spectrum acquisition is proved to have a negatively significant effect on the diversity order.

Improving the outage performance of the network can be achieved by incorporating a specific intra-cluster cooperation scheme where neighboring cognitive relay nodes in a cluster collaborate with a desired cognitive relay node. The combination of this intra-cluster cooperation improves the outage performance significantly, and the full diversity can be achieved if the proper number of neighboring relay nodes participate in the intra-cluster cooperation. In the invited paper [54], Leila et al investigated the performance gains of cognitive radio relay networks under QoS limitations at the secondary users, and spectrum sharing restrictions imposed by the primary users. In their model, secondary users are allowed to gain access to the licensed spectrum band as long as a limit on the primary outage probability is satisfied. An interesting approach is to allow relay selection (from K nodes) by the secondary transmitter to amplify and forward its signal to the destination. Considering that the transmission of the secondary user has to satisfy a statistical delay QoS constraint, the effective capacity of the relaying link degrades as the QoS constraint gets more tight. However, increasing the number of relaying nodes (K) results in an increase of effective capacity. The slope of the effective capacity gain decreases as K increases, indicating that over-dense relay networks do not gain effective capacity as low density ones.
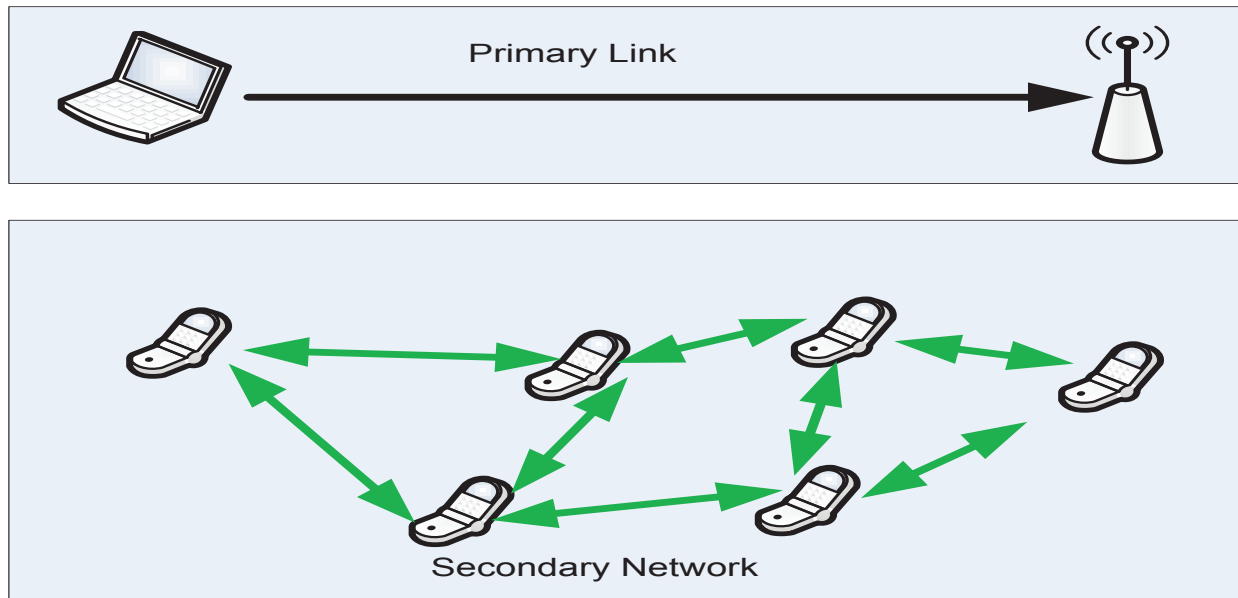
Figure 2.2: Wireless cognitive network with cooperative transmissions between the secondary users.

2.5 Power Allocation in Underlay Relay Networks

With the advantage offered by cooperative communication, the bottleneck that limits the throughput and coverage of underlay cognitive users, is the imposed limitations on their transmitted powers [55]. Therefore, several studies have been conducted to analyze the performance of cooperation among underlay cognitive nodes considering different limitations on the interference and the used transmission powers. For example, the effect of the interference constraint on the diversity gain in DF relaying networks is studied in [56].

In [57], the achievable capacity and the outage probability of cognitive user being assisted by a DF relay are studied. Taking the interference from the primary network into account, the outage probability of a DF cognitive relay network is studied in [58]. The optimal power allocation of the SU achieving maximum throughput is derived in [59] when only one AF relay is used. In the above mentioned works, the cognitive relay network either consists of only one relay or single relay selection is used.

Multiple-relay cognitive networks are studied in [60], where an algorithm is proposed to select multiple relays to maximize the secondary network capacity while preserving the QoS

requirements of the primary network. In [61], a study of the secondary network throughput scaling with the number of relays is conducted while relays either cooperate with full transmission power or do not cooperate at all. Apart from this binary power allocation problem in [60] and [61], beamforming and optimal power allocation are exploited to enhance the performance of cognitive users.

Recently in [62], a simplified suboptimal power allocation for multiple AF relays with individual maximum power constraint is developed. The worst SNR in a multiuser multi-relay cognitive network is maximized using an iterative optimization algorithm in [63]. In [64, 65], performance studies for the multiple-relay cognitive network while nulling the interference generated from the relays to the primary user using zero-forcing beamforming are conducted for both DF and AF relaying. It is shown that the cognitive networks with multiple relays outperform the selective schemes [66] [67] for strict levels of interference temperature.

2.6   LTE Development for MTC and IoT

Although data transmission has been on the rise in the cellular networks for human-involved applications in the last decade, cellular networks are mainly optimized for H2H communication. However, characteristics of M2M traffic are different from the human-generated traffic in the cellular networks. The main differences between H2H and M2M traffic can be expressed as [68] [69]:

- In contrast to human-traffic, in M2M devices, the uplink traffic is higher than downlink.

- While human-traffic is mostly concentrated during daylight and evening, M2M traffic is more uniformly generated by the M2M devices throughout the day.

- In some applications (e.g., involving metering devices), M2M traffic is periodic.

- In some monitoring applications, the volume of traffic increases sharply after the detection of events (burst traffic).

- For many classes of M2M devices, devices have a much lower mobility than human devices. However, for the health care devices, and for accessories such as Google glass

and Apple watch, the mobility is the same as the human devices.

- The quality-of-service requirements of M2M and human devices may be vastly different.

While an M2M device typically sends/receives a small packet of data at each transmission, the extremely large number of M2M devices may cause severe problems in both access channel and traffic channel of a radio access network and congestion in the core network [70] [71]. For these reasons, from the network access perspective, M2M access requests are classified by 3GPP into two groups of uncoordinated/non-synchronized and coordinated/synchronized traffic [72]. Coordinated/synchronized traffic is a type of traffic generated by many similar M2M devices in reaction to an event, whereas uncoordinated/non-synchronized traffic is a result of independent reporting of data. Accordingly, the medium access for M2M devices would require a special attention and hence the medium access techniques have to be revised to address such challenges . For instance, the access channel overhead has been carefully investigated where many approaches, including the classical Back-off techniques, the access class barring scheme, slotted access, and others, are assumed [73]. The reader is encouraged to refer to [74] [75] [76] [77] for more details about the higher layer challenges and solution for M2M devices from 3GPP perspective.

From the physical layer perspective, the 3GPP standardization community has provisioned suitability of LTE to allow MTC communication and connectivity over LTE network. A lot of studies have been conducted to optimize the radio access related technologies and mechanisms. The main task of this effort was to:

- Improve the support of low-cost and low-complexity device types to match low performance requirements (low data rates and delay tolerance) of certain MTC applications.

- Provide extended coverage for MTC devices in challenging locations.

- Prolong long battery life of the UEs by enabling very low energy consumptions.

- Optimize signalling of small data transmission to increase the cell/network capacity to serve very large numbers of devices.

The 3GPP enhancement for LTE to accommodate the requirements of MTC and IoT are summarized next.

2.6.1 CAT-0 in Release-12

Although Category 1 (CAT-1) was the lowest among all LTE UE categories in R11 in terms of transmission capability (10 Mbps peak downlink transmission rate and 5 Mbps for the uplink), it was concluded that a new category will be needed to support the new requirements of MTC and IoT. Category 0 is the new standardized category for this purpose in R12. CAT-0 UEs have a reduced transmission rate of 1 Mbps peak rates for both uplink and downlink. CAT-0 UEs enjoy a reduced complexity by up to 50% compared to CAT-1. The new features of the new category include the use of only one receiver antenna with a maximum receive bandwidth of 20 MHz, which eliminates the use of dual receiver chains. Also the support of FDD half-duplex operation with relaxed switching time eliminating the need for duplex filters, which help the manufacturers to significantly reduce the modem cost compared to more advanced UE categories.

2.6.2 CAT-M or LTE-MTC in Release-13

For further complexity reduction techniques, on top of the ones introduced for CAT-0, a new category, namely Category MTC (CAT-M), is proposed in the recent work of R13 [78]. The aim of the LTE-MTC (CAT-M) Task Force was to provide a market representation to accelerate the wide-spread adoption of 3GPP-based LTE-MTC technology. LTE-MTC is addressing the low-power wide-area IoT market opportunity using licensed spectrum with the intent to launch commercial solutions in 2017. The main objectives of the LTE-MTC (CAT-M) are:

- Facilitate demonstrations and proof of concept trials which strengthen the LTE-MTC solution to meet the low power requirements.

- Lead industry partners to build a strong end-to-end industry chain for LTE-MTC growth, development and deployment.

- Further reduction in complexity of LTE-MTC devices.

Recent studies indicate that CAT-M features a complexity reductions up to 75-80% compared to CAT-1. The most important additional feature is the possibility to implement the

UE transmitter and receiver parts with reduced bandwidth compared to legacy LTE UEs operating with 20 MHz bandwidth. Specifically, a CAT-M UE will operate with a maximum channel bandwidth limited to 1.4 MHz. Another differentiating feature in CAT-M is the coverage enhancements of more than 15 dB (i.e. the received SNR $\approx$ - 15 dB), enabling the reach to the UEs behind the thickest walls or under the ground.

2.6.3   CAT-N or NB-IoT LTE in Release-13

Since the core IoT devices or massive MTC devices typically send small amounts of data and require extended coverage, a special category, namely NB-IoT, has been incorporated to LTE specifications to support IoT features [79]. The design targets for this special category require reduced complexity, promote battery longevity, and enhanced coverage. Furthermore, the need to support high data rates seldom applies to massive MTC. The link budget of NB-IoT has a 20dB improvement over conventional LTE-A [80]. These requirements have been realized by utilizing a single receive antenna system, supporting only QPSK modulation in the downlink side, and employing extended discontinuous reception cycles to reduce the power consumption in deep sleep modes. Moreover, signal repetition is considered as the key factor to provide performance gain [81].

A summary of the main physical layer features of varies LTE developments is presented in Table 2.1. In the following, we present in some details various physical channels introduced in the aforementioned developments. We start by introducing the terminology and different physical channels used with the legacy LTE system. Then, we present the changes made to each channels to accommodate for the requirements of the new specifications.

2.7   Physical Layer Features in Legacy LTE Systems

Among the objectives of the LTE standard is to create a more efficient and streamlined protocol stack and architecture. Many dedicated channels specified in previous 3GPP standards have been replaced by shared channels and the total number of physical channels has been reduced. Logical channels represent the data transfers and connections between the radio link control (RLC) layer and the MAC layer. In LTE, two types of logical channels are

Table 2.1: Summary of the basic requirements for CAT-0, CAT-M, and CAT-N systems

Specification	R12 CAT-0	R13 CAT-M	R13 CAT-N
Downlink peak rate (Mbps)	1	1	0.2
Uplink peak rate (Mbps)	1	1	0.144
Number of UE receive antennas	1	1	1
Duplex mode	Half duplex	Half duplex	Half duplex
UE receive Bandwidth (MHz)	20	1.4	0.2
Maximum UE Transmit power (dBm)	23	23	20

defined: the traffic channels and the control channels. While the traffic logical channel is used to transfer the data of users, the control logical channels communicate the necessary signalling to sustain the connectivity.

Transport channels connect the MAC layer to the physical layer, and the physical channels are processed by the transceiver at the physical layer. Each physical channel is mapped on the resource grid to a set of resource elements (REs) that carry information from higher layers of the protocol stack for eventual transmission on the air interface. The most important transport channel types are the downlink shared channel and uplink shared channel, which are used for data transmission in the downlink and uplink respectively. A physical channel carries the time-frequency resources used for transmission of a particular transport channel. Each transport channel is mapped to a corresponding physical channel. In addition to the physical channels with corresponding transport channels, there are also physical channels without corresponding transport channels. These channels, known as L1/L2 control channels, are used for downlink control information (DCI), providing the terminal with the information required for proper reception and decoding of the downlink data transmission. As for uplink control information (UCI), they are used to provide the scheduler and the Hybrid Automatic Repeat Request (HARQ) protocol with information about the situation at the terminal. The relationship between the logical channels, transport channels, and physical channels in LTE differs in downlink versus uplink transmissions. Next, we will describe -in some details-

various physical channels used in the uplink and downlink as well as some of the important signalling used within each of them.

2.7.1 FDD Frame Structure

For the LTE to feature a high spectrum flexibility, the frequency spectra are formed as concatenation of physical resource blocks (PRBs) each consists of 12 subcarriers. Subcarriers are separated by 15 KHz, hence, the total bandwidth of PRB is 180 KHz. This enables configurations for transmission bandwidth form 1.4 MHz with 6 PRBs to a maximum bandwidth of 20 MHz consisting of 110 PRBs. The available channel bandwidths are (1.4. 3, 5, 10, 15, 20 MHz), with transmission bandwidth occupies 90% of all channels, expect for the 1.4 MHz channel which has only 77% efficiency. The rest of the channel bandwidth is used as a guard band to reduce the unwanted emissions outside the neighbouring bands.

LTE specifies two downlink frame structures. A type 1 frame applies to an FDD deployment and a type 2 frame is used for a TDD deployment. Each frame is composed of 10 subframes and each subframe consists of two time slots. Each time slot is 0.5 msec, thus a radio frame is 10 msec. The three components of a resource grid are used for, user data, control channels, and reference and synchronization signals.

Figure 2.3 shows FDD downlink radio frame structure. The duration of each frame is 10ms, composed of ten 1 ms subframes denoted by indices ranging from 0 to 9. Each subframe is subdivided into two slots of 0.5ms duration. Each slot is composed of seven or six OFDM symbols, depending on whether a normal or an extended cyclic prefix is used. The DCI is placed within the first slot of each subframe. The DCI carries the content of the Physical Downlink Control Channel (PDCCH), (Physical Control Format Indicator Channel (PCFICH), the Physical Hybrid-ARQ Indicator Channel (PHICH), and together they occupy up to the first three OFDM symbols in each subframe. The Physical Broadcast Channel (PBCH) containing the Master Information Block (MIB) is located within subframe 0 and the PSS and SSS are located within subframes 0 and 5. The uplink subframe structure is similar to the downlink frame. It is composed of 1ms subframes divided into two 0.5 ms slots. Each slot is composed of either seven or six single carrier frequency division multiplexing (SC-FDM) symbols, depending on whether a normal or an extended cyclic prefix is used. The
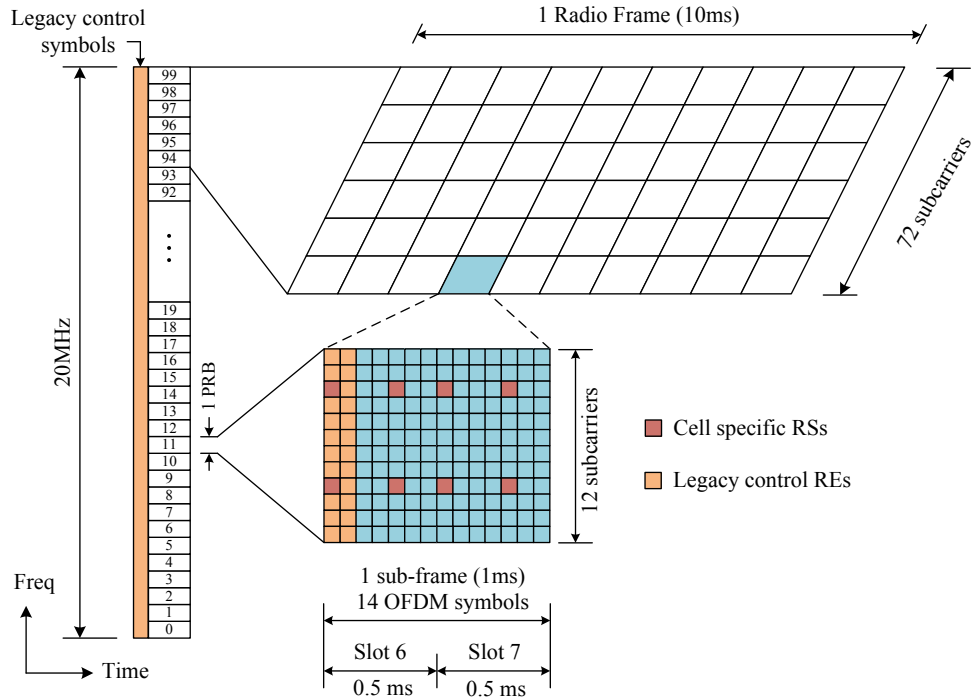
Figure 2.3: Frame structure of legacy LTE systems for FDD with Normal CP type.

inner-band (towards the center) resource blocks are reserved for data resource elements in order to reduce out-of-band emissions, while edges are reserved as a control region. The reference signals necessary for data demodulation are interspersed throughout the data and control channels.

2.7.2 Uplink Physical Channels

LTE has three uplink physical channels namely, the Physical Uplink Shared Channel (PUSCH), Physical Uplink Control Channel (PUCCH), and Physical Random Access Channel (PRACH). The PUSCH carries the user data transmitted from the user terminal. while the PRACH is used for initial access of a UE to the network through transmission of random access preambles. The PUCCH carries the UCI, including scheduling requests, acknowledgments of transmission success or failure (ACKs/NACKs), and reports of downlink channel measurements including the channel quality Indicator (CQI), Precoding Matrix Information (PMI), and Rank Indication (RI). There are two types of uplink reference signals in the LTE standard: the Demodulation Reference Signals (DMRS) and the Sounding Reference Signal (SRS).

Both uplink reference signals are based on Zadoff-Chu sequences [82].

Zadoff-Chu sequences are also used in generating downlink Primary Synchronization Signals (PSSs) and uplink preambles. Reference signals for different UEs are derived from different cyclic shift parameters of the base sequence.

2.7.2.1   Demodulation Reference Signals (DMRS)

DMRSs are transmitted by UE as part of the uplink resource grid. They are used by the uplink channel estimation to equalize and demodulate the uplink control (PUCCH) and data (PUSCH) information. In the case of PUSCH, when a normal cyclic prefix is used, DMRS signals are located on the fourth OFDM symbol of each slot and extend across all the resource blocks. In the case of PUCCH, the location of DMRS will depend on the format of the control channel.

2.7.2.2   Sounding Reference Signals (SRS)

SRSs are transmitted on the uplink in order to enable the base station to estimate the uplink channel response at different frequencies. These channel-state estimates may be used for uplink channel-dependent scheduling. This means the scheduler can allocate user data to portions of the uplink bandwidth where the channel responses are favorable. SRS transmissions are used for timing estimation and control of downlink channel conditions when downlink and uplink channels are reciprocal or identical (TDD mode).

2.7.2.3   Physical Uplink Control Channel (PUCCH)

The PUCCH carries three types of control signaling information: ACK/NACK signals for downlink transmission, scheduling requests (SR) indicator sent by UE when it intends to transmit uplink data on PUSCH, and finally the feedback from the downlink channel information, including the Channel Quality Indicator (CQI), the Precoding Matrix Indicator (PMI), and the Rank Indicator (RI). The last three indicators are representing the channel state information (CSI). Furthermore, the feedback of the downlink channel information relates to MIMO modes in downlink. In order to ensure the correct choice of the MIMO transmission schemes in downlink, each terminal must perform measurements on the quality

of the radio link and report the channel characteristic to the base station. This essentially describes the channel quality functions of the UCI as contained in the PUCCH.

2.7.2.4   Physical Random Access Channel (PRACH)

If a UE would like to transmit on the PUSCH but does not have resource on this channel, it should send a scheduling request on the PUCCH. However, in order to initiate access to the PUCCH, the UE shall initiate the random access procedure. It uses the Physical Random Access Channel (PRACH) to transmit a preamble to begin such procedure. Since this corresponds to the first communication from the UE to the base station, the system does not know the type or specifications of the UE device. After exchanging messages with the UE, the base-station sends the resource grants on the PUSCH and the required time-advance. Various transmission modes, such as Cyclic Delay Diversity (CDD) and Precoding Vector Switching (PVS), provide a transparent way of decoding the preamble information. The PRACH is transmitted on six RBs for the duration up to one subframe long. The exact length and the frequency offset of the PRACH is advertised by the base station using System Information Block-Type 2 (SIB2). A PRACH transmission has a cyclic prefix, a preamble, and a guard period. The preamble sequences have one or two symbols of 800 microseconds, and are generated from Zadoff-Chu sequences. The guard period is used to prevent collisions of the symbols at the base station as the PRACH is sent without timing advance. The preamble format defines the time duration of each field. There are three formats depending on the size of the cell and the signal strength.

2.7.2.5   Physical Uplink Shared Channel (PUSCH)

When the UE receives an uplink scheduling grant, the PUSCH carries uplink user data and signalling transport blocks arriving from the MAC layer to the physical layer. The UE sends one transport block at a time, where CRC is attached to it to help the base station in the error detection process. The resulting block is turbo coded with rate 1/3 and sent through rate matching. Then the UE reassembles the coded transport blocks in the form of codewords, where codewords from the data block are multiplexed with the control signals. Following this process, the transport block is passed to the physical processor where each codeword is

scrambled and the modulation mapper groups the codeword bits into modulation symbols. These modulated symbols go through a forward Fast Fourier Transform (FFT), then mapped to the physical resources using the resource element mapper. Finally, time domain uplink signal is generated using SC-FDMA. On the resource grid, the PUSCH occupies a contiguous set of resource blocks around the center of the uplink band, and the edges of the band are reserved for the PUCCH. Each subframe contains six PUSCH symbols and one demodulation reference symbol.

2.7.3   Downlink Physical Channels and Functionalities

The Legacy LTE has a single type of traffic logical channel which is the Dedicated Traffic Channel (DTCH), and four types of control logical channels: the Broadcast Control Channel (BCCH), the Paging Control Channel (PCCH), the Common Control Channel (CCCH), and the Dedicated Control Channel (DCCH). The dedicated logical traffic channel and all the logical control channels, except for PCCH, are multiplexed to form a transport channel known as the Downlink Shared Channel. The Paging Control Channel (PCCH) is mapped to the Paging Channel (PCH) and combined with the DL-SCH to form the Physical Downlink Shared Channel (PDSCH). The PDSCH and four other physical channels (PDCCH, Physical Downlink Control Channel; PHICH, Physical Hybrid Automatic Repeat Request Indicator Channel; PCFICH, Physical Control Format Indicator Channel; and PBCH, Physical Broadcast Channel) provide all the user data, control information, and system information needed in the unicast mode, which are delivered from higher layers.

2.7.3.1   Reference Signals

Downlink reference signals support the channel estimation functionality needed to equalize and demodulate the control and data information. They are used in CSI measurements (such as RI, CQI, and PMI) needed for channel quality feedback. LTE specifies five types of reference signal for downlink transmission, namely: Cell-Specific Reference Signals (CSR), UE-Specific Reference Signals, Channel-State Information Reference Signal (CSI-RS), MBMS reference signals, and Positioning reference signals. MBMS reference signals are used in the coherent demodulation employed in multicast/broadcast services, and the positioning refer-

ence signal is first introduced in R9 to provide measurements on multiple cells helping in estimating the position of a given terminal.

Cell-Specific Reference Signals

Cell-Specific Reference Signals (CSRs) are common to all users in a certain cell, and are transmitted in every downlink subframe and in every resource block in the frequency domain, thus cover the entire cell bandwidth. The CRSs can be used by the terminal for channel estimation for coherent demodulation of any downlink physical channel except PMCH and PDSCH in the case of transmission modes 7, 8, or 9, corresponding to non-codebook-based precoding. The CRSs can also be used by the UE to acquire CSI. Also the UE measurements such as CQI, RI, and PMI performed on CRSs are used as the basis for cell selection and handover decisions.

UE-Specific Reference Signals

UE-specific reference signals, also known as demodulation reference signals (DMRS), are only used in downlink transmission (modes 7, 8, or 9), where CSRs are not used for channel estimation. DMRSs first introduced in LTE R8 in order to support a single layer, and later in R9 to support up to two layers. Furthermore, an extended specification introduced in R10 aimed to support up to eight simultaneous reference signals.

When only one DMRS is used, 12 reference symbols are inserted in resource blocks pair. CSRs require spectral nulls or unused resource elements on all other antenna ports when a resource element on any given antenna is transmitting a reference signal. This is a major difference between CSR and DMRS. When two DMRSs are used on two antennas, all 12 reference symbols are transmitted on both antenna ports. The interference between the reference signals is mitigated by generating mutually orthogonal patterns for each pair of consecutive reference symbols.

CSI Reference Signals CSI-RSs are designed for cases where we have between four and eight antennas. CSI-RSs were first introduced in LTE R10. They are designed to perform a complementary function to the DMRS in LTE transmission mode 9. While the DMRS supports channel estimation functionality, a CSI-RS acquires CSI. To reduce the overhead resulting from having two types of reference signal within the resource grid, the temporal

resolution of CSI-RSs is reduced. This makes the system incapable of tracking rapid changes in the channel condition. Since CSI-RSs are only used with four to eight MIMO antenna configurations, and this configuration is only active with low mobility, the low temporal resolution of CSI-RSs does not pose a problem.

2.7.3.2 Synchronization Signals

In addition to reference signals, LTE also defines synchronization signals. Downlink synchronization signals are used in a variety of procedures, including the detection of frame boundaries, determination of the number of antennas, initial cell search, neighbor cell search, and handover. Two synchronization signals are available in the LTE: the Primary Synchronization Signal (PSS) and the Secondary Synchronization Signal (SSS). Synchronization signals are related to the PHY cell identity. There are 504 cell identities defined in the LTE, organized into 168 groups, each of which contains three unique identities. The PSS carries the unique identities 0, 1, or 2, whereas the SSS carries the group identity with values 0 to 167. Thus the physical layer cell identity $N_{ID}^{cell} = 3N_{ID}^1 + N_{ID}^2$ is uniquely defined by a number N_{ID}^1 in the range of 0 to 167, representing the cell ID group, and a number N_{ID}^2 in the range of 0 to 2, representing the sector ID within the group. Both the PSS and the SSS are mapped onto the central 62 subcarriers with another 10 subcarriers on the boundaries padded with zeros, forming the central 6 RBs (72 subcarriers located around the DC subcarrier). Using this structure, a UE can receive both synchronization signals without prior knowledge of the downlink bandwidth. In an FDD frame, they are positioned in subframes 0 and 5, next to each other with the PSS and the SSS placed in the last two OFDM symbols of slots 0 and 10 respectively. The PSS determines one of the three possible values of the cell identity within a group. To do so, each cell ID uses one of three Zadoff-Chu root sequences of length 63. The process of the PSS is done by 5 ms monitoring and comparing it to find the used root sequence making use of the good cross-correlation properties of the Zadoff-Chu sequences. Hence, the UE can measure the time at which the PSS arrived and extract a cell identify within a group. Then, the UE uses this timing information to receive the SSS which uses an interleaved concatenation of two binary m-sequences, each of length 31 known as Gold sequences to identify the cell group. The combination of these two sequences differs between

subframes 0 and 5. The concatenated sequence is scrambled with a scrambling sequence given by the primary synchronization signal. Using cross correlation, the UE will be able to identify the CP type (Normal or extended) and the duplex mode (FDD or TDD) as well as exact timing within the frame.

2.7.3.3 Physical Downlink Broadcast Channel (PBCH)

The PBCH carries the Master Information Block (MIB), which contains the basic physical system information and cell-specific information needed during the cell search. After the mobile terminal correctly acquires the MIB, it can then read the downlink control and data channels and perform necessary operations to access the system. The MIB contains four fields of information. The first two fields hold information regarding downlink system bandwidth and PHICH configuration. The downlink system bandwidth is communicated as one of six values for the number of resource blocks in downlink (6, 15, 25, 50, 75, or 100). Those values for the number of resource blocks map directly to bandwidths of 1.4, 3, 5, 10, 15, and 20 MHz, respectively. The PHICH configuration field of the MIB specifies the duration and amount of the PHICH. The PBCH is always confined to the first four OFDM symbols found in the first slot of the first subframe of every radio frame. The base station maps the MIB on the PBCH across 40 ms periods (four radio frames), with portions transmitted in the first subframe of every frame. When using normal CP, the PBCH occupies 72 subcarriers (6 RBs) centered on the DC subcarrier using the first four symbols of slot one.

The data of the broadcast channel arrives to the coding unit in the form of a maximum of one transport block every transmission time interval of 40 ms. Generally there are 14 information bits plus 10 spare bits (set to all zeroes currently), makes total 24 bits. From these information bits, 16 CRC parity bits are computed. The eNodeB can use 1, 2 or 4 antennas for transmission. The CRC bits are scrambled based on the 1, 2 or 4 antenna used in the transmitter. Hence, the total number of bits becomes $14 + 10 + 16 = 40$ bits. After the convolutional encoder, the total number of bits (for normal CP) becomes $= 40 \times 3 = 120$. Then, 24×3 NULLs are appended to these 120 bits to make 192 for sub-block interleaving and inter-column permutations. These bits are repeated 16 times by discarding the appended Nulls resulting in $120 \times 16 = 1920$ bits (or 1728 bits in case of Extended CP), then QPSK

mapped so that the total number of QPSK symbols becomes = 1920/2 = 960 symbols (or 864 symbols in case of Extended CP). These 960 symbols are segmented into four equal sized self-decodable units or segments. These symbols are then placed in PBCH Resource Elements in the second slot of the first subframe (slot 1). That is the first subframe's second slot contains 960/4 = 240 symbols (or 216 symbols in case of Extended CP) and then inserted in the OFDM resource elements. PBCH is restricted to the 72 subcarriers around the DC in the resource grid irrespective of the UE bandwidth. The PBCH is transmitted in the first four OFDM symbols of the second slot of the first subframe in every radio frame. For example, in a subframe which contains PBCH (e.g. first subframe of a frame) there are total $72 \times 7 \times 2 = 1008$ REs (for normal CP). Out of that, currently in that subframe, the total number of CRS (Cell Reference Signal) = $(4 \times 6) \times 6 = 144$ REs (for 4-antennas system). If the system is using single antenna instead of 4 antennas, then 48 REs will be having CRSs and the remaining elements (out of 144) will be Null.

2.7.3.4 Physical Downlink Control Format Indicator Channel (PDCFICH)

The PDCFICH is used to define the number of OFDM symbols that carry the Downlink Control Information (DCI) in a subframe. The PDCFICH information is mapped to specific resource elements belonging to the first OFDM symbol in each subframe. The possible values for PDCFICH (one, two, three, or four) depend on the bandwidth, frame structure, and subframe index. For the 1.4 MHz bandwidth, since the number of resource blocks is quite small, PDCFICH may need up to four symbols for control signaling. However, for the larger bandwidths, the number can take up to three OFDM symbols.

2.7.3.5 Physical Downlink Control Channel (PDCCH)

In order to start communication between the base station and the mobile terminal (UE), a PDCCH is defined for each Physical Downlink Shared Channel (PDSCH) channel. PDCCH mainly contains the scheduling decisions that each terminal requires in order to successfully receive, equalize, demodulate, and decode the data packets. Since the PDCCH information must be read and decoded before decoding of PDSCH begins, in a downlink PDCCH occupies

the first few OFDM symbols of each subframe. The exact number of OFDM symbols at the beginning of each subframe occupied by the PDCCH (typically one, two, three, or four) depends on various factors, including the bandwidth, the subframe index, and the use of unicast or multicast services.

The control information carried on the PDCCH is known as Downlink Control Information (DCI). Depending on the format of the DCI, the number of resource elements (i.e., the number of OFDM symbols needed to carry them) varies. There are 10 different possible DCI formats specified by the LTE standard (known as 0,1,1A,1B,1C,1D,2,2A,2B,2C,2D,3,3A,4), with each format contains a specific set of information and certain purpose. The information carried by DCI format are: resource allocation information, such as resource block size and resource assignment duration; transport information, such as multi-antenna configuration, modulation type, coding rate, and transport block payload size; and information related to the HARQ, including its process number, the redundancy version, and the indicator signaling availability of new data. The scheduling messages transmitted over the PDCCH are addressed to a certain Radio Network Temporary Identifier (RNTI). A variety of RNTI types are used in LTE to define the identity of the intended UE which should read the scheduling messages, and the type of these messages. The type of the RNTI is used to generate the CRC code that will be used by the transport layer to encode the DCI information.

The resource element mapping of the PDCCH is done using control channel elements (CCE), each contains 9 resource element groups (REG). Each REG consists of 4 REs. Based on the length of the DCI message, the base station maps the PDCCH onto 1,2,4 or 8 consecutive CCE. This is called the *aggregation level*. In other words, based on the length of the DCI, PDCCH can be scheduled onto 36, 72, 144, or 288 resource elements.

Further, the CCEs are organized into *common search spaces* and *UE-specific search spaces*. The first type is available to all UE in the cell and have predefined location in the downlink region. However, the second type is assigned to groups of UEs and its location depends on the RNTI type of the UE.

As the aggregation level of a UE changes from a subframe to another, and the length of DCI changes the aggregation level, the UE locates its PDCCH and find the DCI format using blind detection. In other words, a UE attempts to decode using all DCI formats with

candidate locations in the search space, and the correct combination is the one that checks the CRC. The reliability of the PDCCH is enhanced by means of transmit diversity using space-frequency block codes, and is protected against inter-cell interference using a cell-specific scrambling pattern.

Although the described PDCCH functions work fine for most of the situations, it suffers from some limitations as the requirements of the LTE network evolves. First, limiting the channel resources to the first 3-4 symbols of slot 0 has a direct limitation on the cell capacity (number of users could be scheduled). Second, PDCCH is transmitted only in a distributed manner, hence, it cannot benefit from the beamforming using MIMO while the base station enjoys multiple antennas. Third, with the PDCCH transmissions of a certain user spread over the entire frequency band, it does not benefit form frequency selective scheduling nor inter-cell interference coordination.

The aforementioned reasons urged the evolution towards the Enhanced Physical Down-link Control Channel (EPDCCH) in R11. The EPDCCH still carries the same information of PDCCH except that it shares the resources with the traffic PDSCH to increase the capacity. Within each subframe, a resource block pair is either assigned to PDSCH or EPDCCH, which makes the capacity of the new control channel adjustable and also makes use of interference coordination. EPDCCH is transmitted on newly defined four antenna ports (AP 107 - 110), which are associated with the reference signals (occupying the same REs as AP 7-10). EPD-CCH and its reference signals are preceded with a user-specific preceding matrix, and also supports multiuser MIMO (MU-MIMO)with up to 4 layers (i.e. supporting simultaneously 4 different users).

2.7.3.6   Physical Downlink Shared Channel (PDSCH)

After the base station sends the UE a scheduling command, it transmits the data of the DL-SCH using the scheduling commands defined. The PDSCH carries downlink user data and signalling transport blocks arriving from the MAC layer to the PHY. Specifically, transport blocks are transmitted one at a time in each subframe. The base station adds 24-bit CRC to each DL-SCH transport block which is used by the UE for error detection. Following adaptive modulation and coding, the modulated symbols are mapped onto multiple time-

frequency resource grids, which are eventually mapped to multiple transmit antennas for transmission. The type of MIMO technique used in each subframe can be adapted based on the received SNIR (which indicates the channel conditions). It should be mentioned that, the PDSCH and the PUSCH are the only physical channels that can adapt their modulation scheme according to channel quality observed at the mobile terminal. The measurements made at the terminal must be sent back to the base station in order to help the scheduling decisions. At each subframe, the mobile terminal needs to be notified about the scheduling from the base station for each transmitted resource block. Among the information that must be communicated; are the number of resource blocks allocated to a user, the transport block size, the type of modulation, the coding rate, and the type of MIMO mode used per each subframe.

2.8 Physical Layer Features for LTE-MTC Systems

The behaviour of the MTC terminals is different from the legacy LTE users, for which the LTE was optimized. Therefore, in order to accommodate the new requirements, the CAT-M UE category is recently added for MTC communication in R13. A lot of effort was put to specify a new UE for MTC operation in LTE which allows for enhanced coverage compared to existing LTE networks and low power consumption. In details, the LTE-MTC specifies a new R13 low complexity UE category for MTC operation in LTE half duplex FDD mode based on the R12 low complexity UE category supporting additional capabilities. Among these capabilities, is a reduced UE bandwidth of 1.4 MHz for the downlink and uplink with the ability to operate within any system bandwidth. Also, the frequency multiplexing of bandwidth reduced UEs and non-MTC UEs should be accommodated. For the new UE category to have a tangible complexity reduction, the maximum transmit power of the new UE power should be reduced such that an integrated power amplifier (PA) implementation is possible. Also, power consumption reduction is a must for the LTE-MTC UE target ultra-long battery life. The most important feature of the new category, is to improve the LTE coverage corresponding to almost 15 dB for FDD.

A variety of techniques is considered to achieve such requirements, including: subframe

bundling techniques with HARQ for physical data channels (PDSCH, PUSCH), repetition techniques for control channels (e.g. PBCH, PRACH, EPDCCH), uplink Power Spectral Density (PSD) boosting with smaller granularity than 1 PRB, resource allocation using EPDCCH with cross-subframe scheduling and repetition, new physical channel formats with repetition for SIB/RAR/Paging, new SIB for bandwidth reduced and coverage enhanced UEs, and increased reference symbol density and frequency hopping techniques.

2.8.1 MTC Features

More constrains are added on the MTC UE to reduce its cost and complexity. The features of the physical downlink control channel for MTC are summarized as:

- The design of the physical downlink control channel for MTC is based on EPDCCH.

- The introduction of new DCI messages to R13 for low complexity UEs.

- The use of a narrowband (within 6 PRBs) control channel.

- Its usage for other UEs in enhanced coverage.

- The demodulation of the control channel shall be based on CRS and/or DMRS.

2.8.1.1 Modes Of Operation

In Rel-13, the CAT-M UE is referred to as Bandwidth-reduced Low-complexity and Coverage Extension user equipments (BL/CE UE). BL/CE UEs can operate in two different modes of operation: CE Mode A and CE Mode B, each depends on the coverage extension level seen by the UE. The operation mode is determined by the eNodeB and sent to the UE with radio resource control message. The UE selects one of 4 different CE levels, namely level 1,2,3 and 4, based on the reference signal received power. Each level is distinguished by a different random access channel configuration and the time and frequency resources used by the UE for the random access transmissions. For CE Mode A, associated with CE level 1 and 2, a UE would have an equivalent coverage as that of UE CAT-0. This mode requires small number of repetition of different channels, or in the best case no repetitions at all.

Also, the power control mechanism used for Mode A is the same as the legacy users. For the repeated transmissions, the used transmit power remains unchanged during the repetition period. For CE Mode B, the UE is in CE level 3 or 4, and is covered with extended coverage of 15 dB with reference to CAT-0 (equivalent to 155.7 dB Maximum Coupling Loss (MCL) between the transmitter and the receiver). CE Mode B features a medium or large number of repetitions, and the transmission power of the uplink channels is set to the maximum value. Hence, no power control is needed, which makes the control information sent to this category has a unique format as well.

2.8.1.2 Narrowband Concept

The bandwidth choice of a certain base station is configured once and remains unchanged during operation, hence, it would be a good choice to use a bandwidth unit that can be a common divisor of the available bandwidth options in the legacy LTE. Then the choices become limited to 6 RBs or one RB. However, in order for the MTC devices to capture the signature of the LTE signal, it will have to receive the synchronization signals PSS and SSS. These signals occupy the central 6 RBs of the bandwidth of the base station, which makes it desirable for the MTC devices to take 6 RBs as the basic unit of bandwidth. Not only that, but also as mentioned before, the legacy PDCCH is mapped to the full occupied bandwidth, which makes decoding PDCCH is not possible in MTC applications, since the UE is limited to bandwidth of only 1.4 MHz. However, the enhanced version EPDCCH, uses one PRB pair as the basic resource unit, which makes it a good candidate to be used to control MTC UE. Furthermore, the use of only one PRB for the MTC control channels based on EPDCCH was reported to be insufficient, as it could provide the required converge enhancement (CE) [83]. It was concluded in [84] that, increasing the bandwidth of the basic EPDCCH to 6 PRBs in the 1.4 MHz bandwidth on the MTC UE along with repetition will be sufficient to have a good coverage of -14 dB. Furthermore, coverage enhancement can be achieved by employing EPDCCH that supports beamforming which increases coverage by directing the power of the base station towards the UE. For these reasons, it is agreed on to use the 6RBs (or one narrowband (NB)) as the basic bandwidth unit for MTC. A narrowband is defined as six non-overlapping consecutive physical resource blocks in the frequency domain. The total
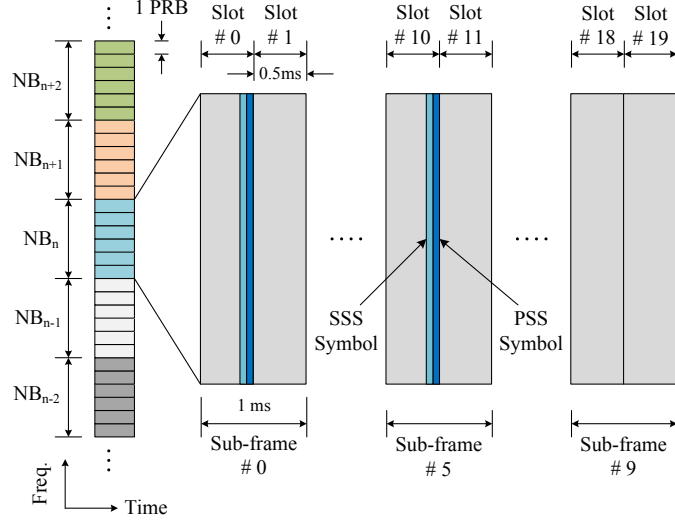
Figure 2.4: Frame structure of LTE-MTC systems for FDD with Normal CP type showing the synchronization signals. The concept of narrowband is highlighted.

number of downlink narrowbands in the downlink transmission bandwidth configured in the cell is given by $N_{NB}^{DL} = \lceil \frac{N_{RB}^{DL}}{6} \rfloor$ and are numbered $n_{NB} = 0, ..., N_{NB}^{DL} - 1$ in order of increasing physical resource-block number. The narrowband concept and numbering is highlighted in Fig. 2.4.

2.8.1.3 Frequency Hopping

With the small bandwidth offered to MTC UE and the use of single receiver chain, the frequency and spatial diversity are taken away. To retrieve some of the lost frequency diversity, the frequency hopping concept is added to the MTC LTE system. In other words, MTC transmissions will hop from one NB to another to make use of transmitting over different channels. Hence, providing frequency diversity. However, frequency hopping shall introduce new challenges due to the fact that the UE will have to re-tune its RF chain every time it hops. The re-tuning consumes some time and might affect the overall behaviour. Therefore a guard period is needed for re-tuning. Rel-13 specifies the re-tuning guard period as the time duration of two orthogonal frequency division multiplexing (OFDM) symbols. No transmission or reception is done by the UE during the guard period. The time of the guard period varies depending on whether it is downlink or uplink.

2.8.1.4 Repetitions

As mentioned before, the limitations forced on the MTC LTE directly affects the downlink control channel, which in turn, has a direct impact on the performance of the downlink. For the downlink to have sufficient link budget to support the prospected coverage enhancement, an enhanced version of the distributed EPDCCH is reused as the base control signal for MTC. Thus, enhancement is obtained by transiting repeated copies of the same signal over time. As a direct result of the use of such repetition code, the link performance can be enhanced through time diversity and boost the control signal energy. On the other hand, the repetition has the effect of increased decoding time (more latency), which requires more wake-up time of the MTC device. The maximum number of repetitions for different physical channels and signals is given in Table 2.2.

Table 2.2: Maximum number of repetitions for different channels.

CAT-M Channel	Mode A Repetitions	Mode B Repetitions
PSS/SSS	1	1
PBCH	1	5
MPDCCH	16	256
PDSCH	32	2048
PUSCH	32	2048
PUCCH	8	32
PRACH	32	128

2.8.2 MTC Physical Random Access Channel (MPRACH)

The legacy design of the PRACH channel is limited to 6 RBs only, which makes it suitable for the MTC use as it signifies the narrowband constraint. However, the legacy PRACH needs some modifications to support the extra path-loss due to the extended coverage. Hence, repetitions and frequency hopping are exploited to provide the necessary diversity to the MPRACH. Like the legacy PRACH, The physical layer random access preamble consists of

a cyclic prefix of length T_{CP} and a sequence part of length T_{SEQ} with different 5 preamble formats (0,1,2,3,4). The values of these parameters depend on the frame structure and the random access configuration and the preamble format is controlled by higher layers. For each coverage enhancement level, UEs with different geographic locations may have different radio conditions and propagation delay. Thus, different PRACH repetition levels could apply to different preamble formats to adapt to different propagation delay and compensate for different propagation losses. For each PRACH coverage enhancement level, there is a PRACH configuration done at higher layers with a PRACH configuration index values from 0 to 63, a PRACH frequency offset, and a number of PRACH repetitions per attempt N_{rep}^{PRACH}. The UE selects the repetition level to use for the initial transmission based on DL measurements, but this is only acceptable if sufficient DL measurement accuracy can be achieved within a reasonable DL measurement time. If sufficient accuracy cannot be achieved, the UE will start at the lowest configured PRACH repetition level. The number of repetitions as well as the starting subframe are also configured by higher layer signalling. It has been proposed that, the UE should remember what PRACH repetition level is used last time and use this information when setting the starting point for the next access. PRACH frequency hopping may provide frequency diversity gain and reduce the number of repetition. From this point of view, the power consumption of enhanced PRACH transmission could be saved due to reduced active time.

2.8.3   MTC Physical Downlink Control Channel (MPDCCH)

EPDCCH has been chosen to be the starting point towards designing the new MTC control channel MPDCCH. However, special requirements have been adapted to best suite the new MTC platform and to support the required coverage with reasonable complexity and power consumption. The new set of features for MPDCCH require defining new set of downlink control formats, adding a possibility for a common UE to access the control channel by introducing the new common search space, and enhancing the control channel assignment procedure to support the new MTC features such as repetition and frequency hopping. A summary of the introduced features to design the new MPDCCH is shown in Fig. 2.5.
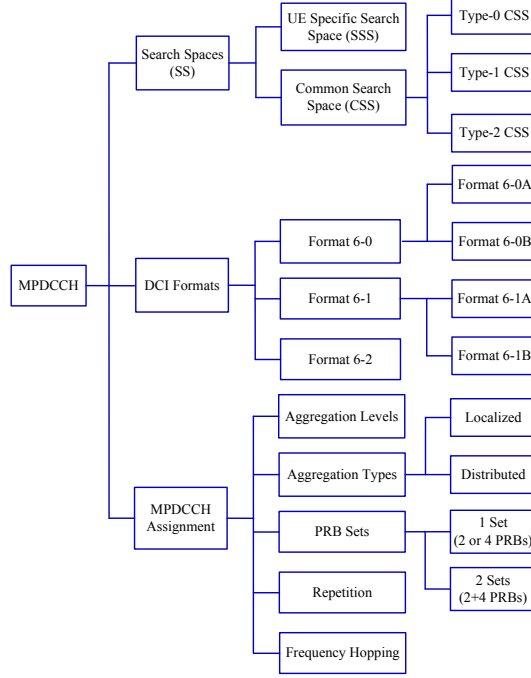
Figure 2.5: Summary for the introduced features for MPDCCH.

2.8.3.1 MTC Search Spaces

In LTE systems, the downlink control region is shared by all UEs in one cell. Each UE should monitor the control region and perform blind decoding to detect whether or not there is control information for itself. In order to reduce the number of blind decoding trials per UE, each UE has a defined search space area of the control region to monitor, rather than having to monitor the whole control region. The search space is defined on the basis of enhanced control channel elements (ECCEs). Control information may occupy 1, 2, 4, or 8 CCEs aggregated together depending on the size of the control information and the channel quality of the UE.

The search space starting point for a UE is determined by a hash function and the search space size is determined by the PDCCH aggregation level. The hash function randomizes the search space locations of different UEs and effectively reduces the blocking probability. The MPDCCH has two broad classes of search spaces: UE-specific search space (USS) for messages directed specifically to the UE and Common Search Space (CSS) for messages directed to multiple users or for messages to a specific UE before the USS has been configured. It is

worth to mention that the legacy EPDCCH has only USS since PDCCH is used for the CSS. In MPDCCH, the UE will have to blindly decode both USS and CSS. The search spaces will differ depending on the CE mode whether mode A or mode B.

2.8.3.2 MTC DCI Formats

Generally, the eNodeB employs the downlink control information messages to send downlink scheduling commands, uplink scheduling grants, and uplink power control commands to the UE. The DCI can be written using several different formats. Indeed, conventional LTE-A systems up to R12 support 14 different formats, namely format 0, 1/1A/1B/1C/1D, 2/2A/2B/2C, 3/3A, 4, and 5. Each format contains a specific set of information and has a specific purpose. However, some formats have been grouped under common name which implies that the main functionality of these downlink messages would have something in common but the details will be different. For instance, the main theme for Format 1 and its group is to mainly provide the downlink scheduling information such as the PRB allocation, modulation and coding, and single or multiple users support. The differences from one format to another in the same group are to which transmission mode and antenna system to use. Also, the basic purpose for Format 2 is to set configuration for MIMO systems. However, they differ on how the MIMO system is configured on being used for open loop, closed loop, beamforming, and multi-user MIMO configurations. Although there have been multiple formats to send various scheduling commands, in LTE-MTC systems, new formats have been introduced to the system. The motivation is to skip the unused parameters such as the number of codewords since LTE-MTC is defined for a single codeword. Also, the DCI messages for both uplink and downlink grants were designed to fit the same number of bits with some indication bits to differentiate between the formats. This is mainly to reduce the blind decoding iterations and hence, reduced UE complexity. Furthermore, with the introduction of enhanced coverage, repetition, and frequency hopping, the UE will mainly require new information to facilitate the use of repetition, narrowband resource assignment, frequency hopping flag. For example, downlink DCI assignment should indicate the MPDCCH repetition factor so that UE can expect when the message is complete. For these reasons and others, three new DCI formats, namely format 6-0, 6-1, and 6-2 have been defined for

LTE-MTC system for uplink grant, downlink scheduling, and paging, respectively. To best suite the operating mode, whether being Mode A or Mode B, there are two versions for each format where the number of information bits differ.

2.9 Physical Layer Features for NB-IoT Systems

2.9.1 Deployment Scenarios and Modes of Operation

As a finite and scarce natural resource, spectrum needs to be used as efficiently as possible. Thus, technologies that use spectrum tend to be designed to minimize usage [85]. To achieve spectrum efficiency, NB-IoT has been designed with a number of deployment options for GSM, WCDMA, or LTE spectrum. There are three deployment scenarios.

1. **In-band Operation:** An NB-IoT carrier is a self-contained network element that uses a single PRB. For in-band deployments with no IoT traffic present, the PRB can be used by LTE for other purposes, as the infrastructure and spectrum usage of LTE and NB-IoT are fully integrated. The base station scheduler multiplexes NB-IoT and LTE traffic onto the same spectrum, which minimizes the total cost of operation for IoT services. To support full flexible design, the specifications define two modes for the in-band operation. The first mode, namely Same-PCI mode, assumes that the NB-IoT carrier has identical cell parameters (i.e., cell ID and number of Tx antennas) as the donor legacy cell. The other mode considers some flexibility of having a different cell ID and different number of Tx antennas.

2. **Stand-alone Operation:** This mode of operation is mainly intended to replace a GSM carrier with an NB-IoT carrier. By steering some GSM traffic to the WCDMA or LTE network, one or more of the GSM carriers can be used to carry IoT traffic. As GSM operates mainly in the 900 MHz and 1,800 MHz bands (spectrum that is present in all markets), this approach accelerates time to market, and maximizes the benefits of a global-scale infrastructure.

3. **Guard band Operation:** this can be applied either in WCDMA or LTE. To operate

in a guard band without causing interference, NB-IoT and LTE need to coexist. The physical NB-IoT layer is designed with the requirements of LTE guard band coexistence specifically taken into consideration. Again, NB-IoT uses OFDM in the downlink and SC-FDMA in the uplink. The design of NB-IoT has fully adopted LTE numerology, using 15kHz subcarriers in the uplink and downlink, with an additional option for 3.75kHz subcarriers in the uplink to provide capacity in signal-strength-limited scenarios.

It should be noted that, NB-IoT supports operation with only one or two Tx antenna ports. For operation with two Tx antenna ports, NB-IoT uses the conventional Space Frequency Block Coding (SFBC) employing the Alamouti mapping. Unlike other LTE-based systems, NB-IoT utilizes the same transmission scheme for all physical channels including Narrowband Physical Downlink Control Channel (NPDCCH), Narrowband Physical Broadcast Channel (NPBCH), and Narrowband Physical Downlink Shared Channel (NPDSCH).

2.9.2 Downlink Physical Channels

2.9.2.1 Frame Structure

With a carrier bandwidth of just 200KHz, an NB-IoT carrier can be deployed within an LTE carrier as one PRB. Fig. 2.6 shows a 3MHz LTE carrier in which a single PRB is assigned to NB-IoT. An operating NB-IoT band is defined as a contiguous set of 12 sub-carriers forming one PRB. A single radio frame is 10ms which consists of 10 subframes with equal duration. Each subframe is divided into two slots with equal periods. Unlike conventional LTE which defines two CP types with different CP patterns, NB-IoT in R13 supports only the normal CP type, where a slot is composed of 7 OFDM symbols. According to the specification [80], if the signal is sampled at 1.92 MSamples/sec, similar to LTE-MTC, the CP length of the first symbol in each slot is 10 samples and those of the other symbols are 9 samples long. Also, in this case, the OFDM symbol spans $N = 128$ sub-carriers.

2.9.2.2 Synchronization Signals

NB-IoT intends to occupy a narrow bandwidth of only 200KHz, which is not backward compatible to the supported bandwidths by the legacy LTE. Therefore, NB-IoT redefines the
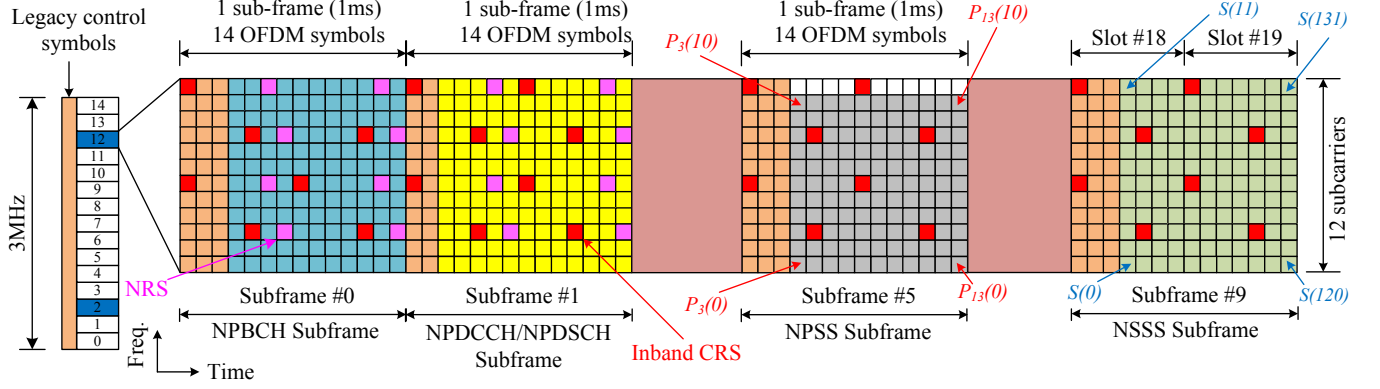
Figure 2.6: Radio frame structure for NB-IoT systems. The allocated RB is expanded in time to show the NPSS/NSSS symbols mapping in addition to the broadcast channel and one data/control subframe.

cell attach procedure including cell search and initial synchronization [86] [85]. During initial synchronization, CFO is estimated and compensated to enable proper signal detection. The UE acquires the physical cell identification by employing the cell search procedure. To cope with these changes, NB-IoT employs new set of synchronization signals, namely Narrowband Primary Synchronization Signal (NPSS) and Narrowband Secondary Synchronization Signal (NSSS) [80]. The new sequences have different bandwidth, mapping, periodicity, and generation when compared to the legacy LTE synchronization signals. Unlike conventional LTE, cell ID is encapsulated only in the secondary sequence without involving the primary sequence.

NPSS and NSSS sequences are constructed from a frequency domain Zadoff-Chu sequence where NPSS length is 11 samples while the NSSS consists of 132 samples. The NPSS, $P_l(n)$, is generated such that $P_l(k) = Q(l)e^{-j\pi uk(k+1)/11}$, where $0 \le k < 11$, $3 \le l < 14$ is the OFDM symbol index, the sequence root $u = 5$, and $Q(l)$ is a modulation sequence given by $\{1, 1, 1, 1, -1, -1, 1, 1, 1, -1, 1\}$, respectively. In NB-IoT system, there are still 504 unique physical cell IDs. However, all of them are only indicated by the NSSS. The NSSS, $S(k)$, is generated according to,

$$S(k) = \bar{C}_q(k') \, e^{-j2\pi\theta_f k} \, e^{-j\frac{\pi uk(k+1)}{131}}, \quad 0 \le k < 132 \tag{2.1}$$

where $k' = k \bmod 128$, the root sequence, u, is related to the cell ID, N_{ID}^{Ncell}, by $u = (N_{ID}^{Ncell} \bmod 126) + 3$, and the cyclic shift, θ_f, is related to the System Frame Number (SFN), n_f, such

that $\theta_f = \frac{31}{132}(n_f/2) \bmod 4$. The modulated sequence, $\bar{C}_q(k')$, is given by $\bar{C}_q(k') = 2C_q(k') - 1$, where q is a cell specific parameter that is given by $q = \lfloor N_{ID}^{Ncell}/126 \rfloor$ and C_q forms four complementary 128-bits binary sequences.

In conventional LTE, primary and secondary synchronization signals (i.e., PSS and SSS, respectively) are mapped to two consecutive OFDM symbols in the same slot with a periodicity of 5msec. However, NPSS is mapped to subframe 5 of every radio frame. NSSS is mapped to the last 11 ODFM symbols of subframe 9 in radio frames having $n_f \bmod 2 = 0$. Sequences are mapped to frequency sub-carriers in an increasing order, then applied across time as shown in Fig. 2.6.

2.9.2.3 Narrowband Reference Symbols (NRS)

Due to the lack of fully adoptable LTE signal structure in case of guard and stand-alone modes, new reference signals or pilots, namely NRS, are inserted within the transmitted signal to assist the channel estimation process which is required for coherent detection at the UE side. Similar to legacy LTE, NRS uses a cell-specific frequency shift derived as the modulo division of the NB-IoT cell ID by 6. The conventional LTE CRS sequence is reused for NRS generation where the centre of LTE CRS sequence is employed as NRS sequence for all PRBs. The NRS is mapped to the last two OFDM symbols of the slot for both antenna ports in case of transmit diversity as shown in Fig. 2.6. As NPSS/NSSS occupy the last 11 OFDM symbols within the subframes transmitting NPSS/NSSS for normal CP, NRS are not mapped to these subframes. To ensure the demodulation and/or measurement performance, it has been agreed to transmit NRS in all valid subframes except the NPSS/NSSS subframes regardless of whether there is downlink transmission in these valid subframes or not.

In in-band operation mode, the LTE CRS REs should be reserved from NB-IoT to avoid pollution to the LTE channel estimation and measurement. However, as a special case, NPBCH decoding shall not rely on LTE CRS due to the lack of knowledge of the legacy PRB index information. This means that the new reference signal (i.e. NRS) alone should be able to provide sufficient channel estimation performance for NPBCH decoding. The NPDCCH and NPDSCH decoding performance can be ensured also based on NRS only. In this sense, LTE CRS is not a must in-band operation mode in terms of DL channel decoding. However,

the standardization is designed to provide the flexibility to UE implementation for the use of LTE CRS although the performance requirements do not rely on it. On the other hand, the extra signalling overhead to support the use of LTE CRS would be limited since the resource mapping information of the LTE CRS needs be anyhow indicated to realize the rate matching around the LTE CRS REs. LTE CRS may also benefit measurement accuracy when available. For these reasons, the specifications allow two modes for in-band operation. The first assumes that the full information of the legacy cell in terms of the cell ID and number of Tx antennas is identical to the NB-IoT carrier. In this case, the UE is free to utilize the CRS for its own demodulation and/or measurements. On the other hand, the other mode assumes that the UE is not aware of the legacy cell ID, but it has the information of the number of its Tx antennas which helps determining the rate matching around the CRS.

2.9.2.4 Narrowband Physical Downlink Broadcast Channel (NPBCH)

Since NB-IoT has various deployment scenarios that require different system configurations, some Narrowband Master Information Block (NB-MIB) fields are required to be operation mode dependent. For example, the UE would require to puncture the CRS in case of in-band operation. Therefore, a field representing the number of legacy Tx antennas is beneficial. In the same mode, the PRB index is needed to validate the working assumption regarding the potential usage of CRS for demodulation. In addition, there should be an indication for the raster frequency offset for the in-band operation. It is understood that, during start, the UE would scan the frequency spectrum searching for a valid NB-IoT carrier. In legacy LTE, the raster frequency is assumed to be 100KHz starting from the center of the LTE band. However, since the NB-IoT in-band deployment assumes that the NB-IoT carrier would be allocated as a single PRB with 180KHz width, the raster frequency to the NB-IoT carrier would not be multiples of 100KHz. Indeed, for odd LTE bandwidths, there is a frequency offset of ±7.5KHz for the raster frequency to be multiple of 100KHz. In fact, the synchronization signal design and mapping are carefully studied so that a UE can lock to the NB-IoT carrier with an ambiguity of ±7.5KHz. It is clear that a new field has to be added to the NB-MIB in order to differentiate between the various frequency offsets as the bandwidth would not be known.

In all cases, similar to LTE-MTC, NB-MIB indicates the scheduling information for the system information messages by defining the TBS size and repetition filed for the first SIB message (i.e., NB-SIB1). For these reasons, it was beneficial to design new NB-MIB fields not only to include the introduced set of fields but also to interpret the fields depending on the operation mode. The decision is to extend the NB-MIB length to 34 bits before CRC attachment. This means that the code word for the broadcast channel becomes 150 bits instead of only 120 bits. Furthermore, it was agreed that NPBCH consists of 8 independently decodable blocks. Thus, after CRC attachment and channel coding, the NB-MIB is rate matched to 1600 bits instead of 1200 bits for Normal CP type.

The rate matched bits are scrambled by the conventional LTE scrambler that is initialized with the NB-IoT Physical Cell Identifier (PCI) in each radio frame fulfilling $n_f \bmod 64 = 0$, where n_f is the SFN. This simply refers to the fact that a single NB-MIB transmission spans 64 radio frames. After the channel interleaver, the bits are QPSK modulated. The modulated bits are mapped to resource elements in a frequency then time fashion. During the mapping, the 800 QPSK modulated symbols are segmented into 8 consecutive segments such that each segment is repeated in 8 consecutive radio frames. In other words, identical symbols carrying the same segment are transmitted with 80ms duration. It is essential to enable the NPBCH decoding without any prior information about the operation mode. Indeed, only cell ID and proper frame timing are required through the conventional cell search procedure. Therefore, it has been agreed that NB-PBCH is transmitted in subframe 0 in every radio frame, where the first 3 symbols in a subframe are not utilized independent of the operational mode. In addition, for rate matching purposes, the CRS are punctured assuming 4 Tx antenna ports even for guard and stand-alone modes. Moreover, the number of NRS ports is considered based on two transmit antennas independent of the actual configuration. However, the number of NRS ports (i.e., whether 1 or 2) is indicated by NB-PBCH CRC masking similar to the conventional system.

2.9.2.5 Narrowband Physical Downlink Control Channel (NPDCCH)

The NB-IoT has its own control channel with customized features and definitions. Although some features have been adopted from LTE-MTC system, there are couple of restrictions that
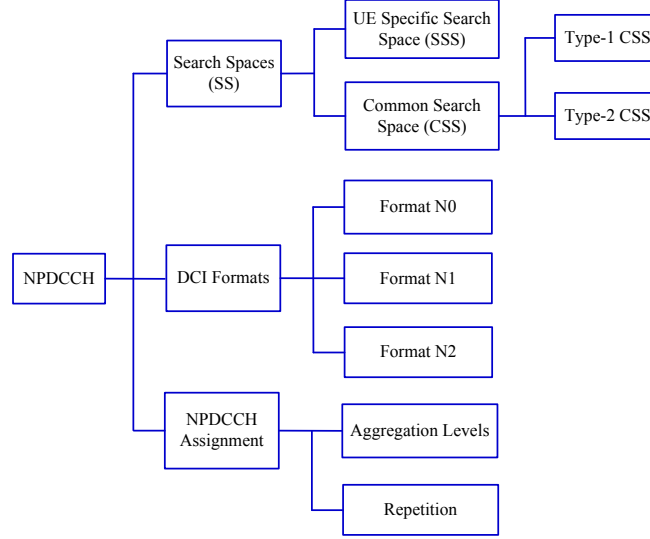
Figure 2.7: Summary for the introduced features for NPDCCH.

mandates redefinitions for some of the control channel concepts. First of all, the NPDCCH transmission becomes packet-based as the system only supports half-duplex mode at least for R13 version. There is no overlapping between the data channel and the control channel within the same subframe. The UE will monitor the NPDCCH when it expects a random access response (RAR), a new DL assignment, paging, or uplink grant. In case of RAR or paging, the UE has to monitor a common search space. Therefore, similar to LTE-MTC and unlike the conventional EPDCCH, two search spaces have been defined for NB-IoT. Second, due to the reduced set of information carried by the DCI messages, three new DCI formats, namely N0, N1, and N2, have been defined only for NB-IoT in R13. Third, NPDCCH assignment relies on repetition to support unconditional coverage enhancement with relatively small aggregation levels again for complexity reduction. Fig. 2.7 shows the essential differences between NPDCCH and other control channels in various LTE systems.

Two broad classes of search spaces have been defined for NB-IoT, namely USS for messages directed specifically to the UE and CSS for messages directed to multiple users, paging, or for messages to a specific UE before the USS has been configured (i.e., RAR message). Similar to LTE-MTC with repetitions enabled, NB-IoT provides the definition for the search space as joint combination of aggregation level and repetition factor. By varying the repetition number, a Type-1 CSS is defined for paging with more possibilities for repetitions (a

maximum of 2048) and another type, namely Type-2 CSS, is specifically defined for RAR with a maximum of 8 repetitions. To avoid blocking, each UE has search space with different values for each parameter (i.e., aggregation level and number of repetitions) so that the scheduler has the ability to avoid blocking and schedule many UEs. For UEs in enhanced coverage, where it is efficient to allocate the whole bandwidth to one NPDCCH, this search space can be based on different repetition levels only, whereas for UEs in normal coverage which there may be a lesser need for repetition, it could be based on fewer repetition levels but more aggregation levels. When the number of candidates is concerned, NB-IoT is designed to monitor the minimum number of blind decodes to reduce complexity and power consumption. Indeed, a maximum of 3 candidates can be monitored every subframe in case of no repetition and only 4 candidates are targeted when repetition is employed. In addition, during the NPDCCH monitoring, the UE is not required to simultaneously process any of the UL channels and/or other DL channels.

To simplify the NPDCCH mapping, the concept of enhanced resource element group (EREG) has not been defined for NPDCCH. The control REs are directly mapped to the Narrowband Control Channel Elements (NCCEs). Only two NCCEs are available in one subframe where one NCCE consists of 6 subcarriers per OFDM symbol in a subframe. Aside from the expected performance mismatch between the two NCCEs due to the frequency selectivity of the channel, it has been agreed that NCCE mapping simply employs Frequency Division Multiplexing (FDM) structure in which the first 6 consecutive subcarriers are assigned to one NCCE and the other 6 subcarriers to the other NCCE. To support transmit diversity and gain some spatial diversity for NPDCCH, REs should be paired with shortest possible distance between REs in each pair. In this way, the instantaneous channel response for both REs within one pair are almost the same and highly correlated, which is necessary for achieving high diversity gain. However, RE-pairs are wrapped around the NRS REs when applicable. Due to the availability of two NCCEs only, two aggregation levels are only supported. In all cases except UE search space with repetition one and two, all candidates are expected to use aggregation level 2 to provide better performance under deep coverage.

An important aspect of physical layer design for NB-IoT system is to keep the UE power consumption low. Consequently, the UE should turn on its receiver for as short periods of

time and in as few occasions as possible during the day. One way to keep this period short is to reduce the DCI size in order to achieve NPDCCH transmissions with small payload and short transmission time. In the DCI design for MTC, this was already considered through various simplifications to reduce the number of DCI bits. The same principles are applied to the coverage modes in NB-IoT. Furthermore to reduce the complexity, it is agreed to target the same DCI format for uplink grant and downlink assignment, as well as different coverage levels. Thus, DCI messages can be carried by NPDCCH using payload size no more than 23 bits for both UL grant/DL assignments which in turn defines a new set of DCI formats. DCI format N0 aims to scheduling of NPUSCH in one UL cell with the essential information about repetition, resource assignment, coding and modulation, and HARQ handling. Format N1, which has the same size as format N0, is used for the scheduling of one NPDSCH codeword in one cell and random access procedure initiated by a NPDCCH order. Last, Format N2 is employed for paging. Here the contents only spans 14 bits with a too short but significantly repeated messages to respect the reachability of all UEs under all coverage conditions.

Finally, DL transmissions to UEs in poor coverage may require many repetitions and thereby block the DL for other UEs. One way to mitigate the risk for blocking is to introduce intermediate transmission gaps at well-defined time instants during long DL transmissions. During these gaps the scheduler can transmit control and data information to other UEs. In our view, using a combination of transmission gaps and time division multiplexing between data and control scheduling allows NB-IoT to keep the basic DL scheduling unit in frequency as full band (i.e., 12 subcarriers).

2.10 Implementation Challenges

2.10.1 Low Power Support

Battery longevity depends on how efficiently a device can utilize various idle and sleep modes that allow large parts of the device to be powered down for extended periods. The NB-IoT specification addresses the physical layer technology and idling aspects of the system. Like LTE, NB-IoT uses two main protocol states: IDLE and CONNECTED. In IDLE mode, de-

vices save power, and resources that would be used to send measurement reports and uplink reference signals are freed up. In CONNECTED mode, devices can receive or send data directly. Discontinuous reception (DRX) is the process through which networks and devices negotiate when devices can sleep and can be applied in both IDLE and CONNECTED modes. For CONNECTED mode, the application of DRX reduces the number of measurement reports devices send and the number of times downlink control channels are monitored, leading to battery savings. 3GPP R12 supports a maximum DRX cycle of 2.56 seconds, which has been extended to 10.24 seconds in R13 (eDRX). However, any further lengthening of this period is as yet not feasible, as it would negatively impact a number of RAN functions including mobility and accuracy of the system information. In IDLE mode, devices track area updates and listen to paging messages. To set up a connection with an idle device, the network pages it. Power consumption is much lower for idle devices than for connected ones, as listening for pages does not need to be performed as often as monitoring the downlink control channel.

Compared with legacy LTE, the link budget of NB-IoT has a 20dB margin, and use cases tend to operate with lower data rates. The coverage target of NB-IoT has a link budget of 164dB, whereas the current LTE is 142.7 dB. The 20dB improvement corresponds to a sevenfold increase in coverage area for an open environment, or roughly the loss that occurs when a signal penetrates the outer wall of a building. Standardization activities in 3GPP have shown that NB-IoT meets the link budget target of 164dB, while simultaneously meeting the M2M application requirements for data rate, latency, and battery life.

2.10.2 Low Cost Support

NB-IoT devices support reduced peak physical layer data rates: in the range of 100-200kbps or significantly lower for single-tone devices. To facilitate low-complexity decoding in devices, turbo codes are replaced with convolutional codes for downlink transmissions, and limits are placed on maximum transport block size (which is 680 bits for DL and 1000 bits for UL). The performance requirements set for NB-IoT make it possible to employ a single receiver antenna. As a result, the radio and baseband demodulator parts of the device need only a single receiver chain. By operating NB-IoT devices in half duplex so that they cannot be scheduled to send and receive data simultaneously, the duplex filter in the device can

be replaced by a simple switch, and only a single local oscillator for frequency generation is required. In fact, these optimizations reduce cost and power consumption. At 200kHz, the bandwidth of NB-IoT is substantially narrower than other access technologies including LTE-MTC systems. The benefit of a narrowband technology lies in the reduced complexity of analog-to-digital conversion (ADC), digital-to-analog conversion (DAC), reduced number of HARQ processes, and subframe buffering. Since all physical channels utilize a unified transmission mode, channel estimation can be adopted for all subframes unlike LTE-MTC in which coherent decoding for the data channel requires a stand-alone channel estimation rather than the control channel one. All these features and others bring benefits in terms of low cost and low power consumption. NB-IoT brings about a significant design change in terms of the placement of the device's power amplifier (PA). Integrating this element directly onto the chip, instead of it being an external component, enables the cheaper single-chip modem implementations.

2.10.3   System-specific Implementation Aspects

2.10.3.1   Initial Synchronization in CAT-M

From CAT-M perspective, in literature, there are various techniques presented to perform initial synchronization, cell search, frequency tracking, and typical chain decoding. During initial synchronization and cell search, all techniques [87] [88] [89] [90] [91] [92] share the same procedure in the following order: (1) A coarse symbol timing has to be obtained first so that the received signal can be converted from time domain to frequency domain. At this stage, there are algorithms to estimate the fractional part of CFO as well [87] [88]. (2) PSS (or sector ID) will be detected in the second step. (3) SSS (or cell ID group) will be found next [89] [90] [93]. (4) The detection of the integer part of CFO can be fulfilled. Some algorithms have been presented to enable this estimation within either Step 2 or Step 3 [91]. Other algorithms are based on different time domain approaches [92].

Since LTE-MTC introduces new challenges to the system represented in the limited degrees of freedom regarding the number of antenna ports and the operating SNR, conventional cell search and initial synchronization techniques have to be revised. One fundamental

approach is defined in [94] by applying time-averaging over different decision statistics to enhance the accuracy of the legacy techniques.

2.10.3.2 Channel Estimation in CAT-M

When it comes to various chain processing, channel estimation and equalization are the main challenges for LTE-MTC systems. Conventionally, in LTE systems, reference signals are inserted within the transmitted signal to assist the channel estimation process which is required for coherent detection. Generally, several channel estimation schemes that vary in their complexity and performance have been presented [95], [96]. A 2-D Minimum-Mean Squared Error (MMSE) channel estimation technique has been introduced in [97]. However the proposed channel estimation technique depends on the knowledge of the channel statistics and the operating SNR which are usually unknown. A robust MMSE channel estimation technique has been introduced in [96], [97] in order to remove the dependency on the exact channel statistics. In this case, filter coefficients are calculated based on worst-case channel conditions and are used in the estimation process at the expense of minor performance degradation. Another simple estimation scheme can be used for systems that have uniformly distributed pilots, and where pilot separation satisfies the sampling theory conditions. In this case, an ideal low-pass filter can be used in order to reconstruct the original signal from its samples [98]. Again, the performance measures for these techniques have been designed and optimized for the legacy operating SNR values and under the assumption that high speed channels are totally supported. Conversely, LTE-MTC would require special treatment to maintain enough performance at low complexity and deep coverage conditions.

It is to be noted that, special reference signal is attached to the new introduced MPDCCH channel to help pilot-aided channel estimation techniques. In [99], the channel power-delay profile is approximated to be only described by the mean delay and the root-mean-square delay spread. A Linear MMSE filter is introduced to estimate those parameters for the LTE Multi-Input Multi-Output (MIMO) system where the user specific pilot pattern (i.e., the same pilot structure utilized by MPDCCH) is employed. The main issue with this approach is the complexity. For the same pilot structure, an iterative 2-D MMSE channel estimation method is considered in a multi-user environment [100]. The approach aims not only to cancel

the interference effect, but also to enhance the channel estimates iteratively by introducing a mean-square error criterion after each iteration. Again, the technique was not designed for a single user downlink reception purpose and it is somehow complex. To the best of the authors knowledge, practical channel estimators for MPDCCH have not been addressed. One can guess that such process has been addressed before and no revisions are required since the DMRS structure for MPDCCH is inherited from the classical EPDCCH channel [99] [101]. However, there are couple of challenges introduced to MPDCCH that would require this revision. (1) The operating SNR for MPDCCH has been reduced to -15dBs. (2) Repetition is supported for MPDCCH and hence channel estimators quality can be enhanced. (3) The channel estimator has to consider frequency hopping. (4) Complexity is a real issue for MTC framework, thus reduced complexity is essential for the channel estimators. For these reasons, channel estimation for MPDCCH requires a revision and new proposals.

2.10.3.3   Channel Estimation in NB-IoT

Although the main theme of the NB-IoT devices to be stationary due to the significant reduced MCL requirements, the specifications left it open for the vendors to support mobility with high Doppler spread [102]. It is unforgotten that even with good coverage NB-IoT UE from the power perspective, the UE losses both frequency and spatial diversities due to the reduced cost and reduced bandwidth features. Therefore, channel estimation algorithms have to be revised to provide reasonable performance at very low SNR values while supporting mobility. Indeed, it is always the tradeoff between performance and complexity to design such channel estimation algorithm. However, in NB-IoT, reduced complexity is a key target and hence the compromise has to be carefully investigated and analysed.

2.11   Conclusion

In this chapter, we addressed a variety of technology candidates to enable the IoT framework. We focused mainly on the underlay cognitive radio networks as the unlicensed candidate for IoT, and the recent developments on the LTE to support MTC and IoT .

The performance of underlay cognitive radios can be enhanced through cooperative com-

munications and MIMO support at the destination. However, the power allocation at the cognitive nodes to achieve the QoS requirement and keep limited interference to the primary users of the spectrum is a challenging problem and requires more investigations. We will address this problem in details in the chapters 3 and 4.

In addition, we addressed in details the development on the LTE to support MTC and IoT. New UE categories are introduced to support the new requirements of each system, namely, CAT-M and CAT-N. Each category has a distinct set of specifications and limitations. Coverage enhancements techniques have been discussed to extract diversity gain through time repetitions and frequency hopping. Introducing and implementing new techniques and algorithms to the support low cost and low power operations is challenging. We will address the problem of the channel estimation in the downlink control channel for LTE-MTC systems, and propose low-complexity power-saving techniques in chapter 5.

Chapter 3

Power Allocation for Non-Orthogonal Underlay Cognitive Relay Networks

3.1 Introduction

A massive number of devices will have the ability to connect to the internat through the IoT framework. With an estimate of 30 billion connected devices (by 2025 [103]), using only the traditional spectrum allocation is impossible, and the "Cognitive Radio" technology is a viable solution to this problem.

Wireless modules equipped with cognitive radios have been proposed to improve the efficiency of the spectrum usage by sharing it as secondary users [104]. The *underlay* access paradigm for cognitive nodes is being promoted as an implementable, where spectrum sharing between primary and secondary users is conditioned on limiting secondary-to-primary interference below a predefined threshold. On the other hand, node cooperation can reduce fading effects and improve the channel reliability or the transmission capacity through diversity gain. Furthermore, the availability of multiple relaying nodes can enhance the performance (in terms of outage probability or achievable capacity). While single relay selection is common [105], the general case of multiple relay selection is addressed in [106], where multiple AF relays transmit over the same frequency band simultaneously (non-orthogonal).

In this chapter, we study a variety of power allocation techniques for underlay cognitive relay networks in order to maximize the received SNR. The system under consideration employs multiple AF relays that use the same frequency band simultaneously. Given an interference threshold on the secondary network activities, we formulate optimization problems
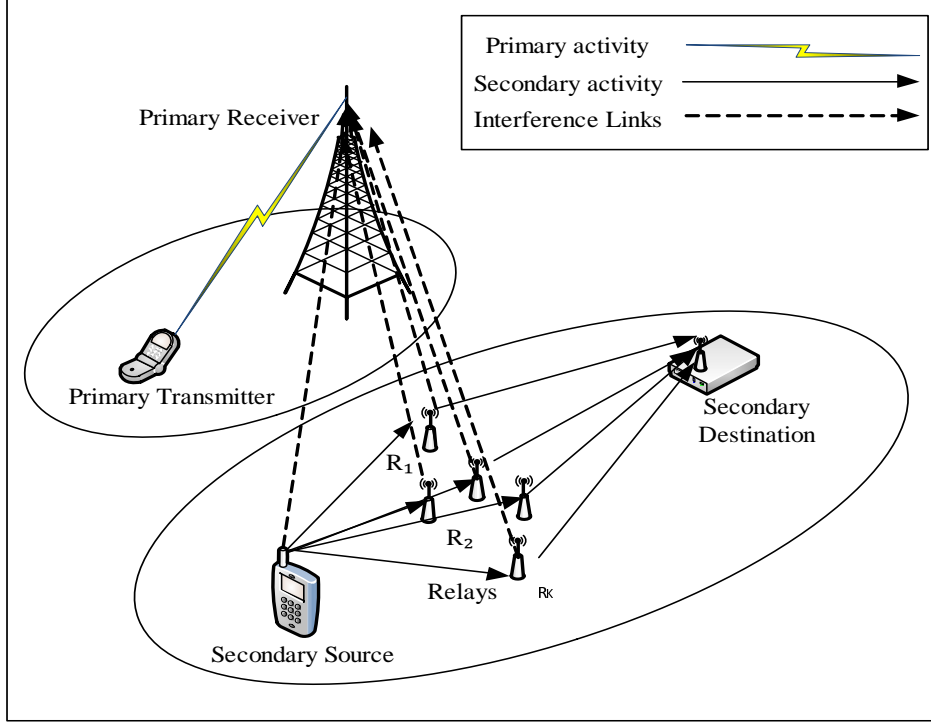
Figure 3.1: Underlay Cognitive Relay Network.

defined for different system constraints and propose the suitable power allocation technique for each problem.

3.2   System Model and Assumptions

We consider an underlay secondary cognitive relay network (Fig. 3.1) with one source S and one destination D and $K \geq 2$ relays denoted $R_1, R_2, ..., R_K$. All nodes are assumed to have only one antenna. The nearby primary system consists of a single transmitter-receiver link. The interference on the primary receiver from secondary transmissions must be smaller than a pre-defined threshold referred to as the *interference temperature* to preserve QoS requirements of the primary network. The interference temperature is a measure of the RF power available at a receiving antenna to be delivered to the primary receiver [107]. Here, interference temperature is measured in dBm when given in absolute value, or in dB when used relative to the noise power. The interference from the primary network to the relays as

well as destination D is treated as Gaussian noise [1].

A block-fading model is assumed, where all channel coefficients are assumed to be independent, identically distributed (i.i.d.) circularly symmetric complex Gaussian random variables (CSCGRV) with zero mean and unit variance, denoted by $\mathcal{CN}(0,1)$.

Assume half duplex AF relays, where direct link between S and D does not exist, and transmission from S to D requires two time slots. In the first time slot, S transmits a data symbol to all relays. The received signal at the ith relay, $(i \in \{1, 2..., K\})$, is then given by

$$y_{R_i} = \sqrt{P_S} \; h_{S,R_i} \; x_S + w_{R_i}, \tag{3.1}$$

where P_S is transmission power of S and x_S is the transmitted data symbol (with $\mathbb{E}[|x_S|^2] = 1$, where $\mathbb{E}[\cdot]$ is the expectation), and h_{S,R_i} is the channel coefficient from S to the ith relay, $i \in \{1, 2..., K\}$. Here w_{R_i} is a complex random variable capturing the effect of the thermal noise and the interference due to the primary activities, and is modeled as CSCGRV with zero mean and variance $\sigma_{R_i}^2$. Each relay scales its received signal by G_{R_i} given by

$$G_{R_i} = \frac{\sqrt{P_{R_i}} \; e^{\jmath \psi_{R_i}}}{\sqrt{P_S \; |h_{S,R_i}|^2 + \sigma_{R_i}^2}}, \tag{3.2}$$

where P_{R_i} is the transmission power used by the ith relay and ψ_{R_i} is the phase correction at the ith relay, which is set to its optimal value $\psi_{R_i} = -(\arg \; h_{S,R_i} + \arg \; h_{R_i,D})$, where $h_{R_i,D}$ is the channel coefficient from the ith relay to D. In the second time slot, each relay retransmits the amplified signal to D. Assuming all relays transmit over the same channel (shared bandwidth) simultaneously, the received signal at D is given by

$$y_D \;\; = \;\; \sum_{i=1}^{K} \left(\frac{\sqrt{P_{R_i}} \; |h_{R_i,D} \; h_{S,R_i}| \sqrt{P_S}}{\sqrt{P_S \; |h_{S,R_i}|^2 + \sigma_{R_i}^2}} \right) x_S + \sum_{i=1}^{K} \left(\frac{\sqrt{P_{R_i}} \; |h_{R_i,D}| \; v_{R_i}}{\sqrt{P_S \; |h_{S,R_i}|^2 + \sigma_{R_i}^2}} \right) + w_D, \tag{3.3}$$

where $v_{R_i} = w_{R_i} e^{-\jmath(\arg \; h_{S,R_i})}$ and w_D is CSCGRV with zero mean and variance σ_D^2 capturing the effect of the thermal noise and the interference due to the primary activities at D.

---

[1]The primary network's overall interference to the secondary network can be modeled as Gaussian random variable based on the Central Limit Theorem. This model is frequently used in the literature [108].

The instantaneous SNR, denoted by γ, is then given by,

$$\gamma = P_S \times \frac{\left(\sum_{i=1}^{K} \frac{|h_{R_i,D}| \, |h_{S,R_i}| \, \sqrt{P_{R_i}}}{\sqrt{P_S \, |h_{S,R_i}|^2 + \sigma_{R_i}^2}} \right)^2}{\sum_{i=1}^{K} \left(\frac{\sqrt{P_{R_i}} \, |h_{R_i,D}| \, \sigma_{R_i}}{\sqrt{P_S \, |h_{S,R_i}|^2 + \sigma_{R_i}^2}} \right)^2 + \sigma_D^2}. \tag{3.4}$$

Hence, the transmission rate of the secondary link for a unit bandwidth is given by

$$R = \frac{1}{2} \log_2 \left(1 + \frac{P_S \times \left(\sum_{i=1}^{K} \frac{|h_{R_i,D}| \, |h_{S,R_i}| \, \sqrt{P_{R_i}}}{\sqrt{P_S \, |h_{S,R_i}|^2 + \sigma_{R_i}^2}} \right)^2}{\sum_{i=1}^{K} \left(\frac{\sqrt{P_{R_i}} \, |h_{R_i,D}| \, \sigma_{R_i}}{\sqrt{P_S \, |h_{S,R_i}|^2 + \sigma_{R_i}^2}} \right)^2 + \sigma_D^2} \right), \tag{3.5}$$

where the $\frac{1}{2}$ factor is due to the dual hop transmission over two time slots and the rate is measured in bits/sec/Hz.

Let $g_{S,P}$ be the channel coefficient from S to the primary receiver. The interference generated by S in the first time slot is $I_S = P_S \, |g_{S,P}|^2$. In the second time slot, with all relays transmitting, the total interference generated at the primary receiver is $I = \sum_{i=1}^{K} P_{R_i} \, |f_{R_i,P}|^2$, where $f_{R_i,P}$ is the channel coefficient from the ith relay to the primary receiver. In order to protect the primary activities, I_S and I should be kept below the interference temperature I_{max} during the first and the second time slots, respectively. It is also assumed that the source and the relays are perfectly synchronized, so the start and the end of the time slots are known to all nodes. If the synchronization is lost, this will cause the source and relays to interfere leading to inter-symbol-interference.

3.3 Optimal Power Allocation

The secondary transmission rate mainly depends on the transmission powers of secondary relays and source. The objective is, thus, to find the set of transmission powers $\{P_S, P_{R_1}, P_{R_2}, ... P_{R_K}\}$ that maximizes the secondary transmission rate and does not violate the interference constraint at the primary receiver. The power allocation problem is, thus, formulated as follows.

$$\textbf{Problem P1}: \max_{\{P_S, P_{R_1}, P_{R_2}, \dots P_{R_K}\}} \mathbb{E}\left[R\right]$$

$$\text{subject to} \quad P_S \left|g_{S,P}\right|^2 \le I_{max}, \tag{3.6}$$

$$\sum_{i=1}^{K} P_{R_i} \left|f_{R_i,P}\right|^2 \le I_{max}. \tag{3.7}$$

Equations (3.6) and (3.7) correspond to the interference constraints during the first and the second time slots, respectively. With the interference constraints being instantaneous (not average), maximizing the average rate is equivalent to maximizing the instantaneous rate. From the system model, the secondary source determines its transmission power P_S independently from the transmission powers of the relays. Hence, the optimal value of P_S, denoted by P_S^*, should be set to the maximum allowable value[2]. Then, from the constraint in (3.6), we get $P_S^* = \frac{I_{max}}{|g_{S,P}|^2}$. The set of relays' powers $\mathbf{P}_R = \{P_{R_1}, P_{R_2}, \dots P_{R_K}\}$ is obtained through the following problem[3]

$$\mathbf{P}_R^* = \arg\max_{\mathbf{P}_R} \left\{ \frac{\left(\sum_{i=1}^{K} \sqrt{P_S^* \, \alpha_i \theta_i} \sqrt{P_{R_i}} \right)^2}{\sum_{i=1}^{K} \left(\sqrt{\theta_i \, \sigma_{R_i}^2} \sqrt{P_{R_i}} \right)^2 + \sigma_D^2} \right\}, \tag{3.8}$$

$$\text{subject to} \quad \sum_{i=1}^{K} \zeta_i \, P_{R_i} \le I_{max}, \tag{3.9}$$

where $\alpha_i = |h_{S,R_i}|^2$, $\beta_i = |h_{R_i,D}|^2$, $\theta_i = \frac{\beta_i}{\alpha_i P_S^* + \sigma_{R_i}^2}$ and $\zeta_i = |f_{R_i,P}|^2$. Finding a global optimal solution for the problem in (3.8) is not obvious. However, we can formulate this problem as a quadratically constrained quadratic problem (QCQP) and get an optimal solution in a simple form as follows.

Let $\mathbf{x} = [x_1, x_2, .., x_K]^T$ be the new optimization vector, where $x_i = \sqrt{P_{R_i}}$ and $[\cdot]^T$ denotes transpose operation. The optimization problem in (3.8) can be reformulated as

$$\mathbf{x}_{opt} = \arg\max_{\mathbf{x}} \left\{ \frac{\mathbf{x}^T \mathbf{A} \mathbf{x}}{\mathbf{x}^T \mathbf{B} \mathbf{x} + \sigma_D^2} \right\}, \tag{3.10}$$

---

[2]As the secondary rate in (3.5) is a monotonically increasing function of P_S.

[3]The $\frac{1}{2}\log_2$ function can be removed as it is monotonically increasing in its argument.

$$\text{subject to} \quad \mathbf{x}^T \mathbf{C} \mathbf{x} \leq I_{max}, \tag{3.11}$$

where $\mathbf{A}$ is a square matrix of size $K \times K$ and its elements $a_{i,j} = P_S^* \sqrt{\alpha_i \theta_i \alpha_j \theta_j}$, for $i, j \in \{1, 2, ...K\}$. $\mathbf{B}$ and $\mathbf{C}$ are diagonal matrices of size $K \times K$ with the diagonal elements $b_{i,i} = \theta_i \sigma_{R_i}^2$ and $c_{i,i} = \zeta_i$, respectively.

Proposition 1. *Define the matrices* $\mathbf{D} = \mathbf{B} + \frac{\sigma_D^2}{I_{max}} \mathbf{C}$ *and* $\mathbf{M} = \mathbf{D}^{-\frac{1}{2}} \mathbf{A} (\mathbf{D}^{-\frac{1}{2}})^T$. *Then, the optimal power allocation is given by*

$$\mathbf{P}_R^* = \mu^2 diag\left\{ (\mathbf{D}^{-\frac{1}{2}})^T \mathbf{v} \, \mathbf{v}^T \mathbf{D}^{-\frac{1}{2}} \right\}, \tag{3.12}$$

and the corresponding secondary rate is, then, given by

$$R^* = \frac{1}{2} \log_2(1 + \gamma^*), \tag{3.13}$$

where $diag\{\cdot\}$ *represents a vector whose elements are taken from the diagonal elements of a matrix, and* $\mu^2 = \frac{I_{max}}{\mathbf{v}^T \mathbf{D}^{-\frac{1}{2}} \mathbf{C} (\mathbf{D}^{-\frac{1}{2}})^T \mathbf{v}}$ *is a scaling factor. Here* γ^* *is the optimal value of the received SNR and equals to* λ_{max} *the dominant eigenvalue of the matrix* $\mathbf{M}$, *and* $\mathbf{v}$ *is the corresponding eigenvector.*

Proof. The proof of the above proposition commences by noting that, the inequality constraint in (3.11) has to be satisfied with equality at the optimal solution $\mathbf{x}_{opt}$, which can be proved by contradiction as follows.

Let $\tilde{\mathbf{x}}$ be the optimal solution for the problem in (3.10) which satisfies the constraint in (3.11) with only the inequality (i.e. $\tilde{\mathbf{x}}^T \mathbf{C} \tilde{\mathbf{x}} < I_{max}$). Then one can find a constant $\kappa > 1$, such that $\hat{\mathbf{x}} = \kappa \tilde{\mathbf{x}}$, that satisfies $\hat{\mathbf{x}}^T \mathbf{C} \hat{\mathbf{x}} = I_{max}$. The last equality comes from the fact that the matrix $\mathbf{C}$ is a diagonal matrix with diagonal elements all being positive $\zeta_i = |f_{R_i,P}|^2 > 0$ (i.e. positive definite), and hence $\mathbf{x}^T \mathbf{C} \mathbf{x}$ is a positive value. Substituting $\hat{\mathbf{x}}$ in the objective function (3.10), we get

$$\frac{\hat{\mathbf{x}}^T \mathbf{A} \hat{\mathbf{x}}}{\hat{\mathbf{x}}^T \mathbf{B} \hat{\mathbf{x}} + \sigma_D^2} = \frac{\tilde{\mathbf{x}}^T \mathbf{A} \tilde{\mathbf{x}}}{\tilde{\mathbf{x}}^T \mathbf{B} \tilde{\mathbf{x}} + \frac{\sigma_D^2}{\kappa^2}}. \tag{3.14}$$

Since it is assumed that $\kappa > 1$ and the value of the objective function in (3.14) is monotonically increasing in κ, then $\hat{\mathbf{x}}$ provides a higher value for the objective function than $\tilde{\mathbf{x}}$. This contradicts the assumption of $\tilde{\mathbf{x}}$ being the optimal solution and proves our claim. Therefore,

the optimal solution $\mathbf{x}_{opt}$ should satisfy the total interference constraint with equality, i.e., $\mathbf{x}_{opt}^T \mathbf{C} \mathbf{x}_{opt} = I_{max}$. Hence, σ_D^2 in (3.10) can be replaced by the quadratic form $\frac{\sigma_D^2}{I_{max}} \mathbf{x}^T \mathbf{C} \mathbf{x}$. Using this substitution, we obtain a homogenous form of the objective function as follows

$$\frac{\mathbf{x}^T \mathbf{A} \mathbf{x}}{\mathbf{x}^T \mathbf{B} \mathbf{x} + \frac{\sigma_D^2}{I_{max}} \mathbf{x}^T \mathbf{C} \mathbf{x}} = \frac{\mathbf{x}^T \mathbf{A} \mathbf{x}}{\mathbf{x}^T \mathbf{D} \mathbf{x}}, \tag{3.15}$$

where $\mathbf{D} = \mathbf{B} + \frac{\sigma_D^2}{I_{max}} \mathbf{C}$ is a diagonal matrix, which is a full rank positive definite matrix and hence can be inverted. Substituting the new objective function (3.15) into (3.10), the optimization problem becomes

$$\mathbf{x}_{opt} = \arg\max_{\mathbf{x} | \mathbf{x}^T \mathbf{C} \mathbf{x} = I_{max}} \frac{\mathbf{x}^T \mathbf{A} \mathbf{x}}{\mathbf{x}^T \mathbf{D} \mathbf{x}}. \tag{3.16}$$

Since the objective function in (3.16) is homogenous, the optimal value is insensitive to any scaling of $\mathbf{x}$. Consequently, the equality constraint can be dropped from (3.16). The solution of the unconstrained problem can thus be scaled to satisfy the constraint. Hence, the simplified problem becomes

$$\mathbf{x}_{opt} = \arg\max_{\mathbf{x}} \frac{\mathbf{x}^T \mathbf{A} \mathbf{x}}{\mathbf{x}^T \mathbf{D} \mathbf{x}}. \tag{3.17}$$

Since the matrix $\mathbf{D}$ is positive definite, it can be decomposed as $\mathbf{D} = \mathbf{D}^{\frac{1}{2}} \left(\mathbf{D}^{\frac{1}{2}} \right)^T$, where $\mathbf{D}^{\frac{1}{2}}$ is the square root of $\mathbf{D}$ [109]. Defining a new optimization vector $\mathbf{y} \triangleq \left(\mathbf{D}^{\frac{1}{2}} \right)^T \mathbf{x}$ (or equivalently $\mathbf{x} = \left(\mathbf{D}^{-\frac{1}{2}} \right)^T \mathbf{y}$) and substituting in (3.17), we get,

$$\mathbf{y}_{opt} = \arg\max_{\mathbf{y}} \frac{\mathbf{y}^T \mathbf{M} \mathbf{y}}{\mathbf{y}^T \mathbf{y}}, \tag{3.18}$$

where $\mathbf{M} = \mathbf{D}^{-\frac{1}{2}} \mathbf{A} \left(\mathbf{D}^{-\frac{1}{2}} \right)^T$. The simple form of the optimization problem in (3.18) can be interpreted as the famous quadratic fractional function and one can trace the matrix $\mathbf{M}$ to be symmetric. According to the min-max theorem [110], the maximum eigenvalue of the matrix $\mathbf{M}$ is the maximal of the objective function (3.18), and the corresponding eigenvector is the optimal $\mathbf{y}$. The optimal secondary rate is, then, given by $R^* = \frac{1}{2} \log_2(1 + \lambda_{max})$, and the optimal power allocation is given by $\mathbf{P}_R^* = \mu^2 diag \left\{ \left(\mathbf{D}^{-\frac{1}{2}} \right)^T \mathbf{v} \ \mathbf{v}^T \mathbf{D}^{-\frac{1}{2}} \right\}$, where μ^2 is a scaling factor to satisfy the equality constraint in (3.16). $\qquad \square$

In order to have more insights of performance gain of the obtained power allocation scheme, we compare the average secondary throughput of different power allocation schemes
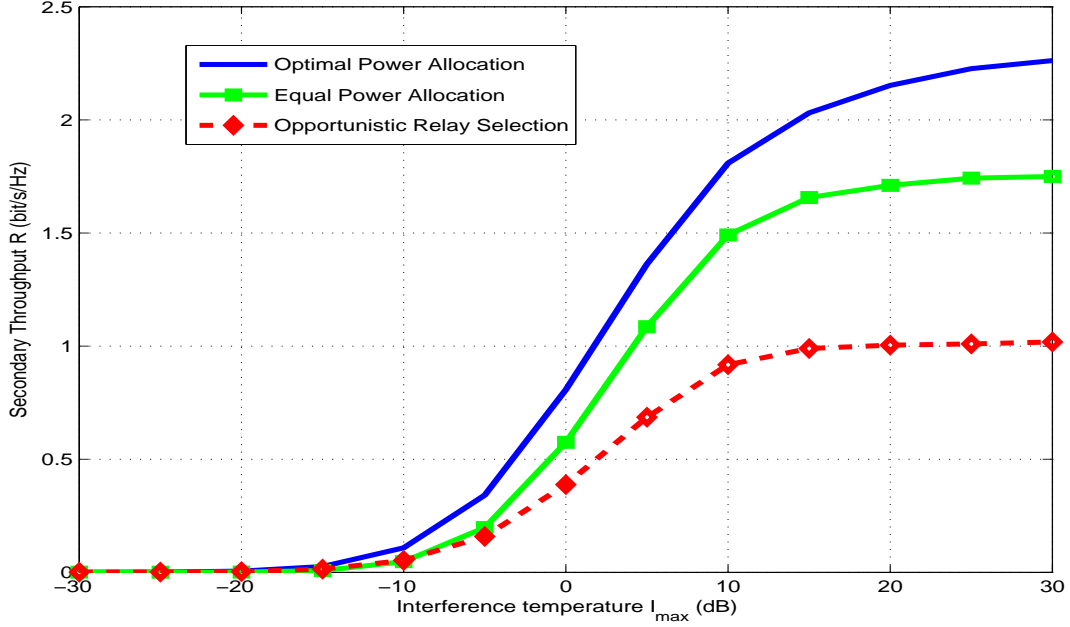
Figure 3.2: The average secondary throughput for different values of interference temperature I_{max}. The system has $K = 5$ relays.

for different interference temperature I_{max} values for a 5-relay network, and present them in Fig. 3.2. Without loss of generality, the variance of the noise at all nodes is set to 1 (i.e. $\sigma^2_{R_i} = \sigma^2_D = 1$). Here, the "Opportunistic Relay Selection" refers to a single relay selection that maximizes the transmission rate. The selected relay R_{i^*} uses the maximum allowed transmission power without violating the interference constraint (i.e. $P_{R_{i^*}} = I_{max}/|f_{R_{i^*},P}|^2$). In the "Equal Power Allocation", all relays use the same transmission power $P_R = I_{max}/\sum_{i=1}^{K} |f_{R_i,P}|^2$. The throughput is calculated using $R = \frac{1}{2}\log_2(1 + \gamma)$, where, γ is the achieved SNR using the power allocation technique. Clearly, our proposed power allocation scheme outperforms the two other schemes. For example, at high I_{max}, the secondary throughput is more than double of that of opportunistic relay selection.
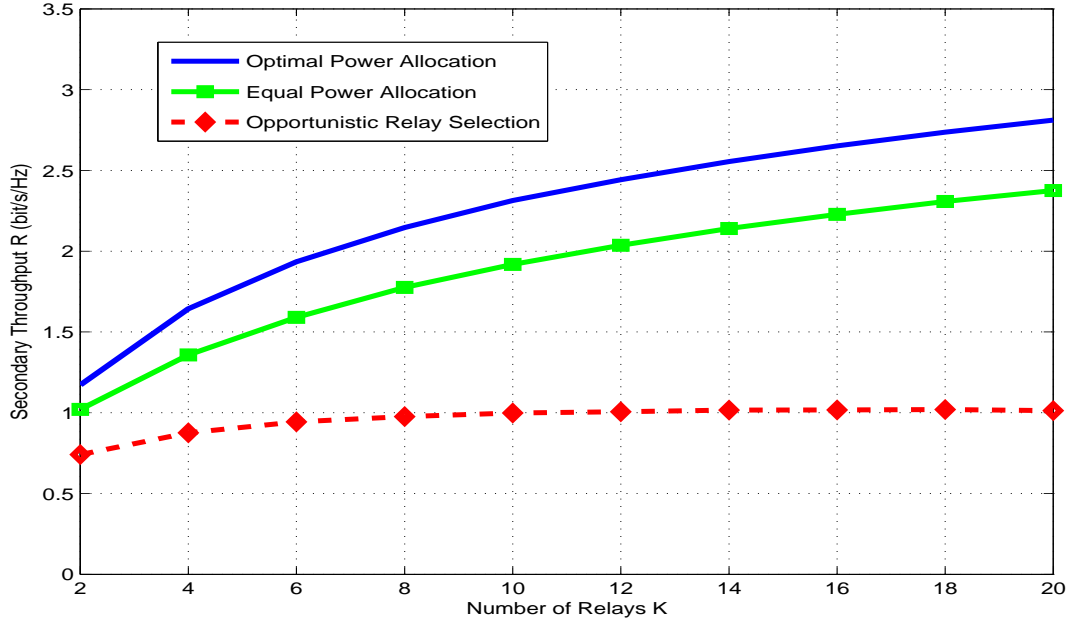
Figure 3.3: The average secondary throughput for different number of secondary relays K. The interference temperature I_{max} is set at 10 dB.

In Fig. 3.3, the effect of the number of relays on the average secondary throughput is shown. The proposed power allocation gains almost 30% increased rate over equal power allocation as K increases, and has a higher growth rate with K compared to the opportunistic relay selection. The proposed power allocation achieves more than twice the rate of the opportunistic relay selection at $K = 20$ relays.

3.4 Evaluation of The Received SNR

Using the optimal power allocation in (3.12) at the secondary relays maximizes the received SNR. The maximum value of this SNR is proved to be the dominant eigenvalue of the matrix $\mathbf{M}$. For any two arbitrary square matrices $\mathbf{G}$ and $\mathbf{Q}$, the eigenvalues of their product $\mathbf{GQ}$ and $\mathbf{QG}$ is the same. Using this fact, the eigenvalues of the matrix $\mathbf{M}$ are given by,

$$
\begin{aligned}
Eigen\{\mathbf{M}\} &= Eigen\{\mathbf{D}^{-\frac{1}{2}}\mathbf{A}(\mathbf{D}^{-\frac{1}{2}})\} \\
&= Eigen\{\mathbf{A}(\mathbf{D}^{-\frac{1}{2}})\mathbf{D}^{-\frac{1}{2}}\} \\
&= Eigen\{\mathbf{AD}^{-1}\}
\end{aligned}
\tag{3.19}
$$

while in the first equality we used $\mathbf{D}^{-\frac{1}{2}} = (\mathbf{D}^{-\frac{1}{2}})^T$, as $\mathbf{D}$ is a diagonal square matrix. This also results in $\mathbf{D}^{-1}$ being diagonal (i.e. full rank). From the construction of the matrix $\mathbf{A}$, it can be shown it is rank one, hence, the product of the two matrices $\mathbf{A}$ and $\mathbf{D}^{-1}$ is also of rank one. This leads to the resulting SNR being the only eigenvalue of the matrix $\mathbf{AD}^{-1}$, calculated using,

$$
Eigen\{\mathbf{M}\} = \text{Tr}\{\tilde{\mathbf{A}}\mathbf{D}^{-1}\}
\tag{3.20}
$$

where $\text{Tr}\{.\}$ is the trace of the matrix, and $\tilde{\mathbf{A}}$ is a diagonal matrix having only the diagonal elements of the matrix $\mathbf{A}$. After some mathematical manipulations, the maximum received SNR can be expressed as,

$$
\gamma^* = \gamma_s \sum_{i=1}^{K} \gamma_i
\tag{3.21}
$$

where $\gamma_s = \frac{P_s}{\sigma^2}$, and γ_i is given by[4]

$$
\gamma_i = \frac{|h_{S,R_i}|^2 |h_{R_i,D}|^2}{|h_{R_i,D}|^2 + \kappa_p |f_{R_i,P}|^2 |h_{S,R_i}|^2 + \kappa_n |f_{R_i,P}|^2}
\tag{3.22}
$$

where $\kappa_p = \frac{P_s}{I_{max}}$, and $\kappa_n = \frac{\sigma^2}{I_{max}}$. Note that (3.21) suggests that the use of the optimal power allocation in (3.12) transforms the nonorthogonal transmission of the secondary relays into parallel channels, resulting in the received SNR to be the summation of the SNRs generated by each relay independently.

---

[4]In this section and the following ones, we will assume that the noise variance is the same at all secondary nodes (i.e. $\sigma_{R_i}^2 = \sigma_D^2 = \sigma^2$)

3.5 SNR Statistics

To study the performance of the system, we first need to drive the statistics of the received SNR γ^*. In order to do so, we start by studying the statistics of the random variable γ_i (with $i \in (1, 2, ...K)$).

3.5.1 Statistics of γ_i

3.5.1.1 Probability Density Function (PDF) and Cumulative Distribution Function (CDF)

Proposition 2. *Given the channel coefficients h_{S,R_i} $h_{R_i,D}$ and $f_{R_i,P}$ are zero mean and unit variance circularly symmetric complex Gaussian random variables (CSCGRV) $\mathcal{CN}(0,1)$, the power gains $|h_{S,R_i}|^2$ $|h_{R_i,D}|^2$ and $|f_{R_i,P}|^2$ are exponential random variables. Hence, The PDF and the CDF of γ_i are given by,*

$$F_{\gamma_i}(t) = 1 - \frac{e^{-t}}{(\kappa_p t + 1)}\left[1 + \frac{t(\kappa_p t + \kappa_n)}{(\kappa_p t + 1)} e^{\frac{t(\kappa_p t + \kappa_n)}{(\kappa_p t + 1)}} Ei\left[-\frac{t(\kappa_p t + \kappa_n)}{(\kappa_p t + 1)}\right]\right], \quad t \geq 0, \qquad (3.23)$$

and

$$\begin{aligned}
f_{\gamma_i}(t) &= \frac{e^{-t}}{(\kappa_p t + 1)^4} \times \left[\kappa_p^3 t^2 + \kappa_p(1 - \kappa_n + 2\kappa_p)t\right. \\
&+ (1 - \kappa_n + \kappa_p) - e^{\frac{t(\kappa_p t + \kappa_n)}{(\kappa_p t + 1)}} Ei\left[-\frac{t(\kappa_p t + \kappa_n)}{(\kappa_p t + 1)}\right] \\
&\times \left.\left(m_1 t^2 + m_2 t + \kappa_n\right)\right], \quad t \geq 0.
\end{aligned} \qquad (3.24)$$

where $m_1 = \kappa_p^2(2 - \kappa_n) - \kappa_p(1 - \kappa_n)$ and $m_2 = 2\kappa_p - \kappa_n(1 - \kappa_n)$.

Proof. Let $X = |h_{R_i,D}|^2$, $Y = |h_{S,R_i}|^2$, $Z = |f_{R_i,P}|^2$, and define $U = \frac{Y}{Z}$ then γ_i is given by,

$$\gamma_i = \frac{XU}{U + \kappa_p X + \kappa_n}.$$

It should be noted that, for the Rayleigh fading scenario under study, the random variables X, Y and Z are Exponential random variables with unit mean. To find the CDF of γ_i, we

start by finding the CDF of U given by,

$$
\begin{aligned}
F_U(u) &= Pr(\frac{Y}{Z} \le u) \\
&= Pr(Y \le uZ|Z) \\
&= \int_0^\infty (1 - e^{-uz})e^{-z}dz \\
&= \frac{u}{u+1}, \qquad u \ge 0.
\end{aligned}
\tag{3.25}
$$

Then,

$$
\begin{aligned}
F_{\gamma_i}(t) &= Pr\left(\frac{XU}{U + \kappa_p X + \kappa_n} \le t \right) \\
&= Pr\left(U(X - t) \le (\kappa_p X + \kappa_n)t | X \right) \\
&= \int_0^t Pr\left(U \ge \frac{(\kappa_p x + \kappa_n)}{x - t} \right) F_X(x)dx \\
&\quad + \int_t^\infty Pr\left(U \le \frac{\kappa_p x + \kappa_n}{x - t} \right) F_X(x)dx \\
&= 1 - \int_t^\infty F_U\left(\frac{\kappa_p x + \kappa_n}{x - t} \right) e^{-x}dx.
\end{aligned}
\tag{3.26}
$$

Substituting (3.25) into (3.26), with some manipulation and using variable change $x = x - t$, then $F_{\gamma_i}(t)$ becomes,

$$
\begin{aligned}
F_{\gamma_i}(t) &= 1 - e^{-t} \int_0^\infty \frac{\kappa_p tx + (\kappa_p t^2 + \kappa_n t)}{(\kappa_p + 1)x + (\kappa_p + \kappa_n)t} e^{-x}dx. \\
&= 1 - e^{-t} \underbrace{\int_0^\infty \frac{\kappa_p t \, x \, e^{-x}}{(\kappa_p + 1)x + (\kappa_p + \kappa_n)t} dx}_{I_1} \\
&\quad - e^{-t} \underbrace{\int_0^\infty \frac{\kappa_p t^2 + \kappa_n t}{(\kappa_p + 1)x + (\kappa_p + \kappa_n)t} e^{-x}dx}_{I_2},
\end{aligned}
\tag{3.27}
$$

Using [111, eq. 3.353.5] and [111, eq. 3.352.4], a closed-form expression for I_1 and I_2 can be obtained. Substituting those results into (3.27) with term arrangement resulting in the CDF (3.23). Differentiating the CDF in (3.23) with respect to the variable t, and after some simple term collection and arrangements, one can easily arrive at the PDF of γ_i in (3.24). $\quad\square$

3.5.1.2 Moment Generating Function (MGF)

Another useful statistic of γ_i is its moment generating function (MGF). Using the CDF of γ_i, the MGF $\mathcal{M}_{\gamma_i}(s)$ is obtained as

$$\mathcal{M}_{\gamma_i}(s) = s \ \mathcal{L}\{F_{\gamma_i}(t)\}, \tag{3.28}$$

where $\mathcal{L}\{x(t)\}$ is the Laplace transform defined by $\int_0^\infty x(t)e^{-st}dt$. Substituting (3.23) into (3.28) results in

$$\mathcal{M}_{\gamma_i}(s) = s + \frac{se^{\frac{s+1}{\kappa_p}}}{\kappa_p} Ei\left[-\frac{s+1}{\kappa_p}\right] - \mathcal{I} \tag{3.29}$$

where $\mathcal{I} = \int_0^\infty \frac{e^{-(s+1)t}}{\kappa_p t+1} Te^T Ei[-T]dt$ and $T = \frac{t(\kappa_p t+\kappa_n)}{(\kappa_p t+1)}$. For the value of $\kappa_n = 1$, the variable T reduces to t, and using Taylor's expansion of $\frac{1}{\kappa_p t+1} = \sum_{n=0}^\infty (-1)^n (\kappa_p t)^n$, a closed-form expression for $\mathcal{I}$ can be obtained using [111, eq. (6.228.2)]. Hence, for $\kappa_n = 1$, $\mathcal{M}_{\gamma_i}(s)$ can be expressed as,

$$
\begin{aligned}
\mathcal{M}_{\gamma_i}(s) &= s + \frac{s}{\kappa_p} e^{\frac{s+1}{\kappa_p}} Ei\left[-\frac{s+1}{\kappa_p}\right] \\
&+ \sum_{n=0}^\infty (-1)^n \kappa_p^n \frac{\Gamma(n+2)s}{(n+2)(1+s)^{n+2}} \times {}_2F_1\left(1, n+2; n+3, \frac{s}{s+1}\right),
\end{aligned} \tag{3.30}
$$

where $\Gamma(.)$ is the Gamma function defined as $\Gamma(z) = \int_0^\infty t^{z-1}e^{-t}dt$, and $2F_1(\alpha, \beta; \gamma, z)$ is the Gauss-hypergeometric function defined in [111, section 9.11]

3.5.2 Statistics of the received SNR γ^*

Since the received SNR at the secondary destination γ^* is expressed as the summation of the SNRs γ_i, its MGF can be expressed as the product of the MGF of $\gamma_i \forall i \in 1, 2, ... K$ as

$$\mathcal{M}_{\gamma^*}(s) = \prod_{i=1}^K \mathcal{M}_{\gamma_i}(s) = \left[\mathcal{M}_{\gamma_i}(s)\right]^K. \tag{3.31}$$

The CDF of γ^*, $F_{\gamma^*}(t)$, can be evaluated as,

$$
\begin{aligned}
F_{\gamma^*}(t) &= \mathcal{L}^{-1}\left\{\frac{\mathcal{M}_{\gamma^*}(s)}{s}\right\}, \\
&= \frac{1}{2\pi j} \lim_{w \to \infty} \int_{c-jw}^{c+jw} \tilde{\mathcal{M}}(s)e^{st} \ ds,
\end{aligned} \tag{3.32}
$$

where $\mathcal{L}^{-1}\{X(s)\}$ is the inverse Laplace transform, $j = \sqrt{-1}$, and $\tilde{\mathcal{M}}(s) = \frac{\mathcal{M}_{\gamma^*}(s)}{s}$. An analytical solution for the inverse Laplace in (3.32) appears intractable. However, some numerical techniques, such as Talbot's Method [112], that inherits a contour deformation approach and improves the numerical stability of the evaluation using fixed point-precision computing, could be used to obtain a solution for the integrating in (3.32) at a desired precision. Obtaining a closed-form expression for the statistics of γ^* using the MGF approach is intractable. While evaluating a numerical solution for these statistics might be useful, obtaining expressions for the overall system performance (outage probability, bit error rate and achievable throughput) is not possible with such solution. Therefore, we suggest approximating the statistics of γ^*. To obtain such approximation, we propose approximating the PDF of γ_i in (3.24) to be an exponential distribution given by,

$$f_{\gamma_i}(x) \approx \frac{1}{\tilde{\mu}_\gamma} e^{\frac{-x}{\tilde{\mu}_\gamma}}, \quad x \geq 0, \tag{3.33}$$

where $\tilde{\mu}_\gamma$ is the mean of exponential distribution obtained by matching the mean of the original distribution in (3.24), and is given by,

$$\tilde{\mu}_\gamma = \frac{-1}{\kappa_p} e^{\frac{1}{\kappa_p}} Ei\left[-\frac{1}{\kappa_p}\right] - \frac{\kappa_n}{\kappa_p} \mathbf{G}_{3,0}^{1,1}\left(\begin{array}{ccc} 0 & 2 \\ 1 & 1 & 0 \end{array}\middle| \begin{array}{c} \kappa_n \\ \kappa_p \end{array}\right). \tag{3.34}$$

where $\mathbf{G}_{p,q}^{m,n}\left(\begin{array}{c} a_1, ..., a_p \\ b_1, ..., b_q \end{array}\middle| z\right)$ is the Meijer G-function defined in [111, eq. 9.3]. A comparison between the empirical PDF of γ_i and the proposed exponential approximation is shown in Fig. 3.4 to show how close is the approximation to the actual PDF.

Proposition 3. *Given the channel coefficients h_{S,R_i} $h_{R_i,D}$ and $f_{R_i,P}$ $\forall i \in \{1,2...K\}$, are i.i.d. $\mathcal{CN}(0,1)$, then the received SNR while using the optimal power allocation, can be approximated as a Gamma random variable with parameters K and $\mu_\gamma = \gamma_s \tilde{\mu}_\gamma$, with the CDF given as,*

$$F_{\gamma^*}(x) \approx 1 - \frac{1}{\Gamma(K)} \Gamma\left(K, \frac{x}{\mu_\gamma}\right), \quad x \geq 0. \tag{3.35}$$

where $\Gamma(a,x) = \int_x^\infty t^{a-1} e^{-t} dt$ is the upper incomplete Gamma function [111]. Accordingly, the approximate PDF of γ^*, is then given by,

$$f_{\gamma^*}(x) \approx \frac{1}{\Gamma(K)\mu_\gamma^K} x^{K-1} e^{\frac{x}{\mu_\gamma}}, \quad x \geq 0. \tag{3.36}$$
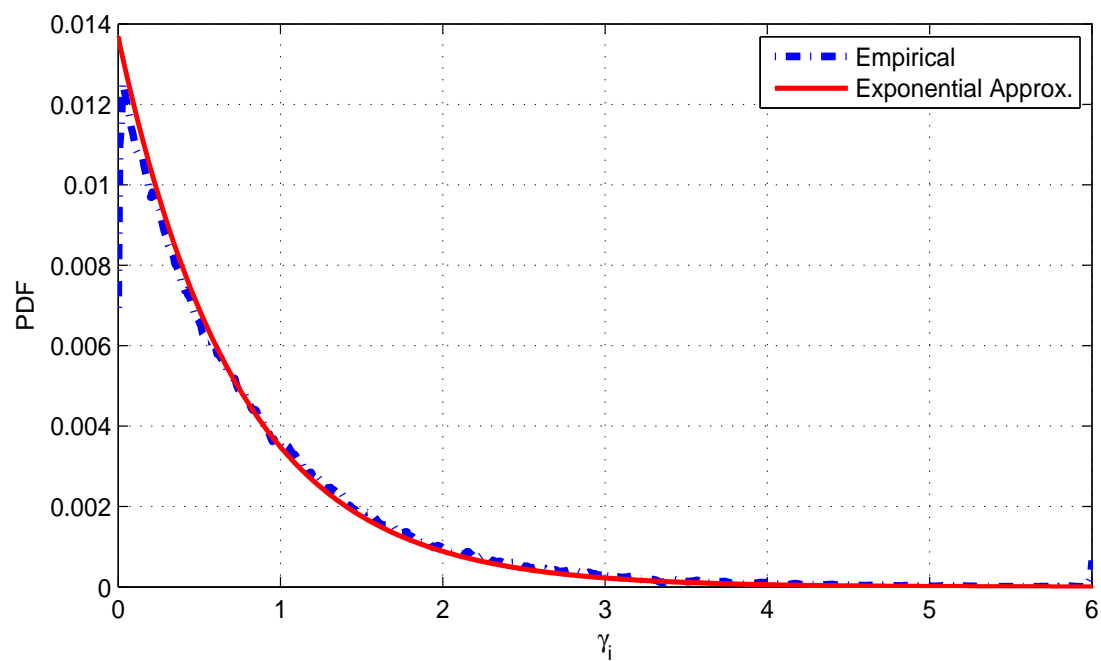
Figure 3.4: The empirical PDF of γ_i compared to the proposed exponential approximation with mean μ_γ.

Simulation results showing the accuracy of the approximated statistics of γ^* are presented in Fig 3.5, 3.6.
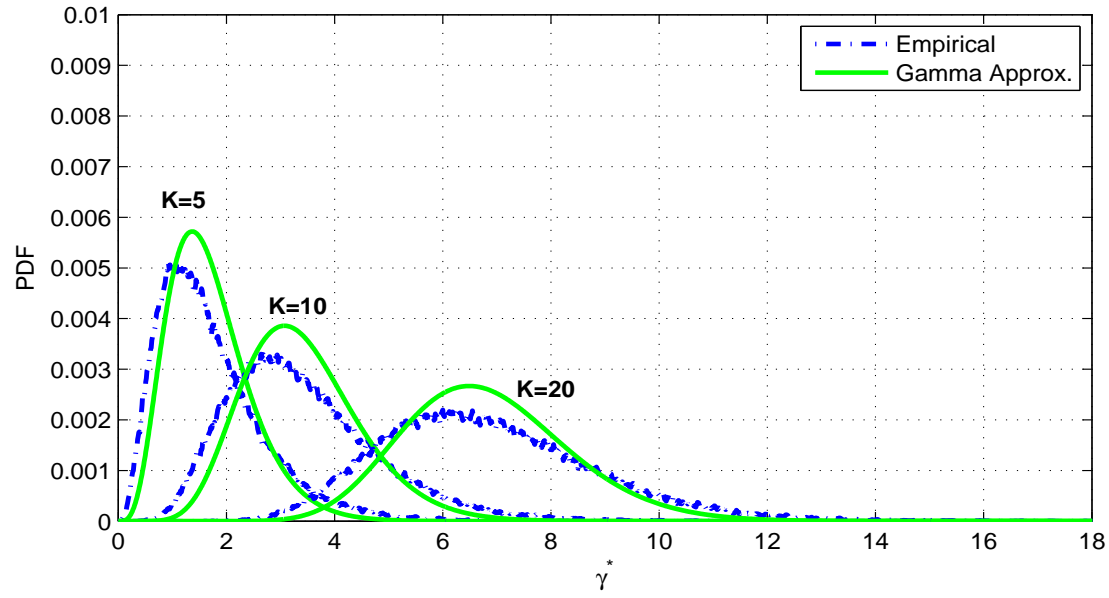
Figure 3.5: The empirical PDF of the received SNR γ^*, compared with the proposed Gamma approximation.
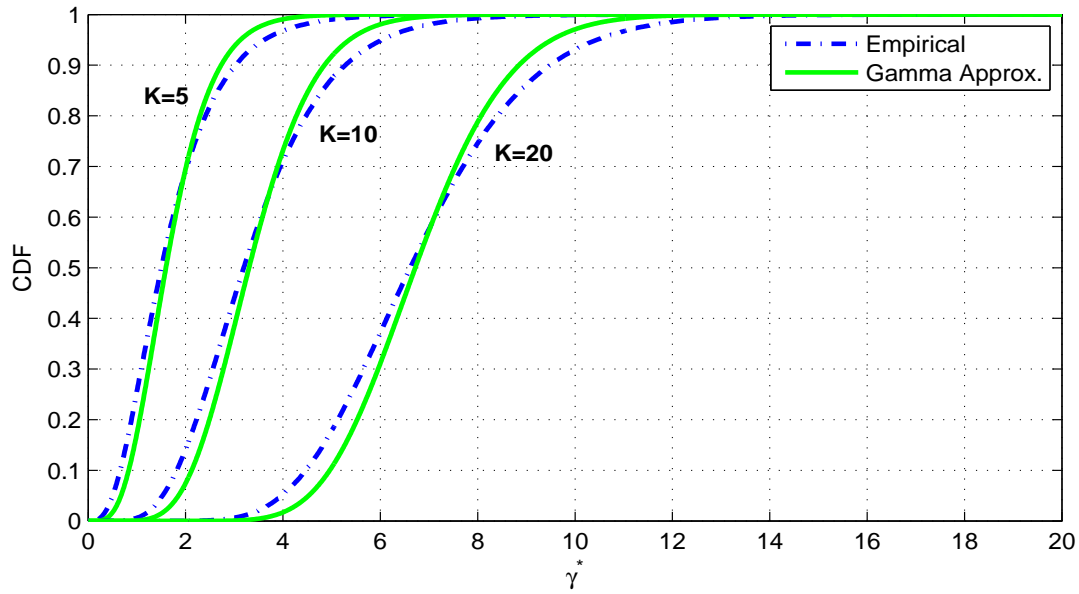
Figure 3.6: The empirical CDF of the received SNR γ^*, compared with the proposed Gamma approximation.

3.6 Performance Analysis

3.6.1 Outage Probability Analysis

In this section, we study the outage probability of the secondary network based on the optimal power allocation discussed in Section 3.3. Using this power allocation, the transmission rate of the secondary network in (3.5) is given by $R^* = \frac{1}{2}\log_2(1 + \gamma^*)$. An outage event occurs when R^* drops below a predefined target rate R_{th}. Let P_{out} be the outage probability, then,

$$
\begin{aligned}
P_{out} &= Pr(R^* \leq R_{th}), \\
&= Pr(\gamma^* \leq \gamma_{th}).
\end{aligned}
\tag{3.37}
$$

where $\gamma_{th} = 2^{2R_{th}} - 1$. Therefore, the outage probability can be simply obtained using the approximate CDF of γ^* in (3.35) as,

$$
P_{out}(\gamma_{th}) = \frac{1}{\Gamma(K)}\gamma\left(K, \frac{\gamma_{th}}{\mu_\gamma}\right).
\tag{3.38}
$$

where $\gamma(a, x) = \int_0^x t^{a-1}e^{-t}dt$ is the lower incomplete Gamma function [111].

3.6.2 Bit Error Rate

Here we analyze the Bit Error Rate (BER) of the secondary network. The average BER denoted by P_e is calculated using

$$
P_e = \int_0^\infty P(e|x)f_{\gamma^*}(x)dx.
\tag{3.39}
$$

where $P(e|x)$ is a modulation-specific BER. Without loss of generality, considering binary phase shift keying (BPSK) modulation, $P(e|x) = \mathcal{Q}(\sqrt{2x})$, where $\mathcal{Q}(.)$ is the Gaussian Q-function. Hence, the average BER is given by,

$$
\begin{aligned}
P_e &= \frac{1}{2\sqrt{\pi}}\int_0^\infty \frac{e^{-x}}{\sqrt{x}}F_{\gamma^*}(x)\ dx \\
&= \frac{1}{2\Gamma(K)\sqrt{\pi}}\int_0^\infty x^{\frac{-1}{2}}e^{-x}\gamma\left(K, \frac{x}{\mu_\gamma}\right)dx.
\end{aligned}
\tag{3.40}
$$

A closed-form expression for the average BER can be obtained by solving the integration in (3.40) using [111, eq. 6.455.2] to yield,

$$P_e = \frac{\Gamma(K + \frac{1}{2})}{2K \ \Gamma(K)\sqrt{\pi}\mu_\gamma^K(1 + \frac{1}{\mu_\gamma})^{K+\frac{1}{2}}} \times {}_2F_1\left(1, K + \frac{1}{2}; K + 1; \frac{1}{\mu_\gamma + 1}\right). \qquad (3.41)$$

3.7 Numerical Results and Simulation

In this section, we present the performance results of the secondary network through the derived expressions and simulation. In Fig.3.7, we simulate the outage probability P_{out} of the cognitive network versus γ_s, the secondary source power P_S measured relative to the noise power at the cognitive nodes σ^2 for a target SNR $\gamma_{th} = 2$. The interference temperature I_{max} is set to 13 dB and the noise power is normalized to 1. The figure illustrates that as the number of relays increases, the outage performance is enhanced. The secondary source can use almost 6 dB less power, and still have the same outage of 10^{-2} if only two more relays are available ($K = 3$ and $K = 5$). This is justified by the diversity gain of using more relays. However, doubling the size of the relaying network from $K = 10$ to $K = 20$ does not provide as much gain as increasing the size from $K = 5$ to $K = 10$. For different values γ_{th} with $K = 5$ relays, Fig. 3.8 plots the simulation results of the outage probability compared to the analytical results.

The average BER of the cognitive network is presented in Fig. 3.9. We considered a strict case where the interference temperature I_{max} is set to a low value as 0 dB. It is shown that, the number of relays greatly affects the BER.The more relays are cooperating, the better the BER performance gets.
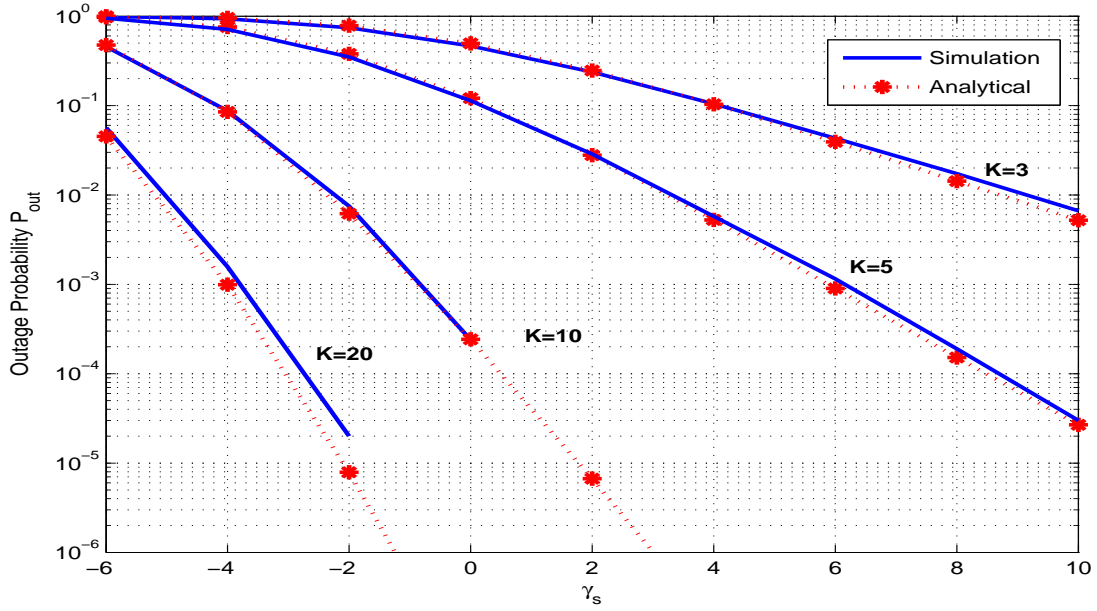
Figure 3.7: The outage probability P_{out} of the cognitive network versus $\gamma_s(dB)$ for different values of K. The target SNR $\gamma_{th} = 2dB$. The interference temperature I_{max} is set at 13 dB.
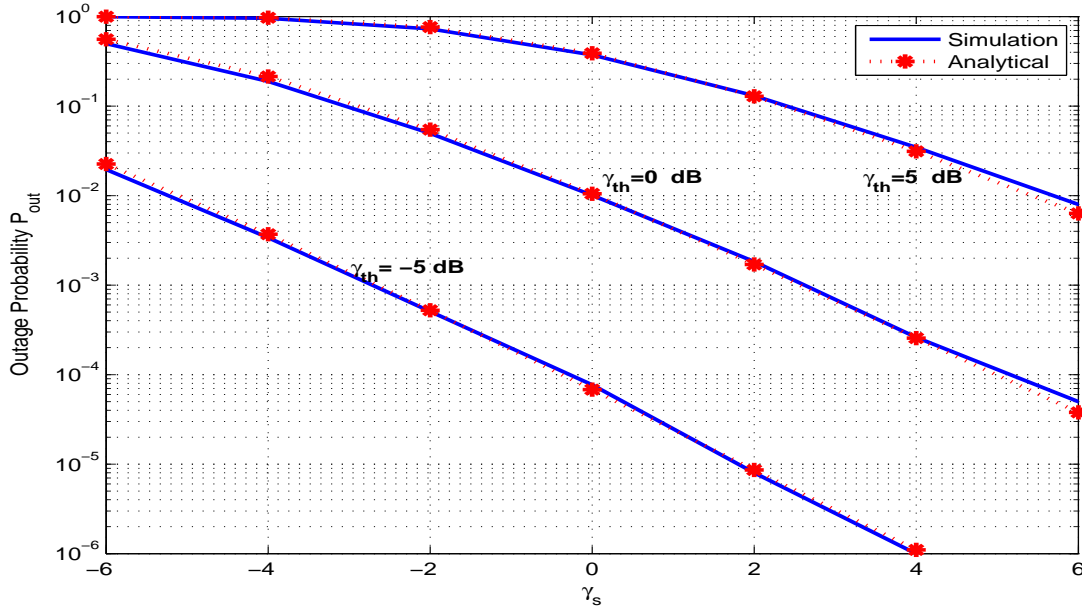
Figure 3.8: The outage probability P_{out} of the cognitive network versus $\gamma_s(dB)$ for different values of γ_{th}. The number of relays $K = 5$. The interference temperature I_{max} is set at 13 dB.
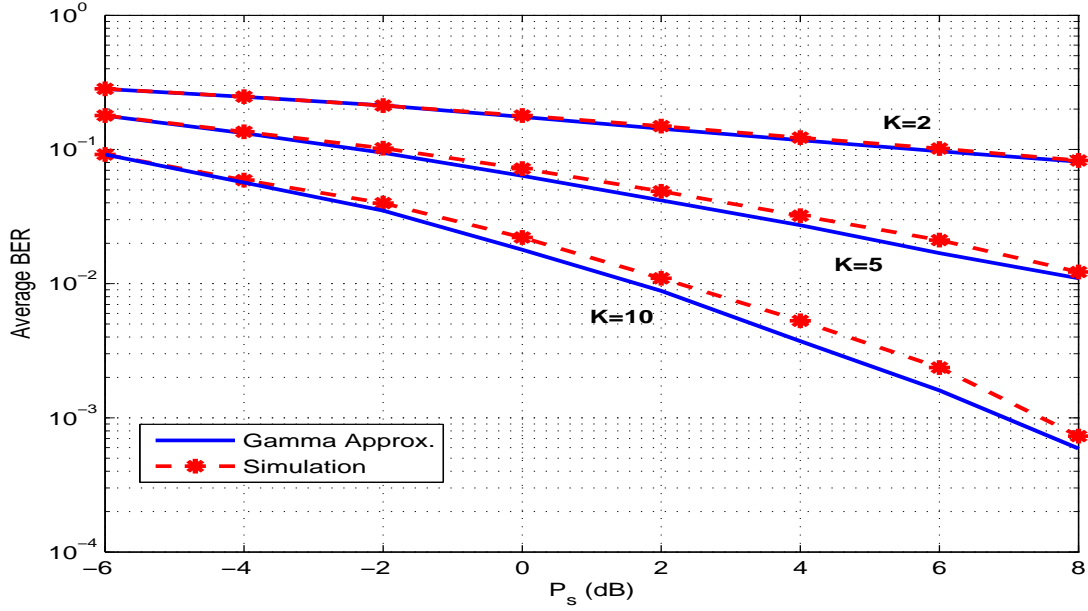
Figure 3.9: The Average BER P_e of the cognitive network versus $\gamma_s(dB)$ for different values for different values of K. The interference temperature I_{max} is set at 0 dB.

3.8 Power Allocation for Nodes with Individual Power Constraints

The problem of power allocation at the cognitive nodes is addressed again in this section while each secondary node has a limit on its maximum transmission power. The objective is to find the set of transmission powers $\{P_S, P_{R_1}, P_{R_2}, ...P_{R_K}\}$ that maximizes the SNR and does not violate the interference constraint at the primary receiver. The power allocation problem is, thus, formulated as follows.

Problem P2

$$\max_{\{P_S, P_{R_1}, P_{R_2}, ...P_{R_K}\}} \gamma,$$

81

$$\text{subject to} \quad P_S \, |g_{S,P}|^2 \leq I_{max}, \tag{3.42}$$

$$0 \leq P_S \leq P_{S_{max}}, \tag{3.43}$$

$$\sum_{i=1}^{K} P_{R_i} \, |f_{R_i,P}|^2 \leq I_{max}, \tag{3.44}$$

$$0 \leq P_{R_i} \leq P_{max}, \forall i = \{1, 2, ...K\}, \tag{3.45}$$

where $P_{S_{max}}$ and P_{max} are the transmission power limits for the secondary source and relays, respectively. Such a limit may be forced by some practical considerations such as, the avoidance of the power amplifiers saturation and having a limited power supply (i.e battery operated nodes). Again, (3.42) and (3.44) correspond to the interference constraints during the first and the second time slots, respectively.

The secondary source determines its transmission power P_S independently from the transmission powers of the relays. Hence, the optimal value of P_S, denoted by P_S^*, should be set to the maximum allowable value. Then, from the constraint in (3.42), we get

$$P_S^* = \min\{P_{S_{max}}, \frac{I_{max}}{|g_{S,P}|^2}\}. \tag{3.46}$$

The set of relays' powers $\mathbf{P}_R = \{P_{R_1}, P_{R_2}, ...P_{R_K}\}$ is obtained through the following optimization problem,

Problem P2.1

$$\mathbf{P}_R^* = \arg\max_{\mathbf{P}_R} \left\{ \frac{\left(\sum_{i=1}^{K} \sqrt{P_S^* \, \alpha_i \theta_i} \sqrt{P_{R_i}} \right)^2}{\sum_{i=1}^{K} \left(\sqrt{\theta_i \, \sigma_{R_i}^2} \sqrt{P_{R_i}} \right)^2 + \sigma_D^2} \right\},$$

$$\text{subject to} \quad \sum_{i=1}^{K} \zeta_i \, P_{R_i} \leq I_{max}, \tag{3.47}$$

$$0 \leq P_{R_i} \leq P_{max}, \forall i = \{1, 2, ...K\}, \tag{3.48}$$

where $\alpha_i = |h_{S,R_i}|^2$, $\beta_i = |h_{R_i,D}|^2$, $\theta_i = \frac{\beta_i}{\alpha_i P_S^* + \sigma_{R_i}^2}$ and $\zeta_i = |f_{R_i,P}|^2$. The problem **P2.1** is a non-convex problem and finding a global optimal solution in a closed-form is not feasible.

3.8.1 Proposed Power Allocation Algorithm

In this section, we propose an algorithm to solve the optimization problem **P2.1**. Following similar steps as in Section 3.3, let $\mathbf{x} = [x_1, x_2, .., x_K]^T$ be the new optimization vector, where $x_i = \sqrt{P_{R_i}}$ and $[\cdot]^T$ denotes transpose operation. The optimization problem in (3.47) can be reformulated as

Problem P2.2

$$\mathbf{x}_{opt} = \arg\max_{\mathbf{x}} \left\{ \frac{\mathbf{x}^T \mathbf{A} \mathbf{x}}{\mathbf{x}^T \mathbf{B} \mathbf{x} + \sigma_D^2} \right\}, \tag{3.49}$$

$$\text{subject to} \quad \mathbf{x}^T \mathbf{C} \mathbf{x} \leq I_{max}, \tag{3.50}$$

$$\varrho_i\{\mathbf{x}\mathbf{x}^T\} \leq P_{max}, \forall i = \{1, 2, ...K\}, \tag{3.51}$$

where $\mathbf{A}$ is a square matrix of the size $K \times K$ with elements $a_{i,j} = P_S^* \sqrt{\alpha_i \theta_i \alpha_j \theta_j}$, for $i, j \in \{1, 2, ...K\}$. $\mathbf{B}$ and $\mathbf{C}$ are diagonal matrices of size $K \times K$ with the diagonal elements $b_{i,i} = \theta_i \sigma_{R_i}^2$ and $c_{i,i} = \zeta_i$, respectively. $\varrho_i\{.\}$ is the i_{th} diagonal element of the inclosed matrix. We propose solving **P2.2** through the following steps. The first step is to find the solution for the problem while relaxing the constraint in (3.51). Next, we find an algorithm to force the satisfaction of (3.51) on the obtained solution.

3.8.1.1 First step

The power allocation maximizing **P2.2** while (3.51) is relaxed, is identical to the solution of **P1** in Section 3.3, which is given by

$$\mathbf{P}_R^* = \mu^2 diag\left\{ \left(\mathbf{D}^{-\frac{1}{2}}\right)^T \mathbf{v} \; \mathbf{v}^T \mathbf{D}^{-\frac{1}{2}} \right\}. \tag{3.52}$$

Then, we satisfy the constraint in (3.51) using the following two steps.

3.8.1.2 Second step

Define the following two complementary sets:

$$\Omega_{max} := \{i : P_{R_i} \geq P_{max}\}, \tag{3.53}$$

$$\Omega := \{i : P_{R_i} < P_{max}\}. \tag{3.54}$$

Ω_{max} denotes the set of relays with power allocation exceeds P_{max}. If the set Ω_{max} is empty, then the power allocation in (3.52) is the optimal solution. Otherwise, we set $P_{R_i} = P_{max}$ for all $i \in \Omega_{max}$.

3.8.1.3 Third step

The powers of other relays (i.e. $i \in \Omega$) are redesigned to satisfy the interference constraint by solving problem in (3.55)

$$\tilde{\mathbf{P}}_R = \arg\max_{\tilde{\mathbf{P}}_R} \left\{ \frac{\left(\sum_{i \in \Omega_{max}} \sqrt{P_S^* \, \alpha_i \theta_i} \sqrt{P_{max}} + \sum_{j \in \Omega} \sqrt{P_S^* \, \alpha_j \theta_j} \sqrt{P_{R_j}} \right)^2}{\sum_{i \in \Omega_{max}} \left(\sqrt{\theta_i \, \sigma_{R_i}^2} \sqrt{P_{max}} \right)^2 + \sum_{j \in \Omega} \left(\sqrt{\theta_j \, \sigma_{R_j}^2} \sqrt{P_{R_j}} \right)^2 + \sigma_D^2} \right\}, \quad (3.55)$$

$$\text{subject to} \quad \sum_{i \in \Omega} \zeta_i \, P_{R_i} \leq \delta I, \quad (3.56)$$

where δI is the residual of the interference limit after the relays in Ω_{max} use P_{max}, and equals $I_{max} - \sum_{i \in \Omega_{max}} \zeta_i \, P_{max}$.

Let $\mathbf{z} = [z_i]^T$, and $i \in \Omega$, be the new optimization problem for relays' powers in Ω. The problem can be casted as a QCQP optimization problem as follows:

$$\mathbf{z}_{opt} = \arg\max_{\mathbf{z}} \left\{ \frac{\mathbf{z}^T \tilde{\mathbf{A}} \mathbf{z} + 2 \, \mathbf{b}^T \mathbf{z} + k_1^2}{\mathbf{z}^T \tilde{\mathbf{B}} \mathbf{z} + k_2} \right\}, \quad (3.57)$$

$$\text{subject to} \quad \mathbf{z}^T \tilde{\mathbf{C}} \mathbf{z} \leq \delta I, \quad (3.58)$$

where $\tilde{\mathbf{A}}$ is a square matrix with elements $\tilde{a}_{i,j} = P_S^* \sqrt{\alpha_i \theta_i \alpha_j \theta_j}$ with $i, j \in \Omega$, $\mathbf{b}$ is a column vector with entries $k_1 \sqrt{P_S^* \, \alpha_i \theta_i}$, $\tilde{\mathbf{B}}$ and $\tilde{\mathbf{C}}$ are diagonal matrices with elements $\tilde{b}_{i,i} = \theta_i \, \sigma_{R_i}^2$ and $\tilde{c}_{i,i} = \zeta_i$, respectively. k_1 and k_2 are constants given by

$$k_1 = \sum_{i \in \Omega_{max}} \sqrt{P_S^* \, \alpha_i \theta_i}, \sqrt{P_{max}},$$

$$k_2 = \sigma_D^2 + \sum_{i \in \Omega_{max}} \left(\sqrt{\theta_i \, \sigma_{R_i}^2} \sqrt{P_{max}} \right)^2.$$

84

Using the interference constraint (3.58), the objective function in (3.57) can be transformed to:

$$\left\{ \frac{\mathbf{z}^T \tilde{\mathbf{D}} \mathbf{z} + 2 \, \mathbf{b}^T \mathbf{z}}{\mathbf{z}^T \tilde{\mathbf{B}} \mathbf{z} + k_2} \right\}, \tag{3.59}$$

where $\tilde{\mathbf{D}} = \tilde{\mathbf{A}} + \frac{k_1^2}{\delta I} \tilde{\mathbf{C}}$. We can further simplify the problem by transforming the non-homogenous form in (3.59) into a homogenous form by using a new optimization vector $\mathbf{y} = [\mathbf{z}^T 1]^T$, which is a vector consisting of the concatenation of the original optimization $\mathbf{z}$ with one element of a value one. The new homogenous form of the problem is:

$$\mathbf{y}_{opt} = \arg\max_{\mathbf{y}} \frac{\mathbf{y}^T \tilde{\mathbf{E}} \mathbf{y}}{\mathbf{y}^T \tilde{\mathbf{F}} \mathbf{y}} \tag{3.60}$$

where $\tilde{\mathbf{E}}$ and $\tilde{\mathbf{F}}$ are given by

$$\tilde{\mathbf{E}} = \begin{bmatrix} \tilde{\mathbf{D}} & \mathbf{b} \\ \mathbf{b}^T & 0 \end{bmatrix}, \quad \tilde{\mathbf{F}} = \begin{bmatrix} \tilde{\mathbf{B}} & \mathbf{0} \\ \mathbf{0}^T & k_2 \end{bmatrix}. \tag{3.61}$$

Now we can obtain the Rayleigh quotient using the decomposition of $\tilde{\mathbf{F}} = \tilde{\mathbf{F}}^{\frac{1}{2}} (\tilde{\mathbf{F}}^{\frac{1}{2}})^T$ and optimizing over $\mathbf{w} \triangleq (\mathbf{F}^{\frac{1}{2}})^T \mathbf{y}$. The solution is the eigenvector corresponding to the maximum eigenvalue of the matrix $\mathbf{G} = \tilde{\mathbf{F}}^{-\frac{1}{2}} \tilde{\mathbf{E}} (\tilde{\mathbf{F}}^{-\frac{1}{2}})^T$. This solution will be scaled to satisfy the interference constraint. One final step is to normalize the solution by the value of its last element. This step is needed to satisfy the use of $\mathbf{y} = [\mathbf{z}^T 1]^T$. Now, excluding the last element will result in the optimal power allocation of the relays which were in the set Ω. If the new power allocation will cause some of the relays to use power greater than P_{max}, the second and the third steps are to be repeated. After finishing all iterations of the algorithm, the power allocation achieving the maximum SNR is selected.

3.8.2 Numerical Results

In this section we present the performance of the proposed power allocation algorithm. For comparison proposes we use the "Equal Power Allocation" scheme as a benchmark. Fig. 3.10 shows the average secondary throughput of 10^6 transmissions for different interference temperature I_{max} values for a 5-relay network. The noise variance at all nodes is set to 1 (i.e. $\sigma_{R_i}^2 = \sigma_D^2 = 1$). The secondary source has a maximum transmission power limit $P_{s_{max}}$
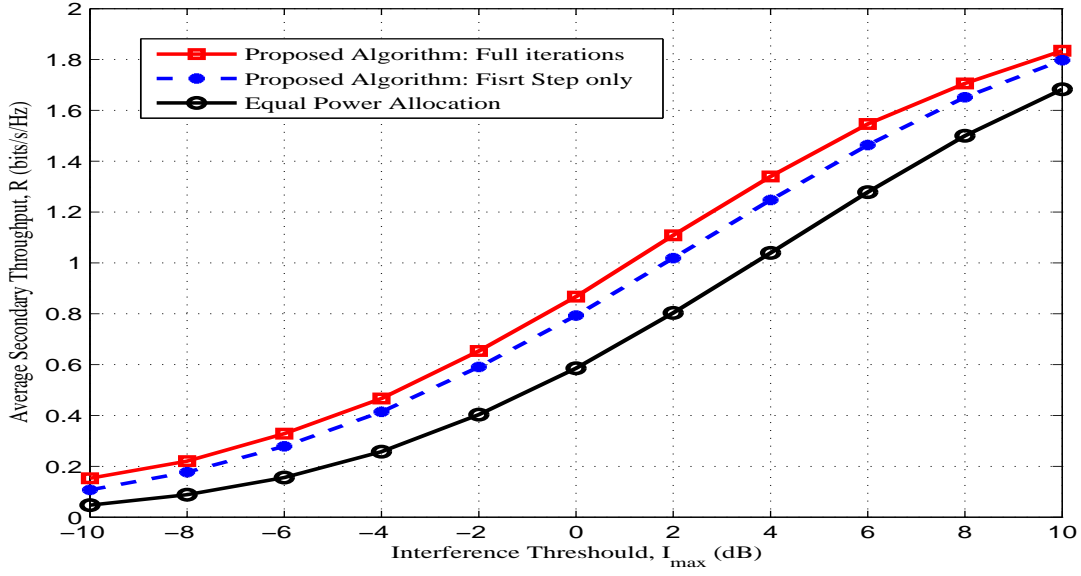
Figure 3.10: The average secondary throughput for different values of interference temperature I_{max}. The system has $K = 5$ relays.

of 7 dB, while all the relays have $P_{max} = 5$ dB. The proposed power allocation maintains a constant performance gap over equal power allocation. Also a 10% increased transmission rate over the one resulting if the algorithm stops after the first iteration as in [62].

In Fig. 3.11, the effect of the number of relays on the average secondary throughput is shown. The proposed power allocation gains almost 20% increased rate over equal power allocation as K increases, and gains a higher growth rate with K. Having more than one iteration in the proposed algorithm improves the achieved throughput for small network sizes. However, as the network size increases, more degrees of freedom is added to the algorithm in the first iteration, leaving little improvement in further iterations.
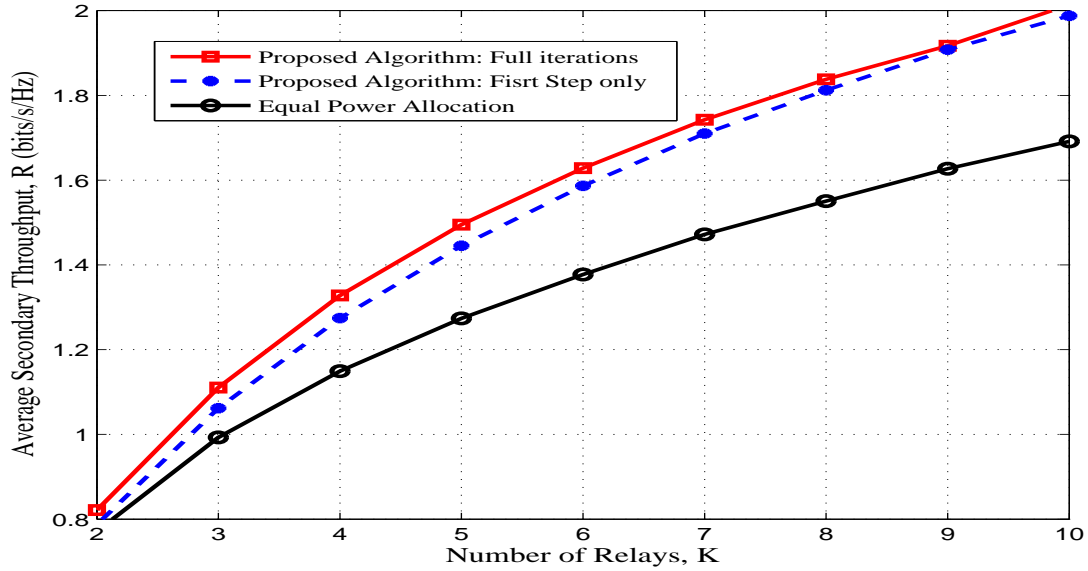
Figure 3.11: The average secondary throughput for different number of secondary relays K. The interference temperature I_{max} is set to 10 dB.

The effect of the maximum transmission power limit of the secondary source, $P_{S_{max}}$, is presented in Fig 3.12. Two different scenarios are considered where the network size changes from $K = 2$ to $K = 4$ relays and each relay has $P_{max} = 0$ dB. For a small network (i.e. K=2), the equal power allocation has a comparable performance to the proposed scheme. However, for a more dense network, a higher throughput is achieved as more transmission power is allowed. Clearly, our proposed power allocation algorithm outperforms the equal power allocation.

On the other hand, in Fig. 3.13, we study the secondary rate for different values of P_{max}, the maximum allowable transmission of the secondary relays with a network size of 5 relays. In this case, we used a source transmission power $P_{S_{max}} = 10$dB and interference temperature $I_{max} = 3$ and 6 dB. It is shown that, for extremely small values of P_{max}, one iteration of the algorithm is not enough to obtain a throughput higher than the equal power allocation. However, as P_{max} increases, significant throughput is gained while the equal power allocation suffers a performance saturation.
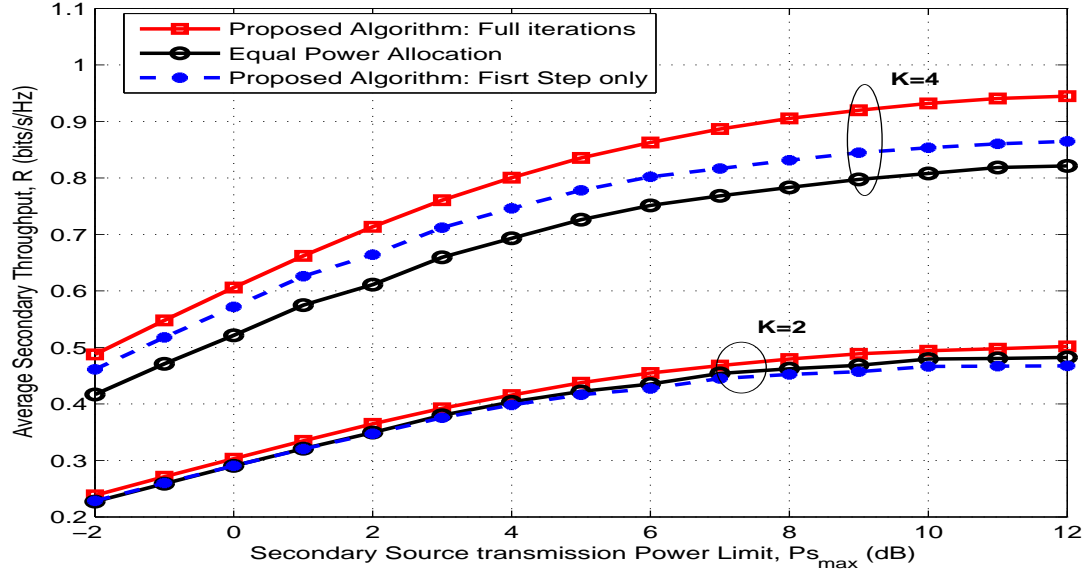
Figure 3.12: The average secondary throughput for different values of the maximum limit on the secondary source transmission power $P_{S_{max}}$ for $K = 2$ and 4. The interference temperature $I_{max} = 7$ dB.
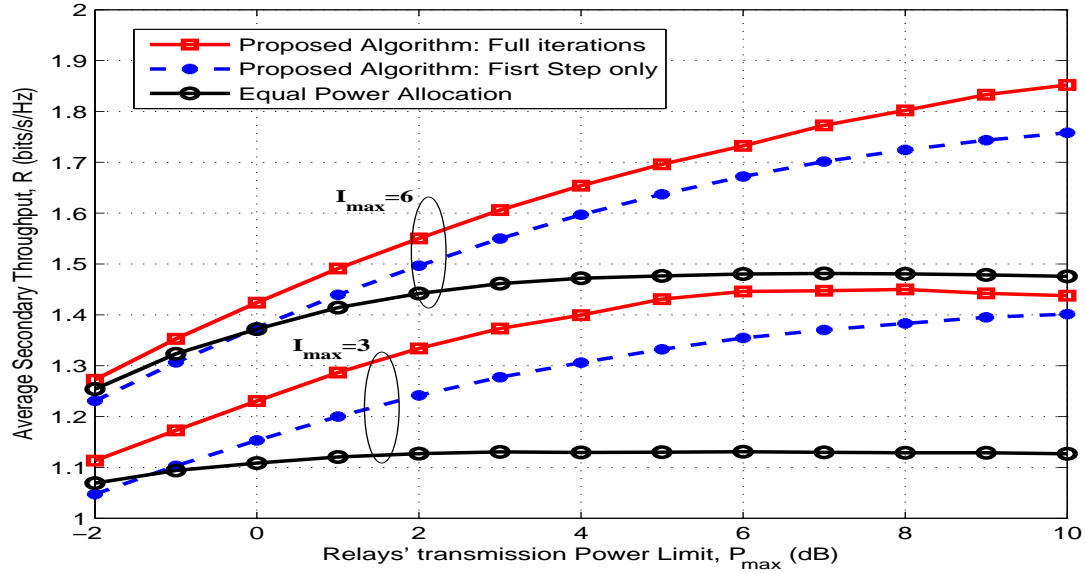
Figure 3.13: The average secondary throughput for different values of the maximum limit on the relays' transmission power P_{max} for $K = 5$ and interference temperature values of $I_{max} = 3$ and 6 dB.

3.9 Energy Efficient Power Allocation

The previously studied power allocation techniques target maximum spectral efficiency (by maximizing the achievable throughput, or equivalently, the received SNR), but they never consider how efficient the power is used to achieve such maximum. A natural efficiency measure for the used energy is defined as the achievable information rate normalized to the used energy (or power). However, such measure traps the system into the low SNR region [113]. A recently proposed measure, namely power-normalized SNR (PN-SNR), defined as the ratio between the received SNR and the transmitted power, is promising as it does not force the system into a low SNR value [114].

Here, we study the power allocation at the cognitive relays in an underlay cognitive network targeting maximum energy efficiency (adopting the measure in [114]). The system under consideration consists of multiple AF relays using the same frequency band simultaneously. Moreover, each relay has a maximum allowable transmission power to prolong the lifetime of the relaying nodes.

3.9.1 Problem Formulation

We adopt the normalized end-to-end SNR at the secondary receiver as a measure of the effectiveness of the power allocation at the secondary relays. As indicated in (3.4), the end-to-end SNR at D, γ, is given by,

$$\gamma = P_S \times \frac{\left(\sum_{i=1}^{K} \frac{|h_{R_i,D}| \, |h_{S,R_i}| \, \sqrt{P_{R_i}}}{\sqrt{P_S \, |h_{S,R_i}|^2 + \sigma^2}} \right)^2}{\sum_{i=1}^{K} \left(\frac{\sqrt{P_{R_i}} \, |h_{R_i,D}| \, \sigma}{\sqrt{P_S \, |h_{S,R_i}|^2 + \sigma^2}} \right)^2 + \sigma^2}.$$

The total power budget of the secondary system during the two time slots, denoted by P_T, is given by,

$$P_T = P_S + \sum_{i=1}^{K} \frac{P_{R_i}}{P_S \, |h_{S,R_i}|^2 + \sigma^2} \tag{3.62}$$

The objective is, thus, to find the set of relays' transmission coefficients $\mathbf{P}_R = \{P_{R_1}, P_{R_2}, ... P_{R_K}\}$ that maximize the normalized end-to-end SNR of the secondary system (i.e. $\frac{\gamma}{P_T}$) while adhering to the interference constraint of the primary network.

As mentioned before, the secondary source determines its transmission power P_S independently from the transmission powers of the relays. Then, the set of relays' power $\mathbf{P}_R$ is obtained through **Problem P3** as follows:

Problem P3:

$$\mathbf{P}_R^* = \arg\max_{\mathbf{P}_R} \left\{ \frac{P_S \left(\sum_{i=1}^{K} \frac{|h_{R_i,D}| \, |h_{S,R_i}| \, \sqrt{P_{R_i}}}{\sqrt{P_S \, |h_{S,R_i}|^2 + \sigma^2}} \right)^2}{\left(P_S + \sum_{i=1}^{K} \frac{P_{R_i}}{P_S \, |h_{S,R_i}|^2 + \sigma^2}\right) \times \left(\sum_{i=1}^{K} \left(\frac{\sqrt{P_{R_i}} \, |h_{R_i,D}| \, \sigma}{\sqrt{P_S \, |h_{S,R_i}|^2 + \sigma^2}} \right)^2 + \sigma^2 \right)} \right\} \tag{3.63}$$

$$\text{subject to} \qquad \sum_{i=1}^{K} P_{R_i} \, |f_{R_i,P}|^2 \le I_{max}. \tag{3.64}$$

$$0 \le P_{R_i} \le P_{max}, \forall i = \{1, 2, ... K\}, \tag{3.65}$$

The problem can be mapped into a quadratic format by using $\mathbf{x} = [x_1, x_2, .., x_K]^T$ as the new optimization vector, where $x_i = \sqrt{P_{R_i}}$ and $[\cdot]^T$ denotes transpose operation. Also, let $\alpha_i = |h_{S,R_i}|^2$, $\beta_i = |h_{R_i,D}|^2$, $\theta_i = \frac{\beta_i}{\alpha_i P_S + \sigma^2}$ and $\zeta_i = |f_{R_i,P}|^2$. The optimization problem in (3.63), is then, formulated as

$$\mathbf{x}_{opt} = \arg\max_{\mathbf{x}} \left\{ \frac{\mathbf{x}^T \mathbf{A} \mathbf{x}}{\mathbf{x}^T \mathbf{B} \mathbf{x} + \sigma^2} \cdot \frac{1}{\mathbf{x}^T \mathbf{C} \mathbf{x} + P_s} \right\}, \tag{3.66}$$

$$\text{subject to} \quad \mathbf{x}^T \mathbf{D} \mathbf{x} \le I_{max}, \tag{3.67}$$

$$\varrho_i\{\mathbf{x}\mathbf{x}^T\} \le P_{max}, \forall i = \{1, 2, ... K\}, \tag{3.68}$$

where $\mathbf{A}$ is a square matrix of size $K \times K$ and its elements $a_{i,j} = P_S \sqrt{\alpha_i \theta_i \alpha_j \theta_j}$, for $i, j \in \{1, 2, ... K\}$. $\mathbf{B}$, $\mathbf{C}$ and $\mathbf{D}$ are diagonal matrices of size $K \times K$ with the diagonal elements $b_{i,i} = \theta_i \sigma_{R_i}^2$, $c_{i,i} = \theta_i/\beta_i$, $d_{i,i} = \zeta_i$ respectively. $\varrho_i\{.\}$ is the i_{th} diagonal element of the inclosed matrix. It is noted that, the problem in (3.66) is a non-convex problem, since the objective function, as well as the constraints, are non-convex.

If the constraint in (3.67) is satisfied with equality, then due to the individual power constraints in (3.68), the feasibility region of the optimization problem (3.66) is a hyper-dimension cube. However, with such constraints in (3.68), the existence of a globally optimum solution is not guaranteed [113]. Given this, we will find a solution based on relaxing the constraints in (3.68). The solution is found through the following steps.

The constraint (3.67) should be satisfied with equality at the optimum solution [115]. Hence, all the zero order terms in (3.66) can be scaled by the quadratic form $\frac{1}{I_{max}}\mathbf{x}^T\mathbf{D}\mathbf{x}$. Using such substitution, we obtain a homogenous form of the objective function as follows,

$$\frac{\mathbf{x}^T\mathbf{A}\mathbf{x}}{\mathbf{x}^T\mathbf{B}\mathbf{x} + \frac{\sigma^2}{I_{max}}\mathbf{x}^T\mathbf{D}\mathbf{x}} = \frac{\mathbf{x}^T\mathbf{A}\mathbf{x}}{\mathbf{x}^T\mathbf{E}\mathbf{x}},$$

$$\frac{\frac{1}{I_{max}}\mathbf{x}^T\mathbf{D}\mathbf{x}}{\mathbf{x}^T\mathbf{C}\mathbf{x} + \frac{P_s}{I_{max}}\mathbf{x}^T\mathbf{D}\mathbf{x}} = = \frac{\mathbf{x}^T\mathbf{D}\mathbf{x}}{\mathbf{x}^T\mathbf{F}\mathbf{x}},$$

where $\mathbf{E} = \mathbf{B} + \frac{\sigma^2}{I_{max}}\mathbf{D}$, and $\mathbf{F} = I_{max}\mathbf{C} + P_S\mathbf{D}$. Both of the matrices $\mathbf{E}$ and $\mathbf{F}$ are diagonal and positive definite, and hence can be inverted. Substituting the new objective function into (3.66), the optimization problem becomes

$$\mathbf{x}_{opt} = \underset{\mathbf{x}|\mathbf{x}^T\mathbf{D}\mathbf{x}=I_{max}}{\arg\max} \frac{\mathbf{x}^T\mathbf{A}\mathbf{x}}{\mathbf{x}^T\mathbf{E}\mathbf{x}} \cdot \frac{\mathbf{x}^T\mathbf{D}\mathbf{x}}{\mathbf{x}^T\mathbf{F}\mathbf{x}}. \tag{3.69}$$

Problem (3.69) is generally neither convex nor concave, since the objective function is a product of two fractional quadratic functions (which can be written in the form of difference-of-convex functions (DC) programming problems). The available literature for solving DC programming problems is mainly based on the so-called branch-and-bound method [116].

3.9.2 Proposed Solution

Let $f_1(\mathbf{x}) = \frac{\mathbf{x}^T\mathbf{A}\mathbf{x}}{\mathbf{x}^T\mathbf{E}\mathbf{x}}$, and $f_2(\mathbf{x}) = \frac{\mathbf{x}^T\mathbf{D}\mathbf{x}}{\mathbf{x}^T\mathbf{F}\mathbf{x}}$. The functions f_1 and f_2 can be put into the form of Rayleigh quotients as:

$$f_1(\mathbf{y_1}) = \frac{\mathbf{y_1}^T\mathbf{M}\mathbf{y_1}}{\mathbf{y}^T\mathbf{y_1}},$$

$$f_2(\mathbf{y_2}) = \frac{\mathbf{y_2}^T\mathbf{N}\mathbf{y_2}}{\mathbf{y_2}^T\mathbf{y_2}},$$

where $\mathbf{M} = \mathbf{E}^{-\frac{1}{2}}\mathbf{A}\left(\mathbf{E}^{-\frac{1}{2}}\right)^T$, and $\mathbf{N} = \mathbf{F}^{-\frac{1}{2}}\mathbf{D}\left(\mathbf{F}^{-\frac{1}{2}}\right)^T$, with $\mathbf{y_1} \triangleq \left(\mathbf{E}^{\frac{1}{2}}\right)^T\mathbf{x}$ and $\mathbf{y_2} \triangleq \left(\mathbf{F}^{\frac{1}{2}}\right)^T\mathbf{x}$.

As mentioned earlier, the Rayleigh quotient has a maximum value at the dominant eigen-mode of the numerator matrix, and the vector achieving this maximum is the corresponding eigenvector. Let $\mathbf{y_1^*}$ and $\mathbf{y_2^*}$ be the vectors maximizing the functions f_1 and f_2 respectively. We propose choosing the solution of (3.69) to be in the subspace spanned by the two vectors $\mathbf{y_1^*}$ and $\mathbf{y_2^*}$. Then the solution can be represented as a linear combination as,

$$\mathbf{x} = \mathbf{y_1^*} + \rho \; \mathbf{y_2^*}. \tag{3.70}$$

Substituting (3.70) into (3.69), will result in the new scalar-valued optimization problem over a single real variable ρ. The optimum ρ is obtained by a 1-D search to maximize the objective function (3.69). Simulation results provided in the next section show that the proposed solution can achieve at least a local optimum, with an acceptable overall performance.

3.10   Numerical Results

In this section, we present the performance of the proposed energy-efficient power allocation algorithm, and compare it to "Equal Power Allocation". It is to be noted that in the equal power allocation all relays use the same transmission power $P_R = \min\{P_{max}, I_{max}/\sum_{i=1}^{K}|f_{R_i,P}|^2\}$. The noise variance at all nodes, σ^2, is set to 1.

In Fig. 3.14, we show the energy efficiency of three power allocation schemes: the proposed algorithm maximizing the energy efficiency, the power allocation in [115] which maximizes the SNR, and the equal power allocation. The simulation results are obtained using 10^6 transmissions. It is shown that, for a 2-relay network, the energy efficiency is almost the same for the three power allocation schemes. However, for larger networks, the gain starts to increase. For small to moderate secondary source transmission power P_S, the proposed power allocation offers higher efficiency compared to the SNR-maximizing allocation. The performance gap increases as the network size increases which is justified by the increased degrees of freedom in the system. However, for high secondary source power, both schemes show almost the same performance, and the efficiency starts to decrease. This is due to the dominance of P_S in the denominator of (3.62) for high secondary source powers.

The corresponding outage probability of the secondary system is given in Fig. 3.15, for interference threshold set to 10 dB, and the individual relays' power P_{max} is set to 0 dB. The SNR threshold is -3 dB. The results in Fig. 3.15 suggest that for small-size networks, the energy efficient power allocation has almost no effect on the outage probability. As the network size increases a slight performance loss is presented by the energy efficient algorithm, compared to the SNR-maximizing allocation. For example, for an 8-relay network, only 0.1 dB loss occurs in the P_S at 10^{-3} probability of outage. The effect of the interference threshold I_{max} on the energy efficiency and the corresponding outage probability is shown in Figs. 3.16,3.17, respectively. The results are obtained at the secondary source transmission power $P_S = 3$ dB, and the individual relays' power P_{max} is also set to 3 dB. It is shown that for small interference threshold values, the proposed algorithm and the SNR-maximizing algorithm have the same efficiency as satisfying I_{max} is the limiting constraint in both problems. However, if this constraint is relaxed by increasing I_{max}, the proposed algo-
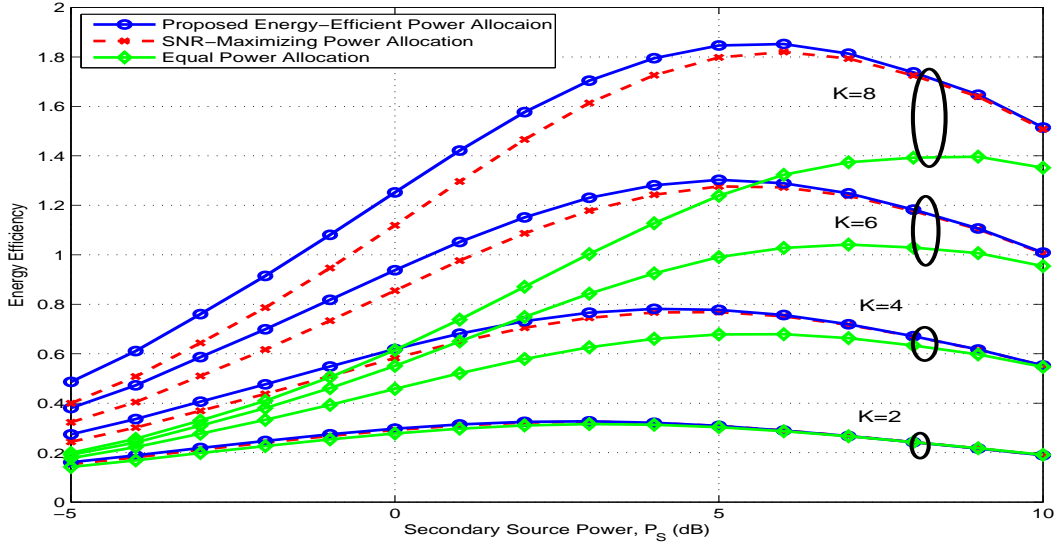
Figure 3.14: The energy efficiency of the secondary network vs the Secondary source transmission power P_S for different network size (K). The interference threshold is set to 10 dB and the individual relays' Power P_{max} is set to 0 dB.
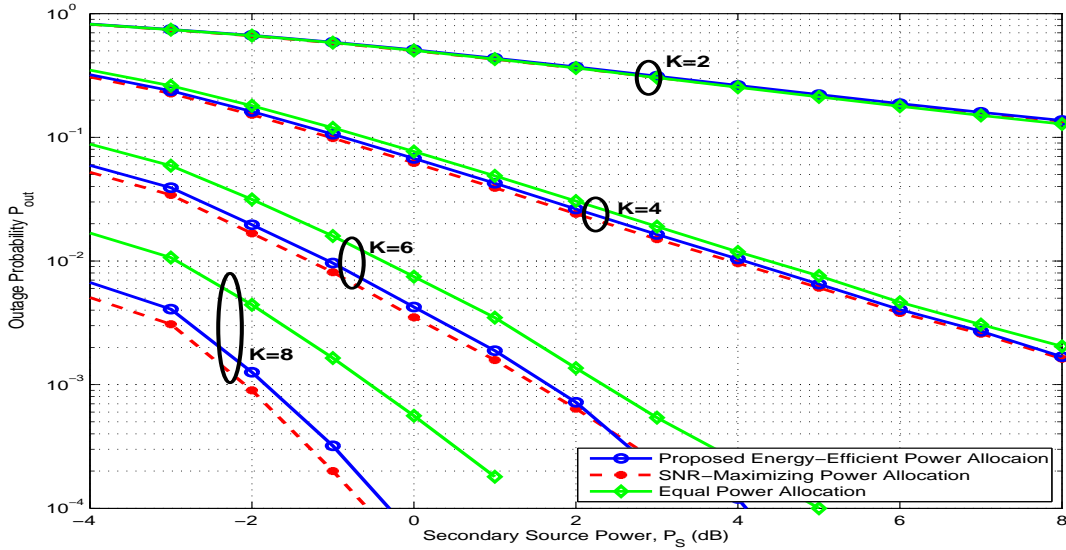
Figure 3.15: The outage probability of the secondary system P_{out} vs the secondary source transmission power P_S for different network size (K).The interference threshold is set to 10 dB and the individual relays' Power P_{max} is set to 0 dB. The SNR threshold is -3 dB.

rithm achieves higher efficiency. As I_{max} increases, more tolerance is given in the secondary network, which allows more power to be used, and hence, the energy efficiency decreases due to the consumption of more power. Fig.3.17 shows the corresponding outage probability. Almost no performance degradation between the two power allocation schemes, and both schemes outperform the equal power allocation.

Next, we show the effect of the individual relay power constraint, P_{max}, on the energy efficiency in Fig. 3.18. The secondary source uses a relatively low transmission power of $P_S = 0$ dB and the interference constraint I_{max} is set at 10dB. It is shown that, the energy efficiency is lower for small values of P_{max}. This results from the constraint in (3.64) being the dominant constraint, and it is satisfied at the upper limit for all relays (i.e. $P_{R_i} = P_{max} \forall i$). As P_{max} increases, more freedom in the power allocation is obtained, which increases the SNR, and consequently increases the energy efficiency. However, for a fixed source power P_S, the energy efficiency will eventually saturate at a certain level. The larger the network size K, the higher is the energy efficiency saturation level. Fig. 3.19 shows the outage probability of the system (for the same setup of Fig. 3.18) at SNR threshold equals -3 dB. The outage probability of the three power allocation schemes is the same for small values of P_{max}. Increasing P_{max} results in almost no performance degradation between the proposed power allocation scheme and the SNR-maximizing power allocation, and both schemes outperform the equal power allocation.
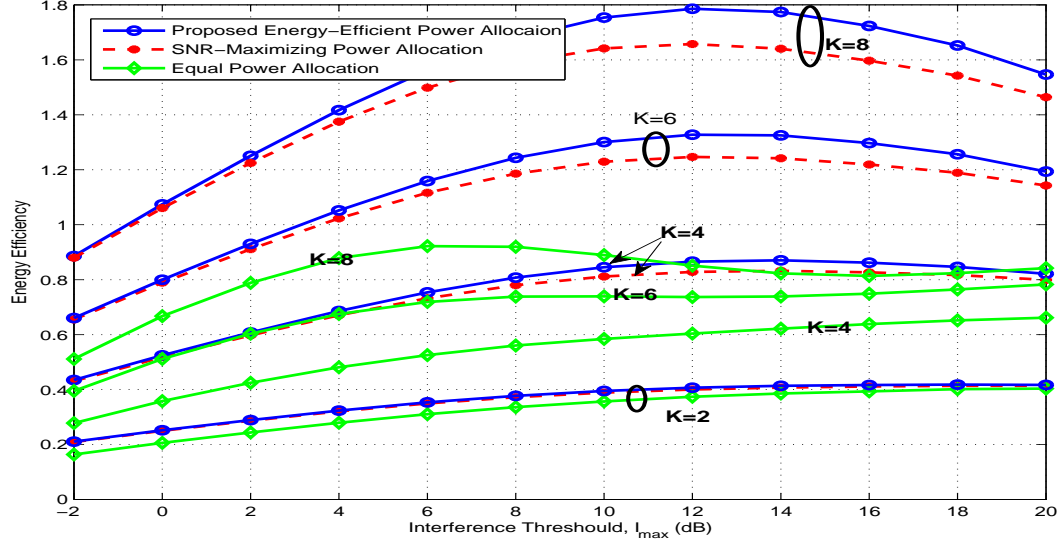
Figure 3.16: The energy efficiency of the secondary network vs the interference threshold I_{max} for different network size (K). The secondary source transmission power P_S is set to 3 dB and the individual relays' Power P_{max} is set to 3 dB.
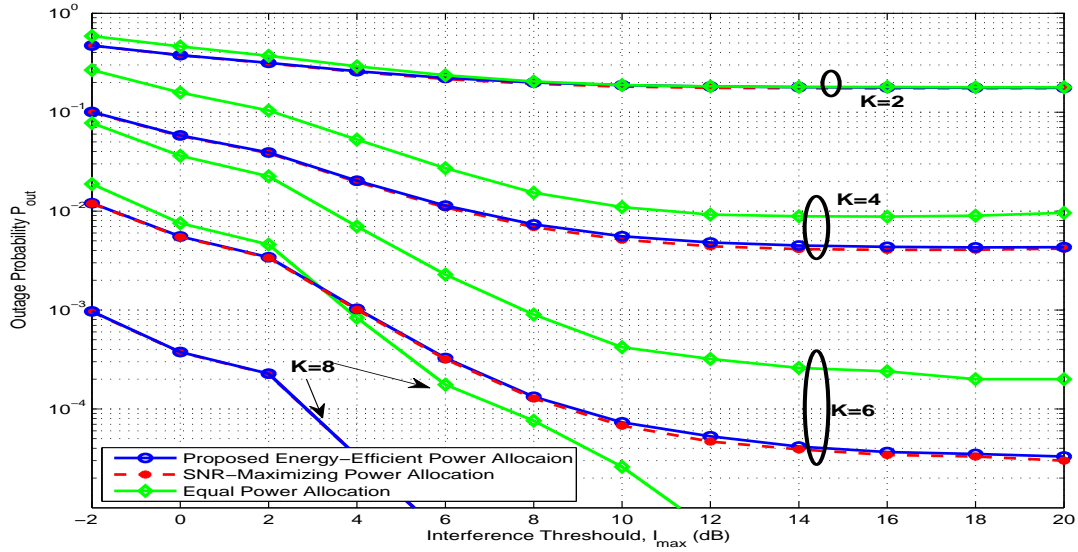
Figure 3.17: The outage probability of the secondary system P_{out} vs the interference threshold I_{max} for different network size (K). The secondary source transmission power P_S is set to 3 dB and the individual relays' Power P_{max} is set to 3 dB. The SNR threshold is -3 dB.
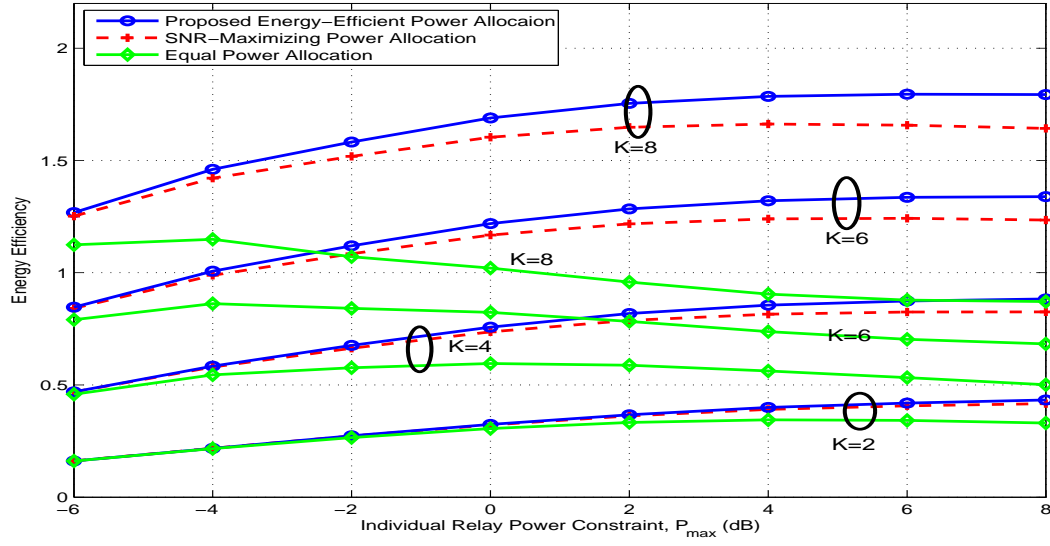
Figure 3.18: The energy efficiency of the secondary network vs the individual relay power constraint P_{max} for different network size (K). The secondary source transmission power P_S is set to 0 dB. The interference threshold I_{max} is set to 10 dB.
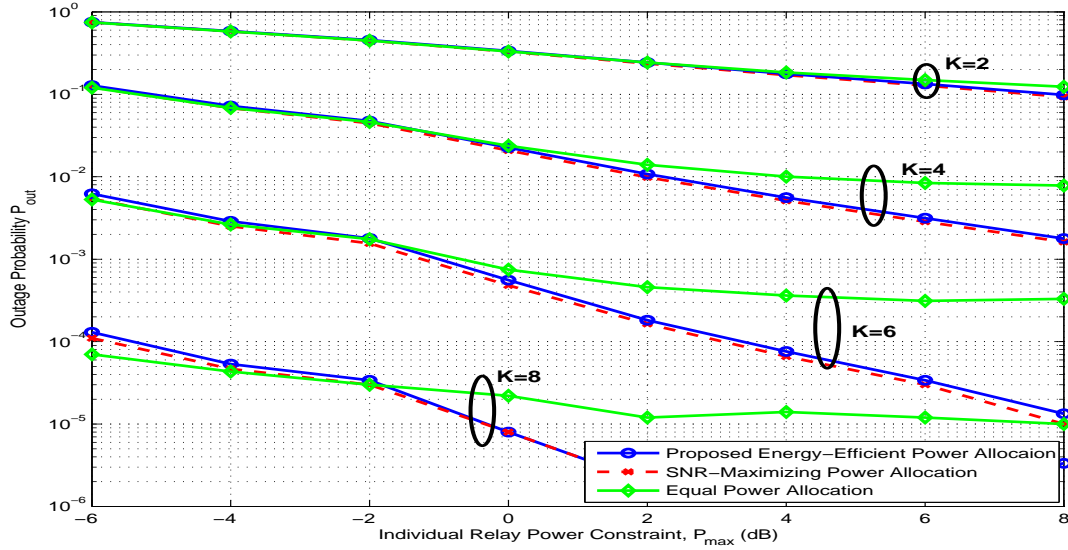
Figure 3.19: The outage probability of the secondary system P_{out} vs the individual relay power constraint P_{max} for different network size (K). The secondary source transmission power P_S is set to 0 dB. The interference threshold I_{max} is set to 10 dB, and the SNR threshold is -3 dB.

3.11 Summary

In this chapter, we addressed the power allocation problem for underlay non-orthogonal cognitive relay networks. A QCQP formulation for the average secondary rate optimization under short-term interference constraint was developed. We obtained the optimal power allocation and the maximum SNR was derived as the maximum eigenvalue of a channel dependant matrix. We also proposed an algorithm to solve the power allocation problem while each secondary node has a limit on its maximum transmission power. Simulation results show that the obtained power allocation offers significant throughput improvement over the existing solutions in the literature for similar problems. Finally, an energy efficiency design for an underlay cognitive network is addressed. A problem for maximizing the power-normalized SNR of the network using the power allocation of multiple non-orthogonal relays is formulated. The problem is shown to be a non-convex product of fractional quadratic functions. Despite the complexity of the problem, we proposed an algorithm to solve the problem using 1-D search. The obtained power allocation is shown to be energy-efficient compared to the SNR-maximizing power allocation, with a slight performance loss in the outage probability.

Chapter 4

Antenna Selection for Dual-hop Cognitive Relay Networks

4.1 Introduction

Multiple antenna systems are known for their enhanced reliability and spectral efficiency [117, 118]. The use of multiple antennas at the cognitive transmitters and/or receivers will help further enhance their performance (along with cooperation). For example, [119] proposed a precoder for non-regenerative MIMO cognitive relay networks to maximize the secondary network capacity. In [120], it is shown that with relay selection and clustering, a MIMO cognitive network with multiple relays can achieve the same growth rate of conventional network (with the absence of the primary system constrains). Using a maximum-ratio combining (MRC) at the receiver, [121] studied the effect of the maximum interference power and the maximum transmit power on the secondary system capacity, while [122] studied the capacity loss due to channel estimation errors.

While MRC achieves the maximum performance in terms of diversity and processing gains, it suffers from the highest complexity. Alternatively, subset selection of the receiver antennas offers a diversity gain but sacrifices the processing gain. In fact, the advantages of subset selection is recognized and implemented in real systems such as IEEE 802.11n and LTE-A. In general, generalized selection combining (GSC) (which is a subset selection form) offers a performance/implementation trade-off [123, 124]. In [125], diversity gain of transmit antenna selection with generalized selection combining is quantified. To further reduce the implementation cost and complexity, GSC shall reduce to the selection of only one antenna,
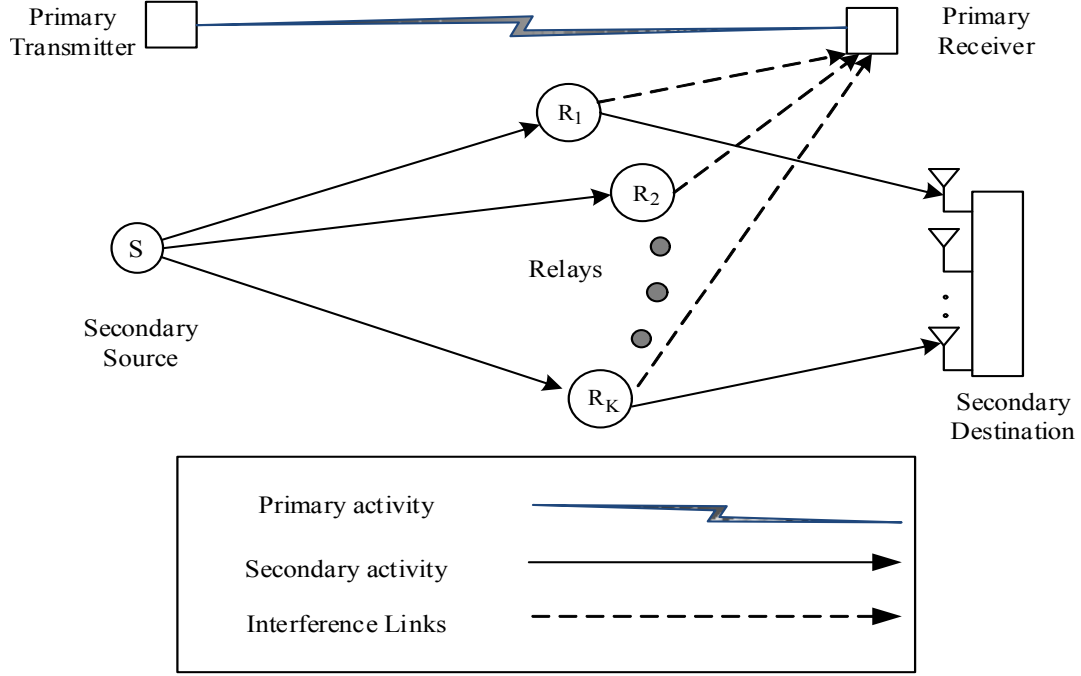
Figure 4.1: Underlay cognitive relay network with secondary receiver equipped with N_D antennas.

namely the selection combining (SC).

In this chapter, we study the performance of cognitive relay networks while the secondary destination has multiple antennas. we aim at reducing the implementation complexity of the cognitive destination by only using one radio frequency (RF) chain despite the existence of multiple receiving antennas. To capture the lost diversity gain, we make use of the availability of multiple cognitive nodes and allow concurrent relays' transmission.

4.2   System Model

We consider an underlay secondary network with one source S and one destination D and $K \geq 2$ relays denoted $R_1, R_2, ..., R_K$. The source S and all relays are assumed to have single antenna, however, the destination D is equipped with N_D antennas. The co-located primary system consists of a single transmitter-receiver link. The interference on the primary receiver generated during secondary transmissions must be kept below a pre-defined threshold referred

to as the *interference temperature*, denoted by I_{max}. Assuming the primary transmitter is far from the secondary relays as well as the destination D, is a typical and valid assumption for large networks. Hence, the effect of the primary network on the secondary receivers may be treated as Gaussian noise or even neglected [59]. Modeling the primary interference as a Gaussian noise is commonly used in literature as in [65, 125, 126] which is justified through the central limit theorem (CLT). In the case of single primary interferer, the structure of the primary signal will have a major role in modelling it into the received secondary SNR. On the other hand, with multiple primary interferers involved, the statistics of either the maximum or the summation can be approximated using the central limit theory leading to a Gaussian approximation.

We also assume block-fading, and all channel coefficients are assumed to be independent. We assume that a direct link between S and D is absent, and the transmission from S to D occurs exclusively through the AF relays using a dual-hop protocol. In the first time slot, S selects the proper transmission power P_S to transmit a data symbol to all relays. The received signal at the ith relay, ($i \in \{1, 2..., K\}$), is given by

$$y_{R_i} = \sqrt{P_S} \ h_{S,R_i} \ x_S + w_{R_i}, \tag{4.1}$$

where x_S is the transmitted data symbol (with $\mathbb{E}[|x_S|^2] = 1$, where $\mathbb{E}[\cdot]$ denote expectation), and h_{S,R_i} is the channel coefficient from S to the ith relay, $i \in \{1, 2..., K\}$, modeled as zero mean and unit variance circularly symmetric complex Gaussian random variables (CSCGRV), denoted by $\mathcal{CN}(0,1)$. Here w_{R_i} is a complex random variable capturing the effect of the thermal noise and the interference due to the primary user activities, and is modeled as CSCGRV with zero mean and variance σ^2, denoted by $\mathcal{CN}(0,\sigma^2)$. Then, each relay amplifies its received signal by a variable gain given by,

$$G_{R_i} = \frac{\sqrt{P_{R_i}} \ e^{\jmath \psi_{R_i}}}{\sqrt{P_S \ |h_{S,R_i}|^2 + \sigma^2}} \tag{4.2}$$

where P_{R_i} and ψ_{R_i} are the transmission power and the phase correction at the ith relay and to be designed in the following section. In the second time slot, each relay forwards the amplified signal to D. To improve the spectral efficiency of the secondary network, all relays are allowed to transmit simultaneously over the available frequency band (non-orthogonal)

following the same model as in Chapter 3. Hence, the received signal vector at D is given by

$$\mathbf{y_D} \;\; = \;\; \sqrt{P_S}\mathbf{H_{R,D}G_Rh_{S,R}}x_S + \mathbf{H_{R,D}G_Rw_R} + \mathbf{w_D}, \tag{4.3}$$

where $\mathbf{H_{R,D}} \in \mathcal{C}^{N_D \times K}$ is the channel coefficient matrix with entries h_{R_i,D_j} being the coefficient from the ith relay to the jth antenna of D, modeled as zero mean and unit variance CSCGRV, denoted by $\mathcal{CN}\,(0,1)$. $\mathbf{G_R} \in \mathcal{C}^{K \times K}$ is the beamforming matrix which is a diagonal matrix with $\{G_{R_i}\}$ for $(i \in \{1,2...,K\})$ as the main diagonal elements, and $\mathbf{h_{S,R}} \in \mathcal{C}^{K \times 1}$ has h_{S,R_i} as entries. Here $\mathbf{w_R} \in \mathcal{C}^{K \times 1}, \mathbf{w_D} \in \mathcal{C}^{N_D \times 1}$ represent the random variables capturing the noise and the primary interference effect at the relays and the destination antennas with entries w_{R_i} and w_{D_j} respectively, both modeled as CSCGRV $\mathcal{CN}(0,\sigma^2)$.

The overall secondary system can be regarded as a single-input multiple-output (SIMO) system by rewriting (3.3) as,

$$\mathbf{y_D} = \sqrt{P_S}\mathbf{h}x_S + \mathbf{w}, \tag{4.4}$$

where $\mathbf{h} = \mathbf{H_{R,D}G_Rh_{S,R}}$ and $\mathbf{w} = \mathbf{H_{R,D}G_Rw_R} + \mathbf{w_D}$ both $\in \mathcal{C}^{N_D \times 1}$. However, in order to reduce the complexity of the secondary destination node, only one RF chain is used with antenna selection.

The secondary interference to the primary receiver caused by S while transmitting in the first time slot has a value of $I_S = P_S\,|g_{S,P}|^2$ where $g_{S,P}$ is the channel coefficient from S to the primary receiver. In the second time slot, with all relays transmitting, the total interference generated at the primary receiver is given by $I_R = \sum_{i=1}^{K} P_{R_i}\,|f_{R_i,P}|^2$, where $f_{R_i,P}$ is the channel coefficient from the ith relay to the primary receiver. To ensure proper operation of the primary user, both I_S and I_R should be kept below the interference temperature I_{max}. It is worth mentioning that, the transmission power of the source P_S is determined independently from the relays power with the only limitation being to satisfy the interference temperature constraint I_{max}. Different designs for P_S can be adopted such as an adaptive allocation in the form of $P_S = I_{max}/|g_{s,p}|^2$, or fixed allocation such as $I_{max}/\mathbb{E}[|g_{s,p}|^2]$.

4.2.1 Receive Antenna Selection

To overcome complexity and cost limitations due to increased number of radio frequency chains at the secondary destination node, and yet still gain from the existence of multiple

antennas, only one RF chain is used with antenna selection. Using channel estimation, the receiver evaluates the received SNR from each antenna $\gamma_{e2e}^{(j)}$, and then selects the antenna that achieves the highest SNR, denoted by γ^*. The index of the selected antenna is obtained by,

$$j^* = \underset{1 \leq j \leq N_D}{\operatorname{argmax}} \left\{ \gamma_{e2e}^{(j)} \right\}. \tag{4.5}$$

How to calculate the values of $\gamma_{e2e}^{(j)}$ mainly depends on the choice of the power allocation and phase correction at the relays. In the following section, we present the optimal design of the beamformer that maximizes the received SNR at a specific antenna.

4.2.2 Optimal Beamforming Design

If the jth antenna at D is selected, the optimal power allocation and the phase corrections applied at the relays can be used to form a directed beam towards the selected antenna. This can be accomplished by first using the optimal phase compensation given by,

$$\mathbf{\Psi}_R^{(j)} = [\psi_{R_i}] = -\arg\{\mathbf{h}_{\mathbf{S},\mathbf{R}}\} - \arg\{[\mathbf{H}_{\mathbf{R},\mathbf{D}}]_j^T\}, \tag{4.6}$$

where $\arg\{.\}$ is the phase of the enclosed vector, $\{.\}^T$ is the transpose, and $[\mathbf{H}_{\mathbf{R},\mathbf{D}}]_j$ is the jth row of the matrix $\mathbf{H}_{\mathbf{R},\mathbf{D}}$. Hence, using (3.2),(3.3), and (4.6), the received signal at the jth antenna can be expressed as,

$$y_{D_j} = \sum_{i=1}^{K} \left(\frac{\sqrt{P_{R_i}} \, |h_{R_i,D_j} \, h_{S,R_i}| \sqrt{P_S}}{\sqrt{P_S} \, |h_{S,R_i}|^2 + \sigma^2} \right) x_S + \sum_{i=1}^{K} \left(\frac{\sqrt{P_{R_i}} \, |h_{R_i,D_j}| \, w_{R_i}}{\sqrt{P_S} \, |h_{S,R_i}|^2 + \sigma^2} \right) + w_{D_j}. \tag{4.7}$$

Hence, one can obtain an expression for the SNR $\gamma_{e2e}^{(j)}$ as,

$$\gamma_{e2e}^{(j)} = P_S \times \frac{\left(\displaystyle\sum_{i=1}^{K} \frac{|h_{R_i,D_j}| \, |h_{S,R_i}| \, \sqrt{P_{R_i}}}{\sqrt{P_S} \, |h_{S,R_i}|^2 + \sigma^2} \right)^2}{\displaystyle\sum_{i=1}^{K} \left(\frac{\sqrt{P_{R_i}} \, |h_{R_i,D_j}| \, \sigma}{\sqrt{P_S} \, |h_{S,R_i}|^2 + \sigma^2} \right)^2 + \sigma^2}. \tag{4.8}$$

Now, the optimal power allocation at the relays that maximizes the received SNR and still satisfies the interference constraint of the primary network is identical to the optimization problem given in chapter 3. The optimization problem is given by:

$$\mathbf{P}_R^{(j)} = \arg \max_{\mathbf{P}_R} \quad \gamma_{e2e}^{(j)},$$

$$\text{subject to} \quad \sum_{i=1}^{K} |f_{R_i,P}|^2 \, P_{R_i} \leq I_{max}. \tag{4.9}$$

The optimal solution of (4.9) is shown in chapter 3 as:

$$\mathbf{P}_R^{(j)} = [P_{R_i}^{(j)}] = \mu_j \, diag\left\{ \left(\mathbf{D}^{-\frac{1}{2}}\right)^T \mathbf{v} \, \mathbf{v}^T \mathbf{D}^{-\frac{1}{2}} \right\}, \tag{4.10}$$

where $diag\{\cdot\}$ is a vector whose elements are the diagonal elements of the enclosed matrix. Here μ_j is a positive scaling factor used to satisfy the interference constraint $\mathbf{x}_{opt}^T \mathbf{C} \mathbf{x}_{opt} = I_{max}$, and is given by $\mu_j = \frac{I_{max}}{\mathbf{v}^T \mathbf{D}^{-\frac{1}{2}} \mathbf{C} \left(\mathbf{D}^{-\frac{1}{2}}\right)^T \mathbf{v}}$.

Expanding the matrices with the definitions of their elements, the power allocation at each relay R_i to form a beam towards antenna j is expressed as:

$$P_{R_i}^{(j)} = \frac{\mu_j |h_{R_i,D_j}|^2 |h_{S,R_i}|^2 (P_S |h_{S,R_i}|^2 + \sigma^2)}{\left[(P_S |h_{S,R_i}|^2 + \sigma^2) |f_{R_i,P}|^2 + I_{max} |h_{R_i,D_j}|^2 \right]^2}. \tag{4.11}$$

It can be seen from (4.11) that, aside from the constant μ_j, the power allocation $P_{R_i}^{(j)}$ can be calculated distributively using local channel-state-information (CSI) at each relay. CSI can be obtained by employing channel estimation techniques using a properly designed signal known at both the transmitter and the receiver. A feedback control channel is used to transmit channel estimates to some nodes to use it, or can be shared on a common control channels.

Now, when the optimal power allocation deployed at the cognitive relays, the corresponding received SNR is maximized to be, $\gamma_{e2e}^{*(j)} = \lambda_{max}$, where λ_{max} is the dominant eigenvalue of the channel matrix $\mathbf{M}$. The maximum received SNR is expressed as,

$$\gamma_{e2e}^{*(j)} = \sum_{i=1}^{K} \gamma_{R_i}^{(j)}, \tag{4.12}$$

where,

$$\gamma_{R_i}^{(j)} = \frac{|h_{S,R_i}|^2 |h_{R_i,D_j}|^2}{|h_{R_i,D_j}|^2 + \gamma_s \theta |f_{R_i,P}|^2 |h_{S,R_i}|^2 + \theta |f_{R_i,P}|^2}, \tag{4.13}$$

104

with $\theta = \frac{\sigma^2}{I_{max}}$. It is to be noted that (4.12) suggests a feasible implementation of the antenna selection algorithm of the previous section. The steps of the antenna selection and power allocation algorithm are summarized in Algorithm 1.

Algorithm 1 Antenna Selection and Power Allocation Algorithm

Assume Global CSI at D, and Local CSI at R_i $\forall$ $i \in \{1, 2.., K\}$

D calculates $\gamma_{e2e}^{(j)}$ from (4.12) $\forall$ $j \in \{1, 2.., N_D\}$

D uses (4.5) to get the index of the selected antenna j^*

D calculates μ_{j^*}

D broadcasts j^* and μ_{j^*} on the control channel

R_i calculates $P_{R_i}^{(j^*)}$ in (4.11) using local CSI and μ_{j^*}

4.3 Clustering

Along with antenna selection, the system complexity can be reduced by allowing only a subset of the relays to transmit. This is done by dividing the total number of the available relays into small groups referred to as Clusters. With only one cluster allowed to communicate with one antenna at the receiver, the complexity of the optimal power calculation and the feedback time are significantly reduced. In what follows, we introduce two clustering schemes and study their performance with the receive antenna selection.

4.3.1 Random Clustering

In this scheme, the total number of relays is uniformly divided over equal-size clusters with the number of clusters equal the number of receive antennas N_D. The indices of the relays R_i are assigned to cluster $\mathfrak{C}_j$, $j \in \{1, 2..N_D\}$ according to the following rule[1]:

$$\mathfrak{C}_j = \left\{ i : \frac{(j-1)K}{N_D} + 1 \leq i \leq \frac{j\,K}{N_D} \right\}. \tag{4.14}$$

Since the relay-cluster association does not change from transmission to another, it can be done once at the setup phase of the communication between D and the relays.

---

[1]It is assumed that, the number of relays K is an integer multiple of the number of the antennas N_D, resulting in the size of the cluster to be an integer.

4.3.2 Max-SNR Clustering

In this scheme, each relay is assigned to the cluster if it maximizes the total received SNR from its corresponding antenna. It should be noted that, the optimal power allocation in (4.10) decouples the received SNR into the summation of the individual SNRs generated by each relay independently. Thus, we propose the Max-SNR clustering scheme where the indices of the relays R_i are assigned to cluster $\mathfrak{C}_j$, $j \in \{1, 2..N_D\}$ according to the following rule:

$$\mathfrak{C}_j = \left\{ i : \gamma_{R_i}^{(j)} \geq \gamma_{R_i}^{(q)}, \quad 1 \leq q \leq N_D \right\}. \tag{4.15}$$

A distributed implementation of this scheme is achievable using the following algorithm:

Algorithm 2 Max-SNR Relay-Cluster Association Algorithm

Assume Local CSI at R_i $\forall$ $i \in \{1, 2.., K\}$

R_i calculates $\gamma_{R_i}^{(j)}$ from (4.13) $\forall$ $j \in \{1, 2.., N_D\}$

R_i solves $j^* = \text{argmax}_{1 \leq j \leq N_D} \left\{ \gamma_{R_i}^{(j)} \right\}$

R_i associates itself with cluster $\mathfrak{C}_{j}^*$

4.4 Performance Analysis

In what follows we analyze the performance of the proposed relay clustering schemes in-terms of the system outage probability.

4.4.1 Random clustering case:

In this section, we derive the statistics of γ^* which will be used to assess the performance of the secondary system. Given the selection rule in (4.5), the output SNR of the selected antenna is given by

$$\gamma^* = \max_{1 \leq j \leq N_D} \left\{ \gamma_{e2e, Random}^{(j)} \right\}, \tag{4.16}$$

where $\gamma_{e2e,Random}^{(j)}$ is the end-to-end SNR resulting at the jth antenna through its connecting cluster using random clustering, and is given by,

$$\gamma_{e2e,Random}^{(j)} = \sum_{\mathfrak{C}_j} \gamma_{R_i}^{(j)}. \tag{4.17}$$

It should be noted that, for random clustering all the clusters have equal and fixed sizes $|\mathfrak{C}_j|$, with $|\mathfrak{C}_j| = A_C = \frac{K}{N_D} \, \forall j$.

The outage probability of the cognitive network with random clustering, P_{out}^R, defined as the probability of the end-to-end SNR of the selected antenna (or cluster) drops below a certain threshold γ_{th}. P_{out}^R is obtained in a closed-form as,

$$P_{out}^R(\gamma_{th}) = \frac{\gamma_{th}^{A_C N_D} e^{\frac{-N_D \gamma_{th}}{\mu_\gamma}}}{[(A_C - 1)!]^{N_D} \mu_\gamma^{A_C N_D}} \sum_{k=0}^{N_D} \alpha_k \gamma_{th}^k. \tag{4.18}$$

4.4.2 Max-SNR clustering case:

In this section we study the outage probability of the Max-SNR clustering scheme. First, we start by analysing the relay-cluster association scheme. It is shown in (4.15) that a relay is associated to a cluster j if the SNR of the corresponding antenna is the maximum. Therefore, the contribution of relay R_i to the total received SNR from its cluster $\mathfrak{C}_j$ is given by,

$$\gamma_{R_i}^{(j^*)} = \max_{1 \leq j \leq N_D} \left\{ \gamma_{R_i}^{(j)} \right\}. \tag{4.19}$$

Hence, the total SNR received from the cluster $\mathfrak{C}_j$, is given by

$$\gamma_{e2e,Max}^{(j)} = \sum_{\mathfrak{C}_j} \gamma_{R_i}^{(j^*)} \tag{4.20}$$

where the size of the cluster $\mathfrak{C}_j$ is A_j.

The outage of the cognitive network occurs when all the clusters/antennas experience outage. This is expressed as follows,

$$P_{out}(\gamma_{th}) = \Pi_{j=1}^{N_D} P_{out,j}(\gamma_{th}|A_j), \tag{4.21}$$

where $P_{out,j}(\gamma_{th}|A_j)$ is the outage probability of cluster $\mathfrak{C}_j$ of size A_j, obtained as follows. Form the description of the clustering scheme and the definition of $\gamma_{R_i}^{(j^*)}$ in (4.19), the CDF

of $\gamma_{R_i}^{(j*)}$, is given by;

$$F_{\gamma_{R_i}^{(j*)}}(x) = \left[F_{\gamma_{R_i}^{(j)}}(x)\right]^{N_D} \tag{4.22}$$

where $F_{\gamma_{R_i}^{(j)}}(x)$ is the CDF of $\gamma_{R_i}^{(j)}$. Given that, $\gamma_{R_i}^{(j)}$ is tightly approximated as an exponential random variable with mean μ_γ given in (3.34), we can rewrite $F_{\gamma_{R_i}^{(j*)}}(x)$ as,

$$F_{\gamma_{R_i}^{(j*)}}(x) = \sum_{n=0}^{N_D} \binom{N_D}{n} (-1)^n e^{-\frac{nx}{\mu_\gamma}}. \tag{4.23}$$

Now, the total SNR received from the cluster $\mathfrak{C}_j$, is given by $\gamma_{e2e,Max}^{(j)} = \sum_{\mathfrak{C}_j} \gamma_{R_i}^{(j*)}$. The outage probability of the cluster $\mathfrak{C}_j$ is, then, given by

$$
\begin{aligned}
P_{out,j}(\gamma_{th}) &= Pr(\gamma_{e2e,Max}^{(j)} \leq \gamma_{th}) \\
&= Pr(\sum_{\mathfrak{C}_j} \gamma_{R_i}^{(j*)} \leq \gamma_{th}) \\
&\leq Pr(\min_{1,2\ldots A_j} \gamma_{R_i}^{(j*)} \leq \frac{\gamma_{th}}{A_j})
\end{aligned}
\tag{4.24}
$$

where the last line in (4.24) made use of the approximation $\sum_{\mathfrak{C}_j} \gamma_{R_i}^{(j*)} \leq A_j \min_{1,2\ldots A_j}\{\gamma_{R_i}^{(j*)}\}$. Let Y be the random variable $\min_{1,2\ldots A_j}\{\gamma_{R_i}^{(j*)}\}$. The CDF of Y is given by

$$
\begin{aligned}
F_Y(y) &= Pr(Y \leq y) = 1 - \Pi_{i=1}^{A_j} Pr(\gamma_{R_i}^{(j*)} \geq y) \\
&= 1 - \left[1 - F_{\gamma_{R_i}^{(j*)}}(y)\right]^{A_j}.
\end{aligned}
\tag{4.25}
$$

Now, substituting (4.23) into (4.25) and replacing $y = \frac{\gamma_{th}}{A_j}$, we obtain

$$P_{out,j}(\gamma_{th}|A_j) = 1 - \left[1 - \sum_{n=0}^{N_D} (-1)^n \binom{N_D}{n} e^{-\frac{n\gamma_{th}}{A_j \mu_\gamma}}\right]^{A_j}. \tag{4.26}$$

Given the probabilistic nature of the relay-cluster assignment, an averaging of all possible combination of cluster sizes should be taken into account. This can be complied by noting that the sizes of clusters are jointly distributed as a multinomial random variable with equal probabilities $p_i = \frac{1}{N_D}$. Hence, the total system outage probability is given by,

$$P_{out}^{max}(\gamma_{th}) = \sum_{\Lambda_K = \{k_1,\ldots k_{N_D}\}} \frac{K!}{k_1!\ldots k_{N_D}! N_D^K} \Pi_{j=1}^{N_D} P_{out,j}(\gamma_{th}|A_j). \tag{4.27}$$

where Λ_K is the set that includes all possible permutations of the N_D numbers $k_1, k_2...k_{N_D}$ that add up to K (i.e $\sum_{i=1}^{N_D} k_i = K$). For instance, if $K = 3$ and $N_D = 2$, then $\Lambda_K = (0, 3), (3, 0), (2, 1), (1, 2)$. It should be noted that $P_{out}(\gamma_{th}|0) = 1$ is the outage probability of an empty cluster.

4.5 Simulation Results

In this section, we present the performance results of the proposed antenna selection scheme and the power allocation at the secondary network through the derived expressions and simulation.

4.5.1 Antenna Selection Only

First, we present the performance of antenna selection at the secondary destination for different network sizes. The outage probability is defined as $P_{out}(\gamma_{th}) = Pr(\gamma_{e2e}^{(j*)} \leq \gamma_{th})$, where $\gamma_{e2e}^{(j*)}$ is the SNR of the selected antenna. Fig. 4.2 shows the outage probability P_{out} versus γ_s (the secondary source power P_S measured relative to the noise power σ^2) for a target SNR $\gamma_{th} = 3$ dB. The interference temperature I_{max} is set at 7 dB and the noise power is normalized to 1. It is noted that, increasing the number of antennas N_D for a fixed relaying network size K enhances the outage performance by increasing the diversity order. However, increasing K from 2 to 3 for a fixed N_D achieves 3 dB SNR gain, while doubling N_D from 2 to 4 only achieves 1.5 dB for a 2-relay network. This leads us to the non-intuitive result, that the network size K has an impact on the outage probability higher than the impact of the number of receive antennas N_D. We also compare the performance of the secondary system with multiple relays and antenna selection to the opportunistic relay selection. In such scheme, a single relay with best SNR is selected and the received signals from all antennas are combined. It can be seen form Fig 4.2 that the system with multiple active relays and antenna selection outperforms opportunistic relay selection while using multiple antennas for reception.
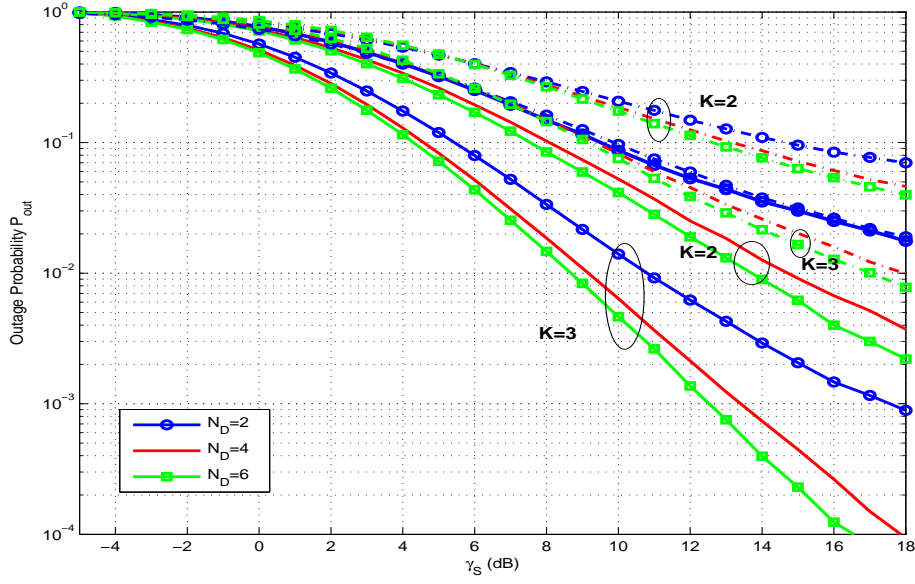
Figure 4.2: Outage probability of antenna selection for different values of N_D, for number of relays $K = 2$ and 3. The interference temperature I_{max}=7 dB and the target SNR $\gamma_{th} = 3$ dB. Solid: Multiple Relays, Dotted: Opportunistic Relay Selection.

4.5.2 Effect of Power Allocation Scheme

Second, we examine the effect of the power allocation at the relays by simulating the outage probability P_{out} of the cognitive network employing the optimal power allocation in (4.10) compared to the equal power allocation where $P_{R_i} = \frac{Imax}{\sum_1^K |f_{R_i,P}|^2}$. We also include the performance of opportunistic relays selection with the power of the selected relay $P_{R_{i*}} = \frac{I_{max}}{|f_{R_{i*},P}|^2}$. While optimal power allocation in (4.10) allows the distribution of the power among the relays such that the interference constraint of the primary user is satisfied, it utilizes the dominant eigenmode of the channel matrix which minimizes the self interference among the relaying channels and transforms them into orthogonal channels. On the other hand, the equal power allocation only satisfies the primary user interference constraint by sharing it equally among the relays. Fig. 4.3 clearly shows that the optimal power allocation outperforms the equal power allocation.

4.5.3 Relay Clustering and Antenna Selection

Up to this end, all relays are allowed to communicate with all the available antennas at the destination. Next, we present the performance of the clustering techniques, where only a subset of the relays is allowed to communicate with only one antenna. We compare the performance of the proposed clustering schemes, namely, the *Random clustering* and the *Max-SNR clustering* in Fig. 4.4. Here, we study the system with $K = 6$ relays for all cases. For *Random clustering*, the size the cluster is fixed and increasing N_D will directly result in decreasing the number of relays per cluster which leads to a performance degradation. This observation agrees with the conclusion form Fig.4.2 and further elaborated in Fig 4.5 and 4.6. However, for the *Max-SNR clustering*, the cluster size is a random variable (binomial with parameters K and $\frac{1}{N_D}$), which suggests that there exist a non-zero probability that the selected cluster/antenna will have a size higher than the *random clustering* case. Hence, a superior performance for the *Max-SNR clustering* scheme is achieved. We also included the case of a single-antenna (no clustering/no-antenna selection) and $K = 6$ as a bench mark as
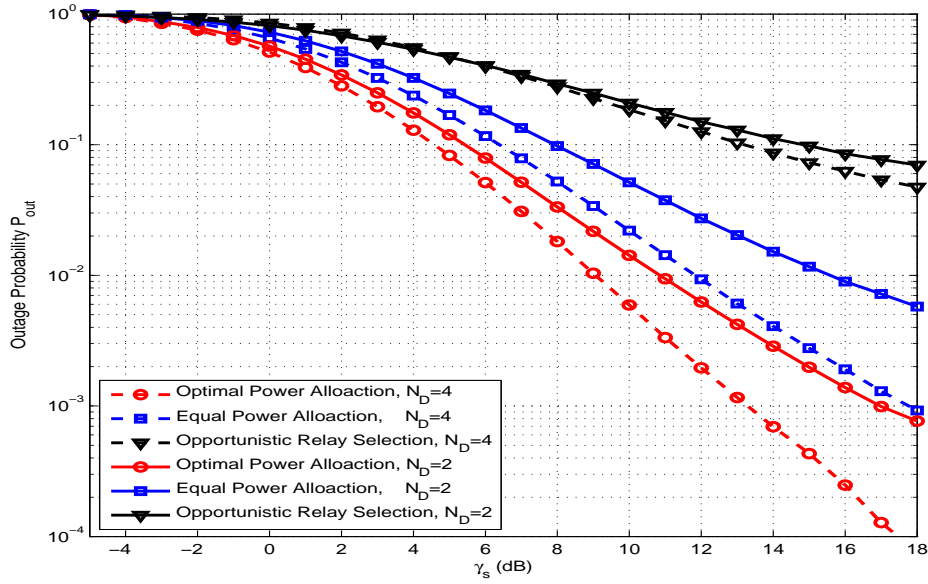
Figure 4.3: Outage probability of antenna selection for different power allocation schemes, with the number of relays $K = 3$, I_{max}=7 dB.
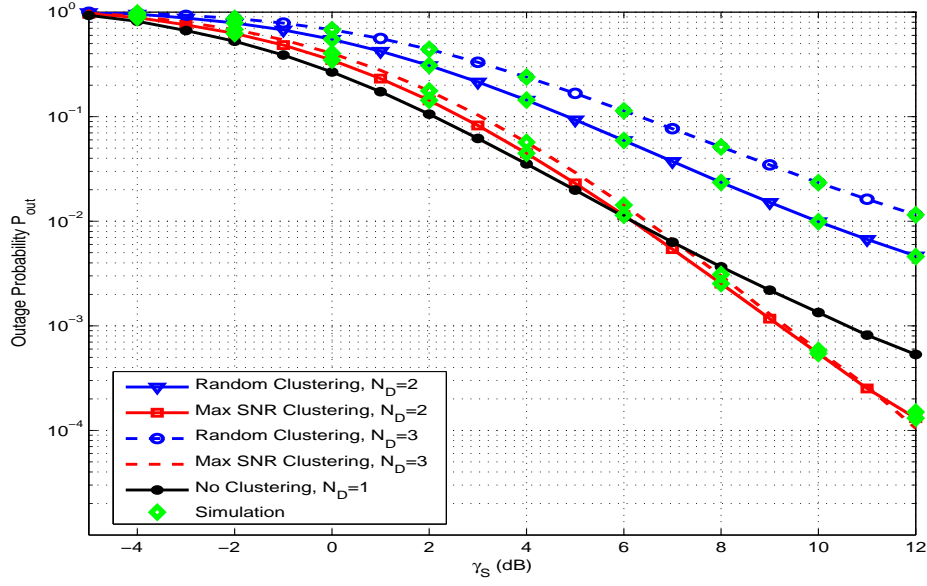
Figure 4.4: Outage probability of antenna selection and relay clustering, for different values of N_D, with number of relays $K = 6$, I_{max}=7 dB using optimal power allocation.

it has the same degrees of freedom. As shown the performance of *Max SNR clustering* with antenna selection is comparable to the single-antenna case for low γ_s. As γ_s increases, the Max-SNR selection shows a better performance than the single-antenna case.

Fig. 4.5 plots the outage probability versus the number of relays K for the two proposed clustering schemes with antenna selection where the secondary destination has $N_D = 2$ antennas. It is shown that, increasing the number of relays (while fixing the number of antennas), results in increasing the number of relays per cluster (in case of *random clustering*) which enhances the performance. Also, the average cluster size increases for the case of *Max SNR clustering* which shows a superior performance compared to the *random clustering*.
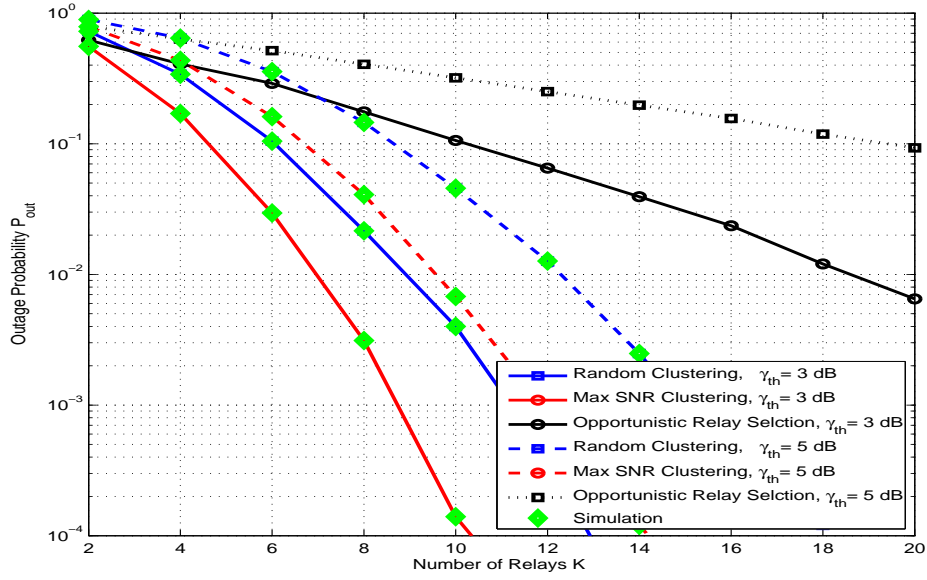
Figure 4.5: Outage probability of antenna selection and relay clustering vs the number of relays K while N_D is fixed ($N_D = 2$), I_{max}=7 dB using optimal power allocation for both random clustering and Max SNR clustering.

Fig. 4.6 completes the picture by plotting the outage probability as the number of antennas increases for a fixed number of relays. A reverse behaviour is encountered as the number of relays per cluster decreases. It is shown that, as the number of antennas increases for a fixed number of relays, the cluster size decreases, and hence the outage probability increases. It is also shown that, both clustering schemes outperform opportunistic relay selection. We also compare the simulation results of the two clustering schemes to the analytical expressions of the outage probability in Fig. 4.7 for *random clustering*, and in Fig. 4.8 for *Max-SNR clustering* where both figures show a perfect match.
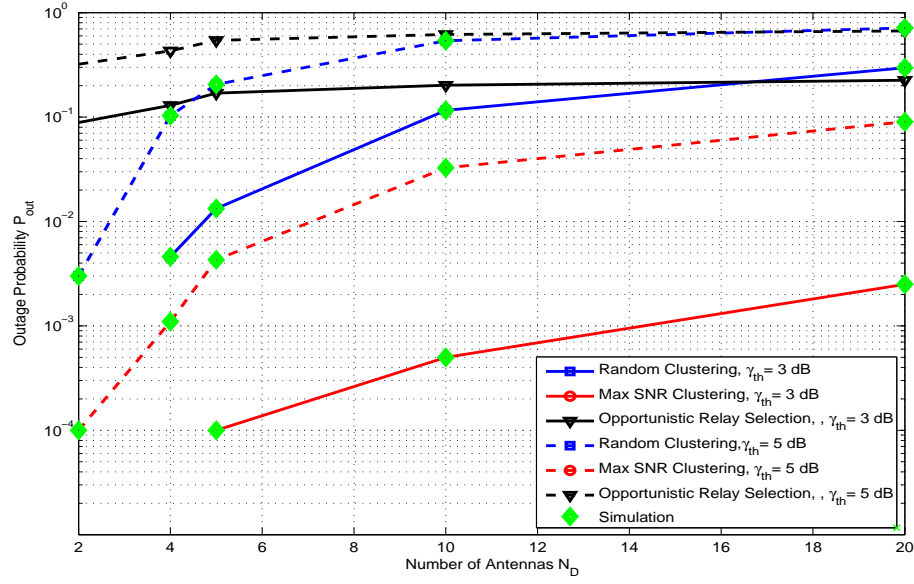
Figure 4.6: Outage probability of antenna selection and relay clustering vs the number of antennas N_D with $K = 20$ relays, I_{max}=3 dB using optimal power allocation.
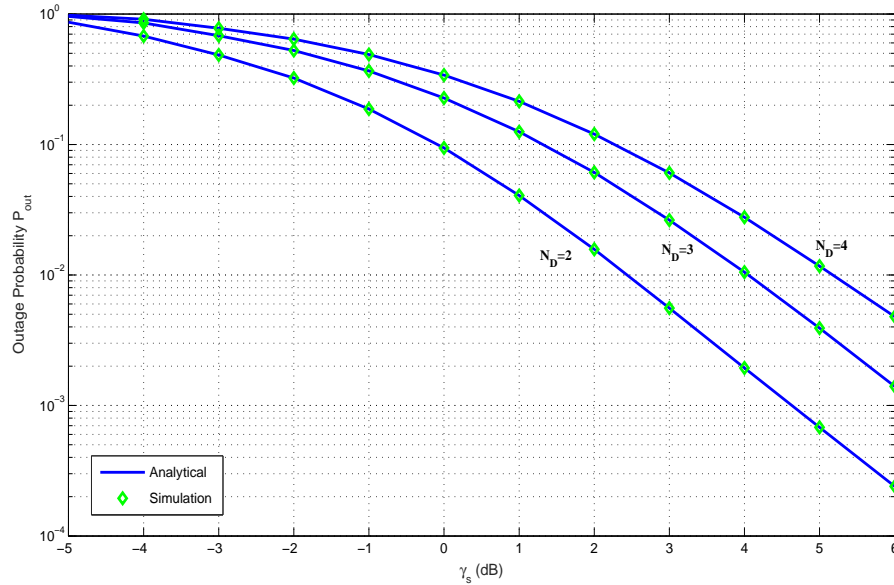
Figure 4.7: Analytical and simulation results of outage probability for $K = 12$ and different N_D setups, I_{max}=5 dB using optimal power allocation for random clustering.

114
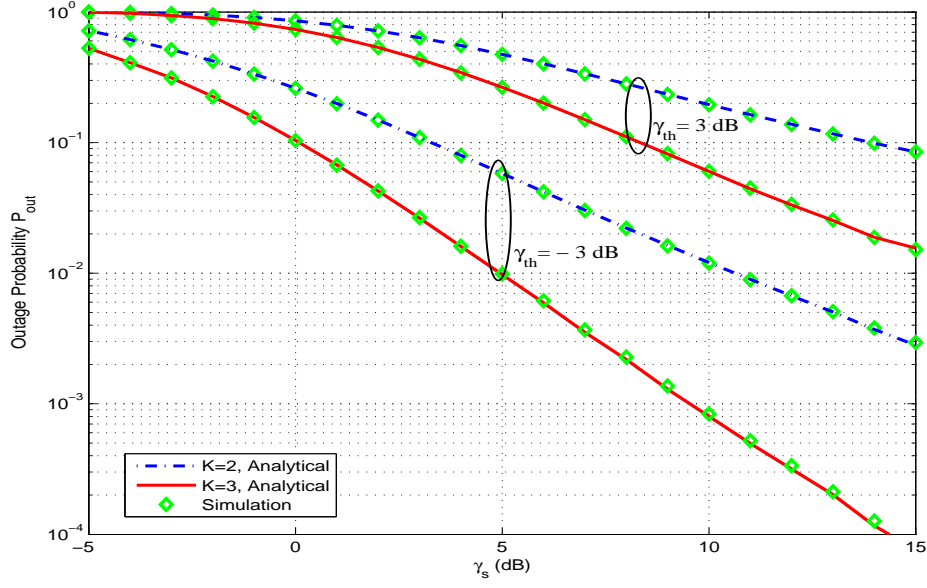
Figure 4.8: Analytical and simulation results of the outage probability for different number of relays K with $N_D = 2$, I_{max}=5 dB using optimal power allocation for Max SNR clustering.

4.6   Summary

In this chapter, an underlay cognitive network employing multiple non-orthogonal AF relays with multiple antennas at the destination is investigated. With the use of optimal power allocation at the relays, we proposed the use of antenna selection at the secondary destination to reduce the system complexity and yet capture the diversity order. Our simulations show that, the number of the secondary relays has a higher impact on the received SNR than the number of receive antennas. To reduce the complexity of the power allocation algorithm, we proposed two clustering schemes with fixed-size and random-size clusters, namely the *random clustering* and *Max-SNR clustering*, respectively. Closed-form expressions for the outage probability are given and are shown to match the simulation results.

Chapter 5

Channel Estimation for LTE-MTC Systems

5.1 Introduction

In the previous chapters, we studied the cognitive relay networks as a strong candidate to enable the IoT framework. However, some of the IoT applications might require transmission priority, wider coverage, or high data rates. In such cases, cellular networks offer a good solution with their large coverage and flexible data rates. Scenarios defined by the 3rd Generation Partnership Project (3GPP) standardization body emerge as the most promising solutions to enable cellular infrastructure of M2M communications. LTE CAT-M is a special category of user equipments supporting MTC features, has been incorporated by the 3GPP to Long-Term-Evolution (LTE) specifications.

In conventional LTE systems, the network provides the UE with Downlink Control Information (DCI) messages sent over the Physical Downlink Control Channel (PDCCH) [127]. An Enhanced PDCCH (EPDCCH) is introduced in LTE-A Release-11 to achieve better spectral efficiency by exploiting frequency selectivity and beamforming and also to provide greater flexibility of dynamic allocation of control channel resources. The DCI messages dynamically provide both downlink and uplink scheduling and detection information on how to receive the data (e.g. modulation, coding, resource assignment, and power control). Thus, the downlink control channel is one of the most important channels and represent the precondition for the correct data decoding. Since LTE-MTC has different challenges and objectives, conventional control channels have to be revised [128]. To cope with the new challenges of MTC, new specifications for the control channel for MTC is defined as MTC-PDCCH or MPDCCH.

Coherent detection of the MPDCCH is a must and requires channel knowledge, hence,

special Demodulation Reference Signals (DMRS) are attached to MPDCCH to allow pilot-aided channel estimation. However, the use of conventional channel estimators with the new MPDCCH will not be efficient in terms of complexity and performance. In fact, channel estimation is identified as one of the main areas that should be further improved for CAT-M UEs [129].

In this chapter, we propose a channel estimation algorithm for the newly introduced MPDCCH in the specifications of the LTE-A CAT-M. The proposed technique aims at reducing the complexity of the channel estimation of the MPDCCH as minimum as possible. In order to achieve this goal, we propose using the simple Least Squares (LS) estimation to estimate the pilots signals, followed by two stage first-order polynomial interpolation (linear) to obtain the channel estimates at every point in the time-frequency grid. We also address the use of the repeated transmissions to enhance the performance of the proposed technique.

5.2   MTC Physical Downlink Control Channel

To improve the spectral efficiency of the control channel, the EPDCCH was introduced to the LTE-A Release-11 standard as an alternative to the legacy PDCCH which is mapped to the full occupied bandwidth. For MTC applications, decoding PDCCH is not possible since the UE is limited to only 1.4MHz. Furthermore, coverage enhancement can be achieved by employing EPDCCH that supports beamforming which increases coverage by directing the base station's power towards the UE. In addition, the EPDCCH can be repeated to achieve SNR gain in the lack of spatial diversity and frequency diversity. For these reasons, EPDCCH has been chosen to be the starting point towards designing the new MTC control channel MPDCCH. However, special requirements have been adapted to best suite the new MTC platform and to support the required coverage with reasonable complexity and power consumption. The new set of features for MPDCCH require defining new set of downlink control formates [130], and adding a possibility for a common UE to access the control channel. In addition, repetition and frequency hopping are introduced to enhance the control channel assignment procedure.
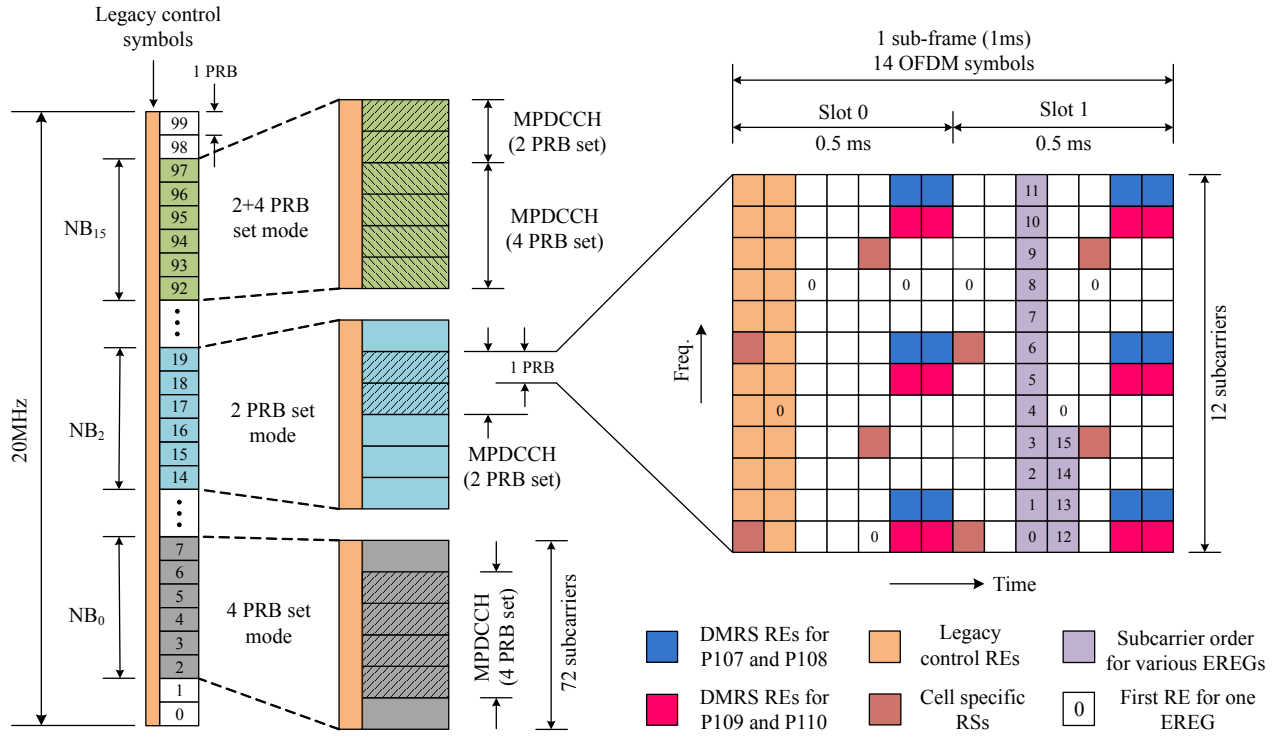
Figure 5.1: A single PRB structure for MPDCCH showing locations of DMRS and EREG start for Normal CP mode.

5.2.1 MTC Control Channel Assignment

5.2.1.1 Control Channel Aggregation and Mapping

Similar to EPDCCH, the MPDCCH can be configured with 1 or 2 physical resource block (PRB) sets. However, for MTC, both sets will either be localized or distributed. Unlike EPDCCH, MPDCCH set sizes can be configured only to be either 2 or 4 PRBs. Thus, the only option to have 6 PRBs allocated to MPDCCH (which is the maximum), is by using 2 sets; one with 2 PRBs and the other with 4 PRBs. Hence, this assignment is referred as the "2+4" configuration. Fig. 5.1 shows the possible set assignment for MPDCCH. The MPDCCH is backward-compatible with the EPDCCH, hence it is frequency-multiplexed with the data channel PDSCH. The mapping of the MPDCCH to the physical resource elements is also similar in principle to the conventional EPDCCH [131]. With the conventional EPDCCH, the REs are grouped together into Enhanced Resource Element Groups (EREGs) (with 9 REs per EREG for Normal CP mode and 8 REs per EREG for Extended CP mode). The

EREGs are then grouped into Enhanced Control Channel elements (ECCEs) with 1 ECCE being formed from 4 EREGs for Normal CP and 8 EREGs for Extended CP type. This gives 36 REs per ECCE for the Normal CP type and 64 REs per ECCE for the Extended CP type. As shown in Fig. 5.1, a single PRB pair is shown for Normal CP mode. First, notice the Demodulation Reference Symbols (DMRS) within the PRB pair. These are used as the coherent reference to demodulate the signal. The remaining REs are numbered from 0 to 15 in a cyclical fashion moving first in frequency and then in time. The REs with the same number form 1 EREG. It is also worth mentioning that during resource element mapping for MPDCCH, the REs will be punctured by the cell specific RS as well as by the legacy control channel REs.

Each MPDCCH is then formed from 1 or more ECCEs being aggregated together. The aggregation levels have been revised for MPDCCH to be 1, 2, 4, 8, 16, or 24 ECCEs for Normal CP and 1, 2, 4, 8, and 12 for Extended CP. The aggregation is the mechanism for rate adaptation to the channel conditions and payload size. The higher the aggregation level, the lower the coding rate and the lower the SNR at which the signal can be demodulated. Unlike the PDCCH/EPDCCH for which the maximum aggregation level is 8, the maximum aggregation level for the MPDCCH is 24 formed by using multiple PRBs. This gives the lowest coding rate, allowing for better coverage. The aggregation level of 24 is achieved using 2 RB sets, one with 2 PRBs and another one with 4 PRBs.

There are two different mappings of the original EPDCCH in forming ECCEs: localized and distributed. MPDCCH inherits similar mapping. In localized mapping, all EREGs that constitute an ECCE are located within the same PRB pair. With the distributed mapping, the ECCE is formed from EREGs in multiple PRBs that are distributed across the allocated PRB pairs for the control channel. In fact, the localized mapping allows the system to exploit frequency selectivity. The distributed mapping gives more diversity for those situations where frequency selectivity can not be exploited.

A significant difference between EPDCCH and MPDCCH is the time relation between the control channel and the corresponding shared channel [132]. To relax the latency requirements at the UE side, 3GPP has decided to schedule an MPDCCH in subframe m for the corresponding shared channel at subframe $m + p$ where p is a positive integer and $p \neq 0$.

Table 5.1: Candidate Table for CE Mode A in LTE-MTC

No. of PRBs		Possible candidate for blind decoding
2+4	2 PRB set	$[\{2,R_1,1\}\{4,R_1,1\}]$ $[\{4,R_2,1\}\{8,R_2,1\}]$
	4 PRB set	$[\{8,R_1,2\}\{16,R_1,1\}][\{8,R_2,2\}\{16,R_2,1\}]$ $[\{8,R_3,1\}\{16,R_3,1\}]$
	2+4 PRB set	$[\{24,R_1,1\}\{24,R_2,1\}\{24,R_3,1\}\{24,R_4,1\}]$
2		$[\{2,R_1,2\}\{4,R_1,1\}\{8,R_1,1\}\{2,R_2,2\}$ $\{4,R_2,1\}\{8,R_2,1\}\{2,R_3,2\}\{4,R_3,1\}$ $\{8,R_3,1\}\{2,R_4,2\}\{4,R_4,1\}\{8,R_4,1\}]$
4		$[\{2,R_1,1\}\{4,R_1,1\}\{8,R_1,1\}\{16,R_1,1\}$ $\{2,R_2,1\}\{4,R_2,1\}\{8,R_2,1\}\{16,R_2,1\}$ $\{2,R_3,1\}\{4,R_3,1\}\{8,R_3,1\}\{16,R_3,1\}$ $\{2,R_4,1\}\{4,R_4,1\}\{8,R_4,1\}\{16,R_4,1\}]$

However, a pipeline assignments may occur such that the PDSCH can be received in sub-frame $m+1$ concurrently with a scheduled MPDCCH that configures the detection of the PDSCH in sub-frame $m+2$, for example.

5.2.1.2 Blind Decoding and Repetition

To blindly decode one candidate in conventional LTE systems, the following is required: static parameters including the CP type, the mapping type, and the user identity represented by the Radio Network Temporary Identifier (RNTI) and dynamic parameters including the candidate index, the DCI size, and the aggregation level. It has been agreed for MTC that the new DCI formats have the same size to reduce the number of trials for blind decodes. Also, to enable low cost UE, MPDCCH has been designed to support a maximum of 20 trials for blind decoding for both common search spaces (CSS) and the user-specific search spaces

(USS). In addition to the static parameters, each blind decode candidate in MPDCCH is then defined by an aggregation level and a number of repetitions. The number of repetitions define the amount of time diversity and soft combining that can be applied to this candidate. 3GPP specifications defines the number of repetitions by signalling the maximum number of repetitions, R_{max}, to the UE. Each CE level has a different value configured through the system information. From R_{max}, a set of repetition levels are defined including (R_1, R_2, R_3, and R_4). For example, this set in the USS is defined as follows: (1) If $R_{max} = 1$, then $R_1 = R_{max}$. (2) If $R_{max} = 2$, then $R_{max} = 2R_1 = R_2$. (3) If $R_{max} = 4$, then $R_{max} = 4R_1 = 2R_2 = R_3$. (4) If $R_{max} \geq 8$, then $R_{max} = 8R_1 = 4R_2 = 2R_3 = R_4$. The set of blind decodes for mode A are defined by Table 5.1 [133]. The entries in the table enumerate the blind decodes as: {aggregation level, repetition index (R_1, R_2, R_3, and R_4), number of blind decodes}.

5.2.1.3 Frequency Hopping

With the small bandwidth offered to MTC UE, there is a significant loss of frequency diversity. To recover portion of this gain, the MTC LTE system will make use of frequency hopping. Thus, transmissions will hop from one narrowband to another [134]. Frequency hopping regains some of the frequency diversity but it introduces new challenges. One issue is that the UE will need to re-tune every time it hops, and this re-tuning takes time which might affect the overall throughput. 3GPP working group has decided that 2 OFDM symbols worth of time is needed for re-tuning. Further, re-turning will take place during the legacy control channel symbols which will be discarded anyway by the MTC UE. This choice of re-tune time and period reduces the chance of loosing the a considerable amount of network throughput. Another issue with frequency hopping is that the UE and eNodeB both need to know the hopping pattern. This needs to be signalled or must be determinable from certain system parameters. The new signalling introduces an overhead to the system. The way that the hopping parameters are signalled depend on the processed channel.

For MPDCCH, the first NB is determined without any new higher layer configuration involved (i.e. it is specified in the system information messages). The other narrowbands are determined using a single configurable offset. The offset, signalled in the system information,

is cell-specifically configured and applicable to all CE levels. In CE mode A, the hopping is turned on or off dynamically by higher-layer signalling in the DCI if the hopping is enabled. The number of NB for hopping is either 2 or 4. This parameter is signalled to the UE and it is cell-specific.

With frequency hopping, the channel estimation will need to be restarted whenever hopping is scheduled. This will have a negative effect of the accuracy of the channel estimates if time diversity is used to enhance the performance. Based on the specifications [135], the MPDCCH transmission will stay on one NB for Y subframes, where Y is in the range of 2-8 subframes to allow some benefit of cross-subframes channel estimation. This value Y is called the frequency hopping interval and it is cell-specific. There are 4 values signalled to specify the frequency hopping interval for all channels in a specific channel direction and UE mode, namely mode A DL, mode B DL, mode A UL, mode B UL. For FDD and mode A, the values that this parameter may take are among the set $\{1, 2, 4, 8\}$. For mode B they take values in the set $\{2, 4, 8, 16\}$.

5.3   System and Signal Models

Fig. 5.2 shows the downlink transmitter/receiver chain for the MPDCCH. At the transmitter side, the control information (DCI payload with length K) is first generated. After CRC attachment which is mainly 16 bits CRC code, the bits are coded with a rate 1/3 tail-biting convolutional code, interleaved, and then rate matched to fit the amount of resources used for the control channel transmission. The rate matching output is scrambled by a cell specific random sequence where the output is QPSK modulated. The resource elements are mapped, along with the reference symbols, to the proper control channel elements on the time/frequency grid according to a predefined scheduler for this control segment. According to LTE-MTC specifications, the control channel candidate will be repeated within a set of consecutive sub-frames. The time domain OFDM symbols are synthesized by employing an Inverse Fast Fourier Transform (IFFT). To reduce the effect of Inter-Symbol Interference (ISI), the last N_g samples of the symbol are copied to the beginning of each OFDM symbol in order to form the cyclic prefix.
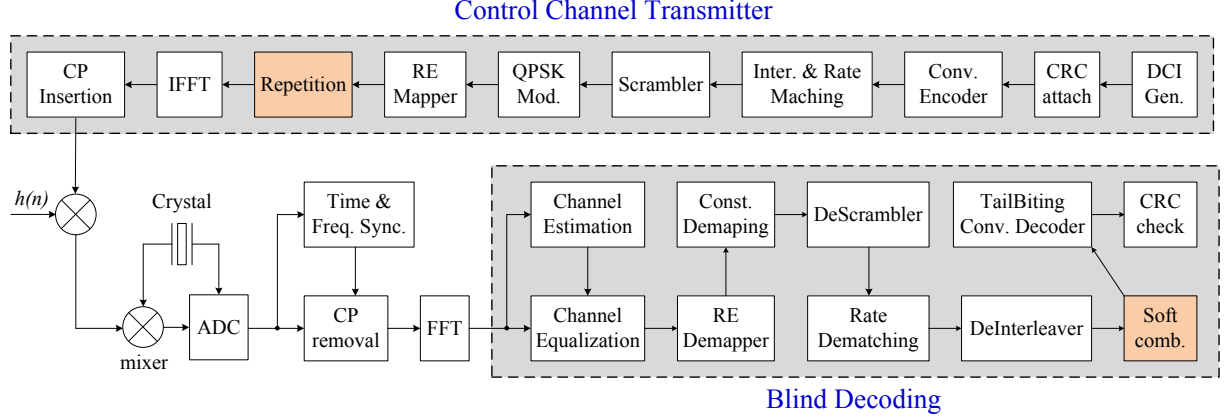
Figure 5.2: Block diagram for the transmitter/receiver model for the control channel simulation in LTE-MTC system

The eNodeB communicates with UE over the channel $h(n)$. The receiver is subjected to AWGN, $z(n)$. In the frequency domain, the channel should be estimated and equalized. As part of the decoding, the CCEs are combined through the resource element demapper to form the control channel candidate back. The constellation demapper is employed to obtain the soft bits which are descrambled by the same sequence applied at the transmitter side. Depuncturing is allowed by the rate dematching to bring the number of soft bits back to $3 \times (K + 16)$ which are then deinterleaved. If repetition is involved at the transmitter side, soft combing is applied across sub-frames to increase the reliability of the soft bits. This combining is assumed to be MRC mechanism. Once the soft combining is complete, the soft bits are decoded by a typical tail-biting convolutional decoder and then CRC check is applied to decide whether the block is correctly received or not.

The complex baseband equivalent channel of the wireless channel impulse response [136] can be represented as,

$$h(t, \tau) = \sum_m \nu_m \delta(t - \tau_m) \tag{5.1}$$

where $\delta(t)$ is the conventional impulse function, τ_m is the mth path delay, and ν_m is the corresponding time varying complex amplitude. The frequency domain transfer function $H(l, k)$ represents the channel gain at each sub-carrier position k in each OFDM symbol l. For a multiple transmit antenna system, the received signal at the receiver antenna represents the combined version of the transmitted streams. Let the frequency domain received signal

$R(l, k)$ at OFDM symbol l and sub-carrier index k be given by (5.2), where $S^j(l, k)$ is the transmitted sub-carrier from antenna port j, $H^j(l, k)$ is the channel transfer function from antenna port j, and $Z(l, k)$ represents the additive white Gaussian noise. All have been considered at OFDM symbol l and sub-carrier k.

$$R(l, k) = \sum_j S^j(l, k)H^j(l, k) + Z(l, k) \tag{5.2}$$

5.4 Channel Estimation For MPDCCH

5.4.1 Pilot Structure

Frequency domain multiplexing of the control information with data was adopted to facilitate frequency selective scheduling of the downlink and uplink assignments and frequency-domain Inter-Cell Interference Coordination (ICIC). The DMRS are employed by antenna ports 107 to 110, where each port may be taken to indicate one physical antenna, for a total of up to 4 transmitting antennas. For normal CP type, antenna ports 107 and 108 share the same subcarrier locations for their DMRS. Similarly antenna ports 109 and 110 share the same subcarrier locations. Note that, the DMRS transmitted by the different antennas that share the same subcarrier locations are orthogonal. Also, it is worth to mention that an MPDCCH candidate can be transmitted through a single layer system when localized transmission is configured. On the other hand, to gain more diversity in distributed transmission mode, the symbols that belong to the same candidate are mapped onto two sets of orthogonal subcarriers. These two sets are transmitted by two transmit antennas which involve orthogonal precoding. Thus, in all cases, a single subcarrier will be observed according to a single antenna transmission.

For the transmitted pilot tones at OFDM symbol l_p and subcarrier index k_p, the transmitted pilot $S^j(l_p, k_p)$ is represented, by,

$$S^j(l_p, k_p) = W^j(l_p, k_p)x(l_p, k_p), \tag{5.3}$$

where $x(l_p, k_p)$ is some pseudo-random unitary signal value (of QPSK nature) transmitted by all antennas at subcarrier (l_p, k_p) and $W^j(l_p, k_p)$ is the value of a binary orthogonal cover

code for antenna port j at subcarrier (l_p, k_p). The cover code is of length 4 and is constructed based on the two vectors [1 1 1 1] and [1 -1 1 -1], where the first vector is attached to odd numbered ports and the second vector is assumed for the even ones. The code sequence for each antenna port is applied in the time dimension either in the forward or reverse order. This order is reversed in the frequency dimension.

5.4.2   Pilot Signal Estimation

Although the general channel estimation problem in case of single antenna systems is two-dimensional [95] (i.e., has to be carried jointly in the frequency and time domains), it is normally separated into two one-dimensional estimation steps to simplify the implementation [137]. In this context, the channel estimation problem can be considered over one OFDM symbol (specifically the symbol containing the DMRS) to exploit the frequency domain characteristics. Prior to any signal processing for the channel estimation algorithm in the MPDCCH, the Channel Transfer Function (CTF) is estimated in the frequency domain at the pilot positions first.

Let (l_p, k_p), (l_p, k_p+5), and (l_p, k_p+10) be the three subcarriers of one resource block that carry consecutive DMRS in the same OFDM symbol. The channel vector from antenna port j at the pilot subcarriers can be defined as $\mathbf{h}_p^j = [H^j(l_p, k_p)\ H^j(l_p, k_p+5)\ H^j(l_p, k_p+10)]^T$, where $(.)^T$ is for the transpose operator. The corresponding pseudo-random signal can be defined by the diagonal matrix $\mathbf{X} = \mathbf{diag}[x(l_p, k_p)\ x(l_p, k_p + 5)\ x(l_p, k_p + 10)]$. If the precoding code for antenna port j is also represented by the diagonal matrix $\mathbf{W}^j = \mathbf{diag}[W^j(l_p, k_p)\ W^j(l_p, k_p + 5)\ W^j(l_p, k_p+10)]$, Then, the received subcarriers vector at the pilot positions can be defined as,

$$\mathbf{r}_p = \mathbf{X}\mathbf{W}^j\mathbf{h}_p^j + \mathbf{X}\mathbf{W}^i\mathbf{h}_p^i + \mathbf{z} \tag{5.4}$$

where $\mathbf{z}$ is the noise vector, $i \in \{107, 108\}$ and $j \in \{109, 110\}$ based on the DMRS of interest. Since $\mathbf{W}^i$ is orthogonal to $\mathbf{W}^j$ and the channels from various antenna ports are typically assumed to be uncorrelated, we get the channel estimation at the pilot locations for antenna port j using the Least Squares (LS) estimation given by,

$$\hat{\mathbf{h}}_p^j = \left(\mathbf{X}^{j\mathbf{H}}\mathbf{X}^j\right)^{-1}(\mathbf{X}^j)^{\mathbf{H}}\mathbf{r}_p \tag{5.5}$$

where, $\mathbf{X}^j = \left[\mathbf{W}^j\right]^{-1}\mathbf{X}$, and $(.)^{\mathbf{H}}$ is the Hermitian.[1]

Because the number of pilot sub-carriers is always fewer than the number of information-carrying sub-carriers, interpolation across time and frequency is required to obtain a channel estimate at each sub-carrier in the time-frequency grid. 2-D interpolation is required in order to obtain a channel estimate for each antenna port at each sub-carrier $\hat{H}$ from $\hat{h}_p$. The channel estimate is obtained using, $\hat{H} = \mathbf{C}\hat{h}_p$, where $\mathbf{C}$ is a matrix representing the filter operation (i.e., the interpolation process) applied to the channel estimates at the pilot positions. Typically, the implementation of interpolation using 2-D filters increases the complexity of the channel estimation algorithm. However, using the separability property [138], 2-D interpolation can be achieved using two cascaded 1-D filters to implement the time and frequency interpolations. In this method, $\hat{H}$ is divided into two sets $\mathbf{C}_t$ and $\mathbf{C}_f$, where $\mathbf{C}_t$ is a filter operating along the time direction, while $\mathbf{C}_f$ is a filter operating in the frequency direction.

In order to calculate these filter coefficients, a variety of techniques can be used. In the following, we will present some of the commonly used techniques and shed some light on their suitability for MPDCCH.

5.4.2.1 MMSE Interpolation Approach

The optimum MMSE interpolation has been well studied in the literature [139]. In [140], using two 1-D Wiener filters can achieve performance near to the optimum 2-D nonseparable Wiener filter but with much reduced complexity. The 1-D Wiener filter for interpolating the kth sub-carrier channel from its neighboring pilots in the lth OFDM symbol is given by

$$\hat{\mathbf{H}}_l^{MMSE} = (\rho_{p,p} + \eta\mathbf{I})^{-1}\rho_{l,p}^H \tag{5.6}$$

where $\rho_{p,p}$ is the autocorrelation matrix of the CFR at the pilot subcarriers, $\rho_{l,p}$ is the cross correlation of CFR between the pilot subcarriers and the one to be estimated, η is a factor depending on the operating SNR, and $\mathbf{I}$ denotes an identity matrix of the right dimension.

---

[1]Similarly, the channel estimates at the pilot positions for antenna port i is formulated as $\hat{H}_p^i = \left[\mathbf{W}^i\right]^{-1}\mathbf{X}^{-1}\mathbf{r}_p$. For simplicity, we will drop the superscripts i and j, and the reader can assume identical processing for both antenna ports.

This type of filter can be used across the time and frequency dimensions. However, the MMSE estimation here requires knowledge about $\rho_{p,p}$, $\rho_{l,p}$ and the operating SNR. To obtain such information, multiple techniques have been proposed to approximate parametric model for the CFR autocorrelation function in the frequency dimension [141]. The model involves the use of two parameters to approximate the power delay profile of the channel that can be estimated from the pilot estimates. This approach is particularly suitable for the case of few reference channel estimates that can be used to estimate the CFR autocorrelation function. The quality of the channel estimates obtained from the MMSE interpolation depends on the length of the used Wiener filter.

5.4.2.2 LPF Interpolation Approach

Low-pass interpolator using 1-D Sinc filtering with Kaiser window was extensively studied in [142] for pilot symbol assisted modulation in frequency flat fading channels. In [142], the improved performance using Kaiser window over fixed window design is due to the flexible window shape offered by the family of Kaiser window. The idea of the Kaiser window design is to push the transition region of the lowpass filter into the zero interval of the channel folded power spectrum and lower the passband and stopband fluctuation in order to minimize the interpolation error caused by the use of non-ideal lowpass filter.

5.4.2.3 DFT Based Lowpass Interpolation

Application of 1-D DFT based lowpass interpolation to the comb pilot case was first investigated in [143]. This technique involves the insertion of a fixed number of zeros into the centre of the Discrete Fourier Transform (DFT) of the data sequence, followed by inverse DFT of the modified DFT sequence and scaling. It is essentially a process of zero-padding plus ideal low-pass filtering. To extend the technique to the 2-D case, zero insertion should be such that pushes the data away from the centre in both dimensions [144].

The aforementioned techniques either require higher order statistics about the channel or require filters with long lengthes to obtain a reasonable performance. However, the low-complexity nature of the CAT-M devices and the associated low operating SNR would require the channel estimation to have a much lower complexity than of those techniques. In the

following section, we will describe our proposed technique that takes into account the constraints of the CAT-M devices and its operating environment.

5.4.3 Proposed Channel Estimation Techniques

Our proposed technique starts by estimating the channel response at the pilot locations using LS as in (5.5). However, assuming low mobility associated with MTC applications, we can assume that the channel response is almost constant on the pilot location of adjacent OFDM symbols l_p and $l_p + 1$ for $l_p \in \{5, 12\}$. Hence, we can enhance the channel estimates at the pilots locations by averaging them on the duration of the two OFDM symbols. Then, the channels estimates at the pilots locations can be obtained as,

$$\hat{H}_{t,k_p} = \frac{\hat{H}_{l_p,k_p} + \hat{H}_{l_p+1,k_p}}{2} \quad \forall\, t \in \{l_p, l_p + 1\}. \tag{5.7}$$

The averaging of (5.7) has the effect of enhancing the noisy channel estimates at the pilot locations by almost 3dBs over the AWGN and hence; reducing its mean-squared error.

In order to calculate the interpolation coefficients with low complexity overhead, polynomial interpolations can be used. In the literature, [145] uses a Discrete Fourier Transform (DFT) filter to interpolate the channel estimation between pilot locations, while in [129] a cubic polynomial interpolation filter is used. Generally speaking, in polynomial interpolation, higher orders give stronger capability to follow the variations. However, an unnecessary higher degree polynomial might create the problem of oscillatory artifacts which causes unwanted modelling mismatch.

Here, our aim is to reduce the complexity of the channel estimation to the lowest possible, so we propose using a first-order linear interpolation. Then the channel estimation at the subcarrier (k) in the OFDM symbol (l_p) carrying the pilots is given by,

$$\hat{H}_{l_p,k} = \hat{H}_{l_p,k_p+a} + (k - k_p + a)\frac{\hat{H}_{l_p,k_p+b} - \hat{H}_{l_p,k_p+a}}{b - a} \tag{5.8}$$

where $k_p + a$ and $k_p + b$ are the frequency indices of the closest pilots with $a \in \{0, 5\}$ and $b \in \{5, 11\}$ respectively. After the interpolation in the frequency direction, the interpolation in the time direction is performed in a similar manner. The channel estimates between the

pilot-carrying symbols are given by,

$$\hat{H}_{l,k} = \hat{H}_{l_p+c,k} + (l - l_p + c)\frac{\hat{H}_{l_p+d,k} - \hat{H}_{l_p+c,k}}{d - c} \tag{5.9}$$

where $l_p + c$ and $l_p + d$ are the time indices of the closest pilots with $c \in \{0, 6\}$ and $d \in \{5, 12\}$ respectively. It should be mentioned that, at the transient subframes (e.g the first subframe in every hopping period), where there is no pilots received until the $6th$ OFDM symbol, channels estimates of the first few symbols can be assumed to be equal to the estimates on the $6th$ OFDM symbol. For the subsequent subframes, the estimates of the first OFDM symbol can be assumed to be equal to the estimates of the $14th$ symbol of the last subframe, and is used in the linear interpolation in the time direction.

5.4.4   Repetitions, De-noising and Fast Decoding

The target for the CAT-M UEs is to operate in extreme coverage conditions where a MCL between the transmitter and the receiver is at its most with ≈ 156 dB which provides a very low SNR. As discussed before, time diversity is used to boost the SNR and enhance the coverage by repeating the transmission of different channels for a number of successive subframes. The receiver can accumulate the received energy from the repeated transmissions to achieve a successful decode. Although the main reason for the repeated transmission is to enhance the decoding probability, we propose using the repetitions to enhance the performance of the channel estimation algorithm. For a subframe repeated for R transmissions, one can assume that the rate of change in the channel response is slow over the repeated subframes. Then, we can enhance the channel estimate of the nth received subframe by *cleaning* it using previously obtained channels estimates. After the first three steps of the channel estimation algorithm are performed (pilots LS, frequency interpolation, and time interpolation), the produced channel estimates at every resource element (the resource grid) are used for decoding for the control symbols. In this decoding process, the channel estimates are used to equalize the received signal and used by the MRC to produce Log-likelihood ratios (LLR), which are then fed to the Viterbi decoder to produce the output control bits.

Let $\hat{B}_r^c$ be the estimate of the decoded control bits of the received rth repetition.

$$\hat{B}_r^c = \Upsilon^{-1}\{R_r, \hat{\mathbf{h}}_r\} \tag{5.10}$$

where R_r is the received signal in the subframe of repetition index r, and $\hat{\mathbf{h}}_r$ is the channel estimates of the resource grid on the same subframe. Υ^{-1} is the receiver processing including: rate matching, de-interleaving and the Vitebi decoding. If the decoded bits are correct, the CRC check will be successful. Once the CRC is successfully checked, there is no need to continue receiving the remaining repetitions and the UE can save some power by switching off the reception of the control channel engine for the rest of the repetitions time. However, if the CRC check is not passed, this means that the collected energy is not sufficient to decode the control massage. We propose using the decoded bits to enhance the channel estimates. This can be done by regenerating an estimate of the control message as in (5.11), and use it to enhance the subsequent repetitions.

$$\Re_r = \Upsilon^{-1}\{\hat{B}_r^c\}. \tag{5.11}$$

The re-modulated signal can be used with the recently received repetition R_r, to update the current channel estimates using LS, as

$$\check{\mathbf{h}}_r = (\Re_r{}^{\mathbf{H}}\Re_r)^{-1}(\Re_r)^{\mathbf{H}}R_r. \tag{5.12}$$

The updated channel estimate $\check{\mathbf{h}}_r$ has the advantage of reduced noise contribution due to the gain obtained from the Viterbi decoder. Further, we can reduce the noise contribution to the channel estimation done for the rth repetition of a certain subframe by using a weighted sum of the some/all of the channel estimates of the pervious repetitions, i.e.,

$$\tilde{\mathbf{h}}_r = \alpha_r\hat{\mathbf{h}}_r + \sum_{i=r-w-2}^{r-1} \alpha_i\check{\mathbf{h}}_i, \tag{5.13}$$

where $\hat{\mathbf{h}}_r = [\hat{H}_{l,k}]_r$ is the channel estimate at all points of the resource grid obtained for the current repetition r (using steps of section 5.4.3), w is the length of the averaging window, and α_i is the associated weight of the channel estimate $\check{\mathbf{h}}_i$ of the ith repetition of the same subframe. The weights α_i should satisfy $\sum_{i=w-r-1}^{r} \alpha_i = 1$. The averaging window length w and the weights α_i are design parameters, and their optimal values depend on many system parameters, such as, the operating SNR, the aggregation level used by the eNodeB, repetition size, and others. Unfortunately, a closed-form solution for these optimal values is extremely difficult (if not impossible) to find. However, in the following section we will present the

130

performance of the proposed channel estimation technique showing the good range of the design parameters to achieve the required block error rate of the control channel.

5.5   Simulation Results

In this section, we present the performance of MPDCCH under different settings using system level simulations. A 1.4MHz LTE-MTC system is considered, with a sampling frequency of 1.92 MHz, 128-point FFT/IFFT, 15kHz sub-carrier spacing, one antenna at transmitter and receiver, and a Normal CP mode. In extended coverage mode, it is not likely for LTE-MTC device to move as fast as a high speed train. Therefore, we have considered low mobility channels. For instance, AWGN and EPA-5 [146] were simulated. EPA-5 is a standard LTE channel with large coherence time (maximum Doppler spread is 5Hz). Simulations were performed over 10^4 subframes over independent channel realizations for the SNR range $[-16, 2]$ dBs in order to cover conventional LTE and the CE LTE-MTC.

5.5.1   MPDCCH with Perfect Channel Knowledge

Fig. 5.3 shows the performance, represented by the Block Error Rate (BLER), for decoding a single MPDCCH candidate with aggregation level 2. A single set assignment is assumed with 2 PRBs for this case. Different repetition levels are assumed for both channels. It is very clear that the gain of repetition appears significantly at very low SNR values. For EPA-5, perfect channel estimation is assumed for the presented simulation. The objective is to evaluate the performance loss due to the fading channel without incorporating any implementation or complexity loss. That way, the EPA-5 effect is obvious when compared to AWGN. From Fig. 5.3, one can notice that enhanced coverage LTE-MTC UE operating at SNR=-16dBs requires repetitions in the order of 64 and higher for aggregation level 2 to achieve BLER of 1% and less. The conventional EPDCCH performance is characterized by the case in which $R = 1$. It is clear that classical EPDCCH has no ability to decode the control channel correctly at very low SNR values for this aggregation level.

Fig. 5.4 shows the effect of increasing the aggregation level size, L, for a given repetition factor, namely $R = 8$. In case of $L \leq 8$, a single set of 2 PRBs is utilized. However, $L = 16$ is
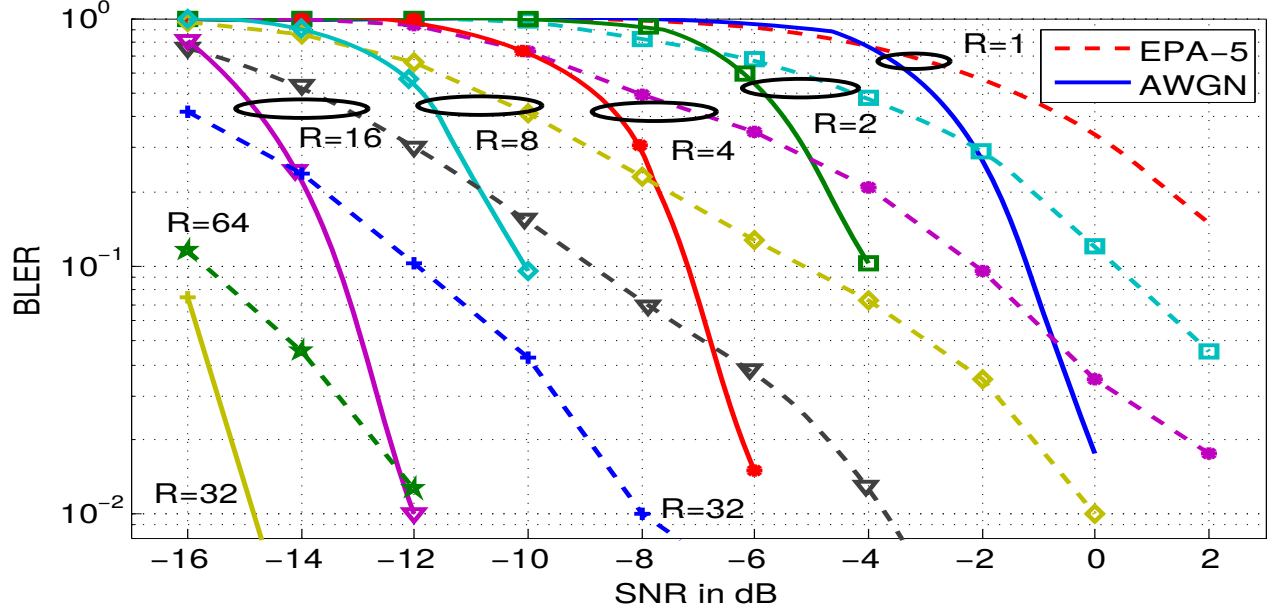
Figure 5.3: BLER versus SNR for aggregation level L=2. Different repetition factors, $R \in \{1, 2, 4, 8, 16, 32, 64\}$, are considered for various channel conditions.

only achieved with 4 PRBs set, while $L = 24$ is only allowed for the "2+4" set configuration. In reality, increasing the aggregation level may be enough to achieve 1% BLER for AWGN channel. However, the effect of fading is significant, and the only way to reduce the BLER is to increase the repetition factor even with higher aggregation levels. Fig. 5.5 better interprets the effect of repetitions and aggregation level sizes for a given SNR value which has been chosen to be the operating point for deep coverage enhancement UE, namely SNR=-14 dBs. It is obvious that EPDCCH (achieved at $R = 1$) cannot decode any control message at this SNR. Further, heavy repetitions are required for MPDCCH to achieve the target 1% error even for high aggregation levels.

5.5.2 Proposed Channel Estimation

We present the performance of the proposed channel estimation technique in-terms of the mean-squared error (MSE) define by:

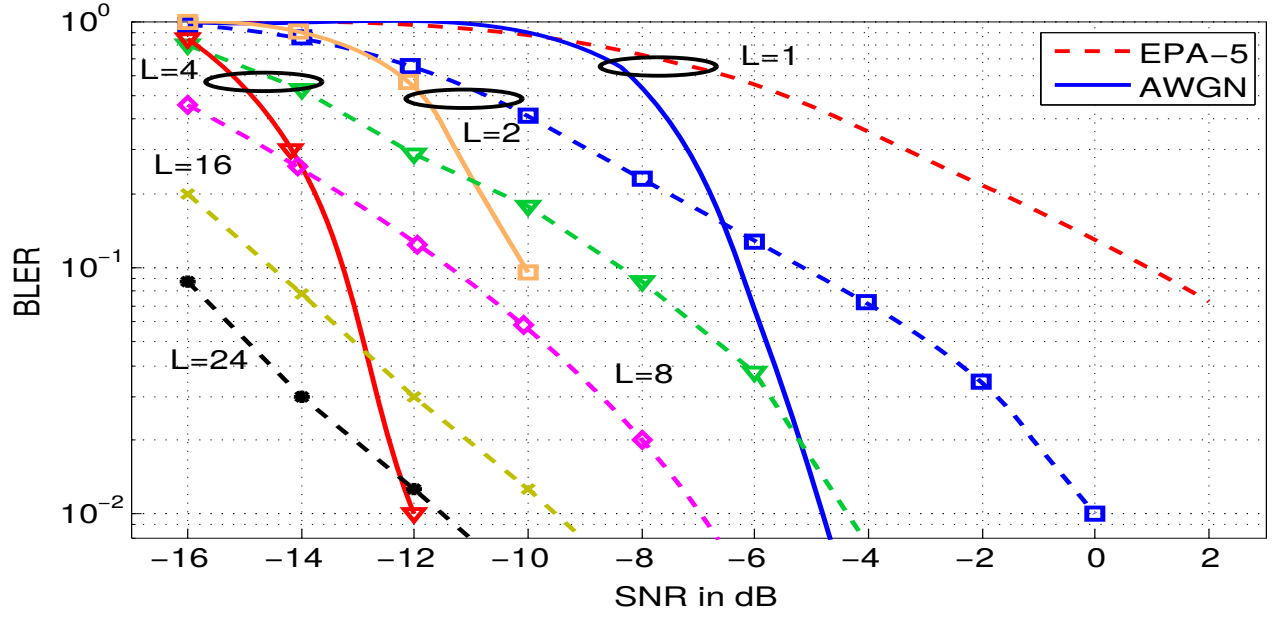$$MSE = \mathbb{E}\{|\mathbf{h} - \tilde{\mathbf{h}}|^2\}. \tag{5.14}$$

Figure 5.4: BLER versus SNR for repetition factor R=8. Different aggregation levels, $L \in \{1, 2, 4, 8, 16, 24\}$, are considered for various channel conditions.
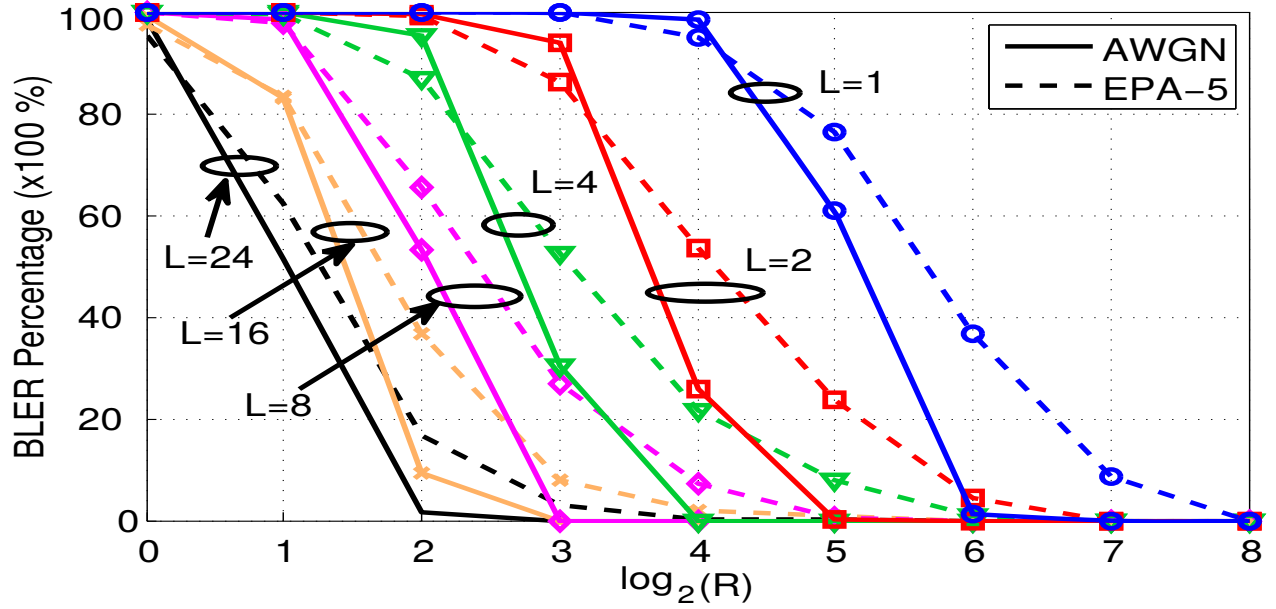

Figure 5.5: BLER versus the repetition factor for a given SNR = -14dB. Different aggregation levels, $L \in \{1, 2, 4, 8, 16, 24\}$, are considered for various channel conditions.

Here, we consider the following simulation parameters. The MPDCCH candidate carries a DCI message of 16 bits using a distributed transmission mode. The MPDCCH uses 4 PRB with aggregation level $L = 16$ and different repetition orders. The transmission is assumed to happen over the EPA-5 wireless channel. We first start by showing the effect of cleaning the channel estimates using decision-feedback (DFB). Through extensive simulations, we noted that decision-feedback best works when using only the channel estimates from the pervious repetition, i.e. $\tilde{\mathbf{h}}_r = (1 - \alpha)\hat{\mathbf{h}}_r + \alpha\check{\mathbf{h}}_{r-1}$. In other words, using a leaky-bucket filtering with weight α . Fig. 5.6 shows the MSE vs. the weight factor for different SNR values for the case of $R = 64$ repetitions. Using simulation results, we found that, the optimal weight is in the range of $\alpha \in [0.035 - 0.05]$ depending on the SNR and increases as the SNR increases. This is justified as the lower the SNR, the reconstructed channel estimates from the decisions feedback add more noise to the new channel estimates.
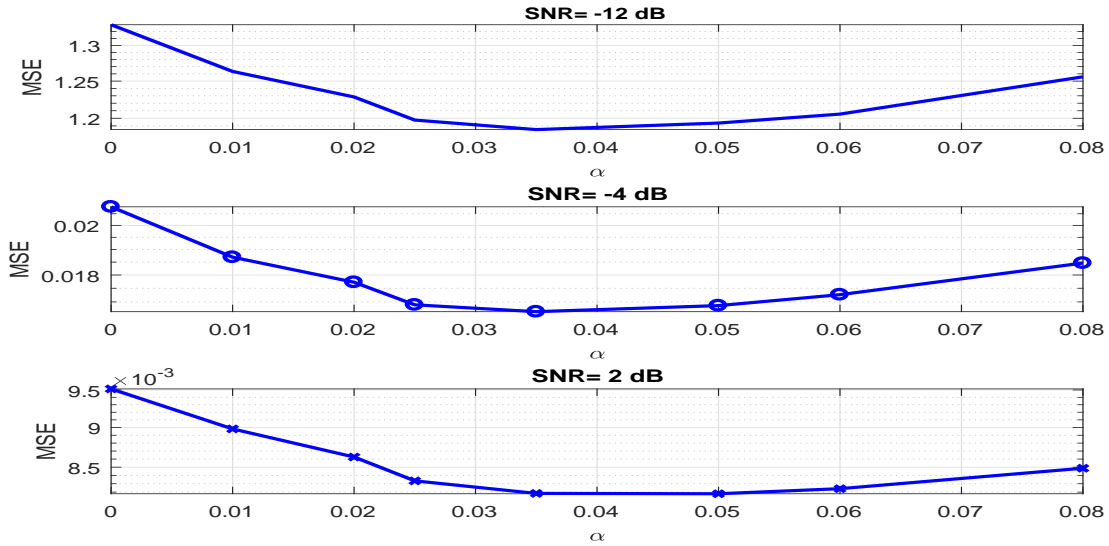
Figure 5.6: MSE versus the weight factor α for different SNR $= -12$dB, -4dB, and 2dB top to bottom.

The MSE of the proposed technique using the optimal weight factor is shown in Fig. 5.7. We compare the MSE of the channel estimates obtained using our proposed technique with the denoising step using the DFB (solid lines) to the MSE of the channel estimates obtained using only the linear interpolation. The results show that, the denoising step in the algorithm

Figure 5.7: The MSE versus SNR for aggregation level $L = 16$ of the proposed channel estimation technique. Different repetitions, $R \in \{16, 64, 128, 256\}$, are considered for EPA-5 channel. Solid lines are for the channel estimation with denoising using DFB, and dotted lines are the case of no denoising.

significantly reduces the MSE of the channel estimates at different repetition factors. It is shown that, the MSE of the proposed technique saturates at a lower level than the MSE of only using linear interpolation. This enhancement in the MSE will improve the decoding performance of the MPDCCH.

In Fig. 5.8, the BLER for decoding a single MPDCCH candidate with aggregation level 16 using the proposed channel estimation technique is shown. Using the proposed low-complexity algorithm, a UE in extended coverage mode can decode the MPDCCH candidate at very low SNR of -13 dB with 1% BLER. Fig. 5.8 depicts that, the proposed denoising step offers almost 2 dB of SNR gain for high-order repetitions. The channel estimate obtained using the proposed technique helps the UE to use only few of the sent repetitions to decode the control message. Hence, the decoding time of the MPDCCH candidate is reduced, which allows the UE to save more power.

In Fig. 5.9, we plot the average decoding index of a subframe needed to reach a successful decoding for the MPDCCH candidate using the proposed technique. It is shown that, not all the sent repetitions are needed to reach a successful decode which increases the energy
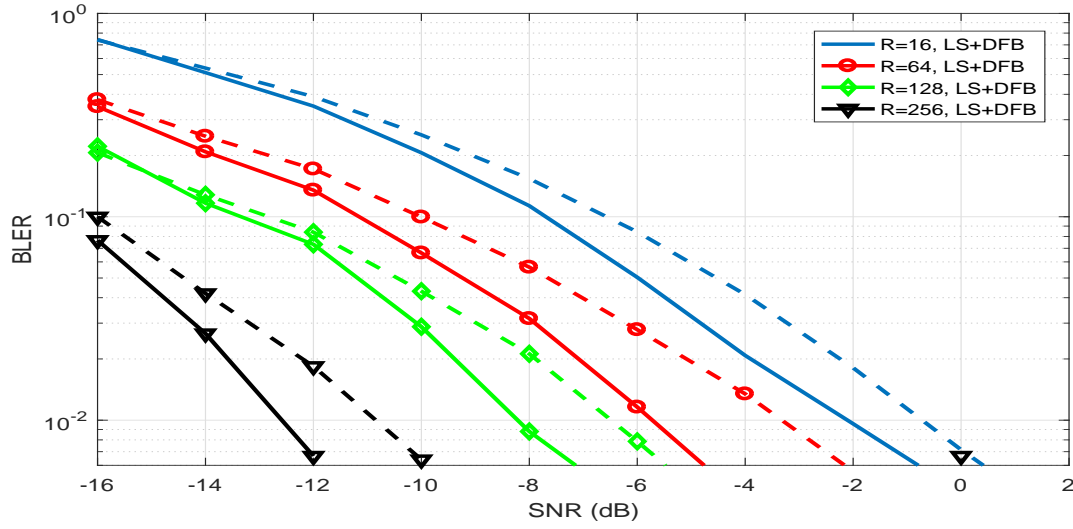
Figure 5.8: BLER versus SNR for aggregation level $L = 16$. Different repetitions, $R \in \{16, 64, 128, 256\}$, are considered for EPA-5 channel using the proposed channel estimation technique. Solid lines are for the channel estimation with denoising using DFB, and dotted lines are the case of no denoising.

efficiency of the UE during the MPDCCH reception. In Fig. 5.10, it shown that, less than 30% of the repetitions will be used by the UE in extended coverage mode B (i.e. high repetitions) at the low SNR of -12 dB. As the SNR increases, less number of repetitions shall be used, and hence more power saving.
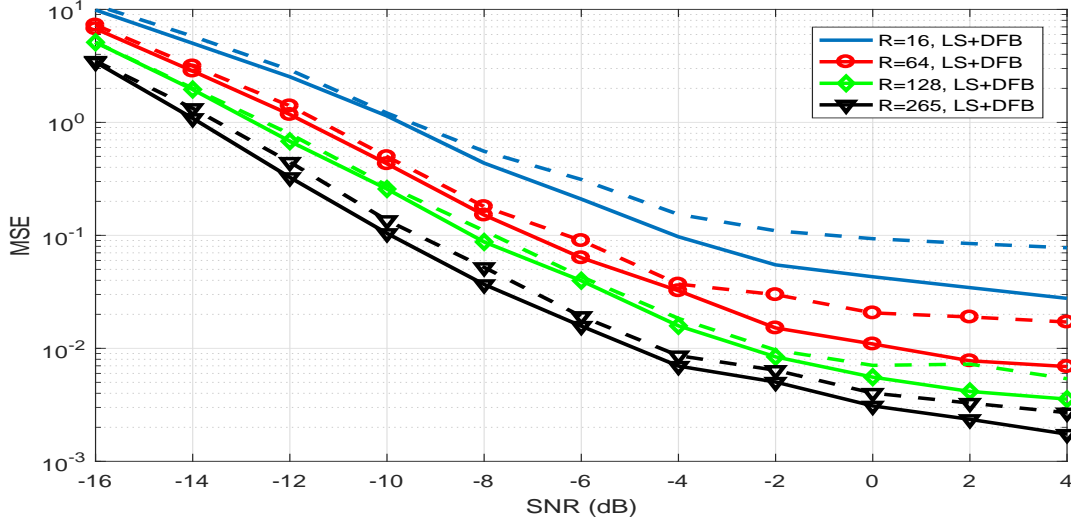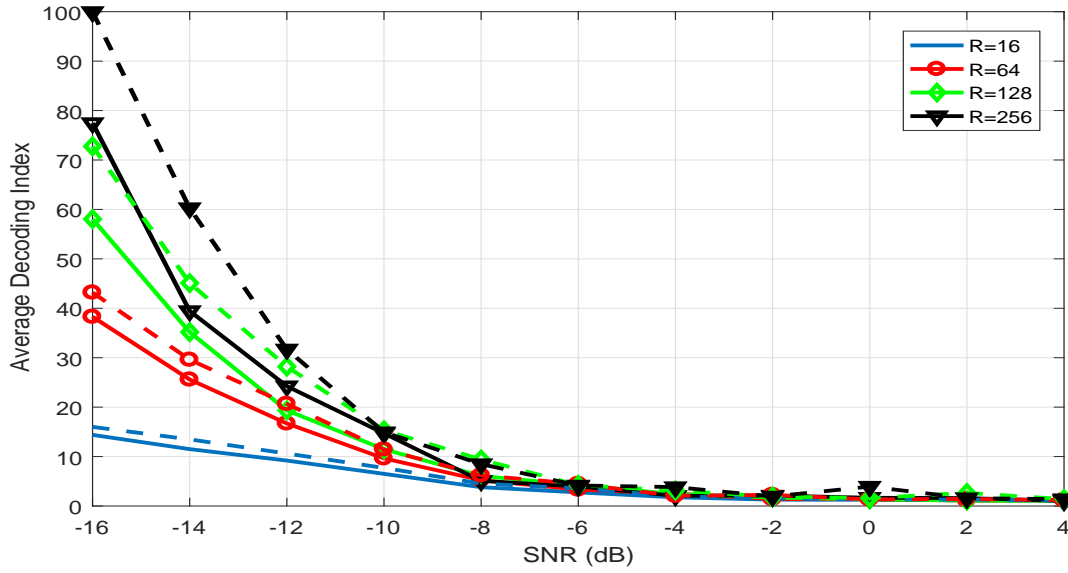
Figure 5.9: The index of successful decoding versus SNR for aggregation level $L = 16$ of the proposed channel estimation technique. Different repetitions, $R \in \{16, 64, 128, 256\}$, are considered for EPA-5 channel. Solid lines are for the channel estimation with denoising using DFB, and dotted lines are the case of no denoising.
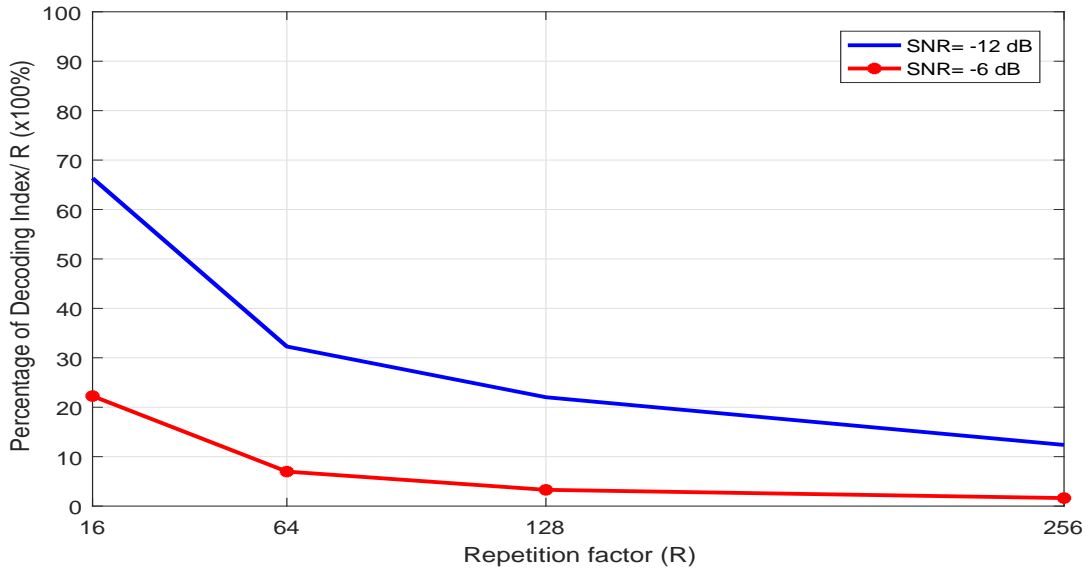
Figure 5.10: Percentage of average successful decoding index to the maximum repetition factor R.

5.6 Summary

In this chapter, we discussed the main challenges for new physical control channel of LTE-MTC systems. We evaluated the performance of the new control channel for various aggregation levels, SNR values, channel conditions, and repetition factors. Using assumptions from the MTC environment, we proposed a channel estimation algorithm, that is specific for the MPDCCH. The proposed technique offers low-complexity and features a fast-decoding criterion that helps the UE to save more power and increase its energy efficiency. The proposed scheme is able to use less than 30% of the supported repetitions in extended coverage modes to achieve the required detection error rate at moderate and low SNRs.

Chapter 6

Conclusions and Future Work

6.1 Conclusions

In the near future, a massive number of machines will have the ability to connect to the Internat through the IoT framework. With the accelerating pace of marketing such framework, the new wireless communication systems have to offer efficient solutions to incorporate the services needed for the IoT. However, a single technology will not be able to support all the requirement of different applications. Therefore, in this thesis, we tackled some of the promising technological candidates to enable such framework. In particular, we addressed research problems related to: (1) unlicensed access using non-orthogonal cognitive relay networks, (2) licensed access through the MTC framework that is recently introduced in the LTE-A standard. Our research in both topics led to significant contributions, that is perceptible in the record of publications resulted from this work. Next, we briefly summarize those accomplishments.

In chapter 3, we addressed the use of underlay cognitive radios to enable the unlicensed access of the users to the spectrum. With the existence of multiple nodes in the same area, we suggested the use of non-orthogonal multiple relays to increase the spectral efficiency. In particular, we optimized the power allocation at all the nodes in the system to maximize the throughput of the cognitive network while keeping the interference to the primary users within acceptable values. In addition, the limitations forced on the designers of MTC devices, such as the low-complexity and low-power operation, were taken into consideration. Hence, we solved the power allocation problem with more constraints on the maximum transmission power to maximize the energy-efficiency of the system. Our proposed power allocation techniques

can be implemented locally at the nodes with minimal feedback from the destination, which reduces the complexity of the overall system.

In chapter 4, we addressed the throughput maximization problem of the underlay cognitive network when the destination node is equipped with multiple antennas. We proposed using antenna selection at the destination to enable the use of only one RF chain. This also helps to further reduce the system complexity. We investigated the design of the optimal beamformer at the relaying nodes to maximize the end-to-end SNR. Then, we obtain close-form solutions for the BER and the outage probability of the system for two different relay-clustering schemes. Relay-clusters are formed of smaller groups of the available nodes to help increase the overall lifetime of the cognitive network.

In chapter 5, we presented the recent specification introduced to the LTE-A standard to accommodate for the MTC, namely CAT-M. The new UE category offers huge complexity reduction at the expense of losing performance gains from spatial and frequency diversity. Such loss introduced more challenges to the important procedure necessary for adequate operation, such as, the cell search and the channel estimation for different channels. We focused on the channel estimation problem of one of the most important physical channels in LTE-A systems, namely, MPDCCH. In this front, we proposed low-complexity power-saving channel estimation techniques that maximize the benefit from the time diversity offered by the system.

6.2 Future Work

In our research, we addressed the power allocation problem of non-orthogonal multiple cognitive relay network. The proposed power allocation technique, and hence, the performance of the system, was derived assuming the Rayleigh channel model. However, in the context of MTC, different channel models with line-of-sight components, such as the Nakagami channels, can be of interest. Analysis of the performance of the proposed power allocation in such environment can be done to assess the overall system performance.

Our proposed power allocation algorithms assumed perfect and instantaneous channel knowledge at all the secondary nodes, which provides an upper limit for the achievable

performance of the system. However, in practical systems, channel state information may be delayed or distorted due to quantization errors. These errors will clearly affect the power allocation problem, and consequently the secondary system throughput and the induced interference to the primary network. Hence, one direction for future research is to assess the performance of the secondary system while using outdated channel state information. Also, we can investigate robust power allocation techniques that decrease the sensitivity of the secondary system to channel estimation errors.

We investigated the clustering problem for physically co-located secondary nodes. However, this work can be extended to include the density of the network nodes, hence, analysing the associated problems with these Dense-Relay Networks.

In the direction of the cellular support for IoT, we investigated channel estimation techniques for the control channel of the CAT-M. However, the proposed techniques assumed perfect synchronization at the receiver. The effect of RF impairments, such as carrier frequency offset, may greatly affect the achieved performance. Therefore, a direct extension to the current work is to consider such impairments. Last but not least, investigating channel estimation techniques for CAT-N is another challenging problem, specially for the extremely low bandwidth where very few pilot signals are inserted.

References

[1] A. Ali, W. Hamouda, and M. Uysal, "Next generation M2M cellular networks: challenges and practical considerations," *IEEE Commun. Mag.*, vol. 53, no. 9, pp. 18–24, September 2015.

[2] V. Gazis, "A Survey of Standards for Machine to Machine (M2M) and the Internet of Things (IoT)," *IEEE Commun. Surveys Tuts.*, vol. PP, no. 99, pp. 1–1, 2016.

[3] Z. Fan, R. J. Haines, and P. Kulkarni, "M2M communications for E-health and smart grid: an industry and standard perspective," *IEEE Wireless Commun. Mag.*, vol. 21, no. 1, pp. 62–69, February 2014.

[4] L. Atzori, A. Iera, and G. Morabito, "The Internet of Things: A survey," *Computer Networks*, vol. 54, no. 15, pp. 2787 – 2805, 2010. [Online]. Available: http://www.sciencedirect.com/science/article/pii/S1389128610001568

[5] A. Al-Fuqaha, M. Guizani, M. Mohammadi, M. Aledhari, and M. Ayyash, "Internet of Things: A Survey on Enabling Technologies, Protocols, and Applications," *IEEE Commun. Surveys Tuts.*, vol. 17, no. 4, pp. 2347–2376, Fourthquarter 2015.

[6] B. Panigrahi, H. K. Rath, R. Ramamohan, and A. Simha, "Energy and spectral efficient direct Machine-to-Machine (M2M) communication for cellular Internet of Things (IoT) networks," in *Int. Conference on Internet of Things and Applications*, Jan 2016, pp. 337–342.

[7] A. Damnjanovic, J. Montojo, Y. Wei, T. Ji, T. Luo, M. Vajapeyam, T. Yoo, O. Song, and D. Malladi, "A survey on 3GPP heterogeneous networks," *IEEE Wireless Commun. Mag.*, vol. 18, no. 3, pp. 10–21, June 2011.

[8] M. Levesque, F. Aurzada, M. Maier, and G. Joos, "Coexistence Analysis of H2H and M2M Traffic in WiFi Smart Grid Communications Infrastructures Based on Multi-Tier Business Models," *IEEE Trans. Commun.*, vol. 62, no. 11, pp. 3931–3942, Nov 2014.

[9] T. Adame, A. Bel, B. Bellalta, J. Barcelo, and M. Oliver, "IEEE 802.11AH: the WiFi approach for M2M communications," *IEEE Wireless Commun. Mag.*, vol. 21, no. 6, pp. 144–152, December 2014.

[10] T. Taleb and A. Kunz, "Machine type communications in 3GPP networks: potential, challenges, and solutions," *IEEE Commun. Mag.*, vol. 50, no. 3, pp. 178–184, March 2012.

[11] U. Raza, P. Kulkarni, and M. Sooriyabandara, "Low power wide area networks: An overview," *IEEE Commun. Surveys Tuts.*, vol. PP, no. 99, pp. 1–1, 2017.

[12] W. Guibene, K. E. Nolan, and M. Y. Kelly, "Survey on Clean Slate Cellular-IoT Standard Proposals," in *2015 IEEE Int. Conf. on Computer and Information Technology; Ubiquitous Computing and Commun.; Dependable, Autonomic and Secure Computing; Pervasive Intelligence and Computing*, Oct 2015, pp. 1596–1599.

[13] J. P. Bardyn, T. Melly, O. Seller, and N. Sornin, "IoT: The era of LPWAN is starting now," in *ESSCIRC Conf. 2016: 42nd European Solid-State Circuits Conf.*, Sept 2016, pp. 25–30.

[14] F. Ghavimi and H. H. Chen, "M2M communications in 3GPP LTE/LTE-A Networks: Architectures, Service Requirements, Challenges, and Applications," *IEEE Commun. Surveys Tuts.*, vol. 17, no. 2, pp. 525–549, Secondquarter 2015.

[15] Sigfox. (2018). [Online]. Available: http://www.sigfox.com/

[16] LoRa. (2018). [Online]. Available: https://www.lora-alliance.org/What-Is-LoRa/Technology

[17] Semtech. (2017). [Online]. Available: http://www.semtech.com/

[18] J. Petajajarvi, K. Mikhaylov, A. Roivainen, T. Hanninen, and M. Pettissalo, "On the coverage of LPWANs: range evaluation and channel attenuation model for lora technology," in *2015 14th Int. Conf. on ITS Telecommunications (ITST)*, Dec 2015, pp. 55–59.

[19] K. E. Nolan, W. Guibene, and M. Y. Kelly, "An evaluation of low power wide area network technologies for the Internet of Things," in *2016 Int. Wireless Commun. and Mobile Computing Conf. (IWCMC)*, Sept 2016, pp. 439–444.

[20] T. Petri, M. Goessens, L. Nuaymi, L. Toutain, and A. Pelov, "Measurements, performance and analysis of LoRa FABIAN, a real-world implementation of LPWAN," in *2016 IEEE 27th Annual Int. Symp. on Personal, Indoor, and Mobile Radio Commun. (PIMRC)*, Sept 2016, pp. 1–7.

[21] P. Neumann, J. Montavont, and T. Nol, "Indoor deployment of low-power wide area networks (LPWAN): A LoRaWAN case study," in *2016 IEEE 12th Int. Conf. on Wireless and Mobile Computing, Networking and Commun. (WiMob)*, Oct 2016, pp. 1–8.

[22] Ingenu Tech. (2018) RPMA technology for the Internet of Things. [Online]. Available: http://theinternetofthings.report/Resources/Whitepapers/ 4cbc5e5e-6ef8-4455-b8cd-f6e3888624cb_RPMATechnology.pdf

[23] IEEE, "IEEE standard for local and metropolitan area networks– part 15.4: Low-rate wireless personal area networks (lr-wpans)–amendment 5: Physical layer specifications for low energy, critical infrastructure monitoring networks." *IEEE Std 802.15.4k-2013 (Amendment to IEEE Std 802.15.4-2011 as amended by IEEE Std 802.15.4e-2012, IEEE Std 802.15.4f-2012, IEEE Std 802.15.4g-2012, and IEEE Std 802.15.4j-2013)*, pp. 1–149, Aug 2013.

[24] M. Centenaro, L. Vangelista, A. Zanella, and M. Zorzi, "Long-Range Communications in Unlicensed Bands: the Rising Stars in the IoT and Smart City Scenarios," *IEEE Wireless Commun. Mag.*, vol. 23, October 2016.

[25] T. Myers, D. Werner, K. Sinsuan, J. Wilson, S. Reuland, P. Singler, and M. Huovila, "Light monitoring system using a random phase multiple access system," Jul. 2 2013, uS Patent 8,477,830. [Online]. Available: https://www.google.com/patents/US8477830

[26] S.-Y. Lien, K.-C. Chen, and Y. Lin, "Toward ubiquitous massive accesses in 3GPP machine-to-machine communications," *IEEE Commun. Mag.*, vol. 49, no. 4, pp. 66–74, 2011.

[27] E. Soltanmohammadi, K. Ghavami, and M. Naraghi-Pour, "A Survey of Traffic Issues in Machine-to-Machine Communications over LTE," *IEEE Internet of Things Journal*, vol. PP, no. 99, pp. 1–1, 2016.

[28] A. Rico-Alvarino, M. Vajapeyam, H. Xu, X. Wang, Y. Blankenship, J. Bergman, T. Tirronen, and E. Yavuz, "An overview of 3GPP enhancements on machine to machine communications," *IEEE Commun. Mag.*, vol. 54, no. 6, pp. 14–21, June 2016.

[29] T. A. Weiss and F. K. Jondral, "Spectrum pooling: an innovative strategy for the enhancement of spectrum efficiency," *IEEE Communications Magazine*, vol. 42, no. 3, pp. S8–14, Mar 2004.

[30] J. Mitola and G. Q. Maguire, "Cognitive radio: making software radios more personal," *IEEE Personal Communications*, vol. 6, no. 4, pp. 13–18, Aug 1999.

[31] S. Haykin, "Cognitive radio: brain-empowered wireless communications," *IEEE Journal on Selected Areas in Communications*, vol. 23, no. 2, pp. 201–220, Feb 2005.

[32] S. Srinivasa and S. A. Jafar, "Cognitive radios for dynamic spectrum access - the throughput potential of cognitive radio: A theoretical perspective," *IEEE Communications Magazine*, vol. 45, no. 5, pp. 73–79, May 2007.

[33] A. Giorgetti, M. Chiani, D. Dardari, R. Minutolo, and M. Montanari, "Cognitive radio with ultra-wide bandwidth location-capable nodes," in *MILCOM 2007 - IEEE Military Communications Conference*, Oct 2007, pp. 1–7.

[34] S. Sridharan, S. Vishwanath, S. A. Jafar, and S. Shamai, "On the capacity of cognitive relay assisted gaussian interference channel," in *2008 IEEE International Symposium on Information Theory*, July 2008, pp. 549–553.

[35] B. A. Fette, "Copyright page," in *Cognitive Radio Technology (Second Edition)*, 2nd ed., B. A. Fette, Ed. Oxford: Academic Press, 2009, pp. iv –. [Online]. Available: https://www.sciencedirect.com/science/article/pii/B9780123745354000254

[36] I. F. Akyildiz, W.-Y. Lee, M. C. Vuran, and S. Mohanty, "Next generation/dynamic spectrum access/cognitive radio wireless networks: A survey," *Computer Networks*, vol. 50, no. 13, pp. 2127 – 2159, 2006. [Online]. Available: http://www.sciencedirect.com/science/article/pii/S1389128606001009

[37] M. A. L. Thathachar and P. S. Sastry, *Networks of Learning Automata: Techniques for Online Stochastic Optimization*. Secaucus, NJ, USA: Springer-Verlag New York, Inc., 2003.

[38] J. Mitola, "Cognitive radio: An integrated agent architecture for software defined radio, doctor of technology," *Royal Inst. Technol*, pp. 271–350, 01 2000.

[39] T. Cover and A. E. Gamal, "Capacity theorems for the relay channel," *IEEE Transactions on Information Theory*, vol. 25, no. 5, pp. 572–584, September 1979.

[40] A. Sendonaris, E. Erkip, and B. Aazhang, "User cooperation diversity. part i. system description," *IEEE Transactions on Communications*, vol. 51, no. 11, pp. 1927–1938, Nov 2003.

[41] J. N. Laneman, D. N. C. Tse, and G. W. Wornell, "Cooperative diversity in wireless networks: Efficient protocols and outage behavior," *IEEE Transactions on Information Theory*, vol. 50, no. 12, pp. 3062–3080, Dec 2004.

[42] J. N. Laneman and G. W. Wornell, "Distributed space-time-coded protocols for exploiting cooperative diversity in wireless networks," *IEEE Transactions on Information Theory*, vol. 49, no. 10, pp. 2415–2425, Oct 2003.

[43] W. Chang, S. Kotagiri, J. N. Laneman, S. Y. Chung, and Y. H. Lee, "Compress-and-forward relaying over parallel gaussian channels," in *2007 2nd IEEE International Workshop on Computational Advances in Multi-Sensor Adaptive Processing*, Dec 2007, pp. 305–308.

[44] G. Kramer, M. Gastpar, and P. Gupta, "Cooperative strategies and capacity theorems for relay networks," *IEEE Transactions on Information Theory*, vol. 51, no. 9, pp. 3037–3063, Sept 2005.

[45] Q. Zhao and B. M. Sadler, "A survey of dynamic spectrum access," *IEEE Signal Processing Magazine*, vol. 24, no. 3, pp. 79–89, May 2007.

[46] Y. Chen, Q. Zhao, and A. Swami, "Joint design and separation principle for opportunistic spectrum access in the presence of sensing errors," *IEEE Transactions on Information Theory*, vol. 54, no. 5, pp. 2053–2071, May 2008.

[47] B. Wild and K. Ramchandran, "Detecting primary receivers for cognitive radio applications," in *First IEEE International Symposium on New Frontiers in Dynamic Spectrum Access Networks, 2005. DySPAN 2005.*, Nov 2005, pp. 124–130.

[48] A. Sahai, N. Hoven, and R. Tandra, "Some fundamental limits on cognitive radio," *Proceedings of Allerton Conference on Communication, Control, and Computing*, 10 2004.

[49] A. Sahai, N. Hoven, S. Mubaraq, and M. R. Tandra, "Fundamental tradeoffs in robust spectrum sensing for opportunistic frequency reuse," IEEE J. Select. Areas Commun, Tech. Rep., 2006.

[50] A. Nosratinia, T. E. Hunter, and A. Hedayat, "Cooperative communication in wireless networks," *IEEE Communications Magazine*, vol. 42, no. 10, pp. 74–80, Oct 2004.

[51] D. Cabric, S. M. Mishra, and R. W. Brodersen, "Implementation issues in spectrum sensing for cognitive radios," in *Conference Record of the Thirty-Eighth Asilomar Conference on Signals, Systems and Computers, 2004.*, vol. 1, Nov 2004, pp. 772–776 Vol.1.

[52] A. Ghasemi and E. S. Sousa, "Collaborative spectrum sensing for opportunistic access in fading environments," in *First IEEE International Symposium on New Frontiers in Dynamic Spectrum Access Networks, 2005. DySPAN 2005.*, Nov 2005, pp. 131–136.

[53] Z. Yang, Z. Ding, P. Fan, and G. K. Karagiannidis, "Outage performance of cognitive relay networks with wireless information and power transfer," *IEEE Transactions on Vehicular Technology*, vol. 65, no. 5, pp. 3828–3833, May 2016.

[54] L. Musavian and S. Aissa, "Cross-layer analysis of cognitive radio relay networks under quality of service constraints," in *VTC Spring 2009 - IEEE 69th Vehicular Technology Conference*, April 2009, pp. 1–5.

[55] M. Elsaadany, M. Abdallah, T. Khattab, M. Khairy, and M. Hasna, "Cognitive relaying in wireless sensor networks: Performance analysis and optimization," in *Proc. IEEE Global Telecomm. Conf. (GLOBECOM)*, Dec. 2010.

[56] J. pyo Hong, B. Hong, T.-W. Ban, and W. Choi, "On the cooperative diversity gain in underlay cognitive radio systems," *IEEE Trans. Commun.*, vol. 60, no. 1, pp. 209–219, 2012.

[57] V. Asghari and S. Aissa, "End-to-end performance of cooperative relaying in spectrum-sharing systems with quality of service requirements," *IEEE Trans. Veh. Technol.*, vol. 60, no. 6, pp. 2656–2668, 2011.

[58] W. Xu, J. Zhang, P. Zhang, and C. Tellambura, "Outage probability of decode-and-forward cognitive relay in presence of primary user's interference," *IEEE Commun. Lett.*, vol. 16, no. 8, pp. 1252–1255, 2012.

[59] J. Lee, H. Wang, J. Andrews, and D. Hong, "Outage probability of cognitive relay networks with interference constraints," *IEEE Trans. Wireless Commun.*, vol. 10, no. 2, pp. 390–395, 2011.

[60] M. Naeem, D. Lee, and U. Pareek, "An efficient multiple relay selection scheme for cognitive radio systems," in *Proc. IEEE Int. Conf. Commun. ICC*, 2010.

[61] Y. Li and A. Nosratinia, "Spectrum-sharing capacity enhancement with distributed relaying," in *Proc. IEEE ICC, 2012*, 2012, pp. 2197–2201.

[62] M. Choi, J. Park, and S. Choi, "Simplified power allocation scheme for cognitive multi-node relay networks," *IEEE Trans. Wireless Commun.*, vol. 11, no. 6, pp. 2008–2012, 2012.

[63] K. Zarifi, S. Affes, and A. Ghrayeb, "Joint source power control and relay beamforming in amplify-and-forward cognitive networks with multiple source-destination pairs," in *Proc. IEEE Int. Conf. Commun. (ICC)*, Jun. 2011, pp. 1–6.

[64] A. Afana, V. Asghari, A. Ghrayeb, and S. AFFES, "Enhancing the performance of spectrum-sharing systems via collaborative distributed beamforming and af relaying," in *Proc. IEEE Global Telecomm. Conf. (GLOBECOM)*, Dec. 2012, pp. 1314–1319.

[65] ——, "On the Performance of Cooperative Relaying Spectrum-Sharing Systems with Collaborative Distributed Beamforming," *IEEE Trans. Commun.*, vol. 62, no. 3, pp. 857–871, Mar. 2014.

[66] Y. Guo, G. Kang, S. Qiaoyun, M. Zhang, and P. Zhang, "Outage performance of cognitive-radio relay system based on the spectrum-sharing environment," in *IEEE Global Telecomm. Conf. (GLOBECOM)*, Dec. 2010, pp. 1–5.

[67] Z. Yan, X. Zhang, and W. Wang, "Exact outage performance of cognitive relay networks with maximum transmit power limits," *IEEE Commun. Lett.*, vol. 15, no. 12, pp. 1317–1319, Dec. 2011.

[68] M. Z. Shafiq, L. Ji, A. X. Liu, J. Pang, and J. Wang, "Large-scale measurement and characterization of cellular machine-to-machine traffic," *IEEE/ACM Trans. Netw.*, vol. 21, no. 6, pp. 1960–1973, Dec 2013.

[69] X. Jian, X. Zeng, Y. Jia, L. Zhang, and Y. He, "Beta/m/1 model for machine type communication," *IEEE Commun. Lett.*, vol. 17, no. 3, pp. 584–587, March 2013.

[70] M. S. Ali, E. Hossain, and D. I. Kim, "LTE/LTE-A random access for massive machine-type communications in smart cities," *IEEE Commun. Mag.*, vol. 55, no. 1, pp. 76–83, January 2017.

[71] M. Laner, P. Svoboda, N. Nikaein, and M. Rupp, "Traffic models for machine type communications," in *ISWCS 2013; 10th Int. Symp. on Wireless Communication Systems*, Aug 2013, pp. 1–5.

[72] 3GPP-TR, "Study on ran improvements for machine-type communications (release 11)," Technical specification group radio access network, Tech. Rep. 37.868, 2011.

[73] A. Laya, C. Kalalas, F. Vazquez-Gallego, L. Alonso, and J. Alonso-Zarate, "Goodbye, aloha!" *IEEE Access*, vol. 4, pp. 2029–2044, 2016.

[74] A. Laya, L. Alonso, and J. Alonso-Zarate, "Is the random access channel of lte and lte-a suitable for m2m communications? a survey of alternatives," *IEEE Commun. Surveys Tuts.*, vol. 16, no. 1, pp. 4–16, First 2014.

[75] J. Choi, "On the adaptive determination of the number of preambles in rach for mtc," *IEEE Commun. Lett.*, vol. 20, no. 7, pp. 1385–1388, July 2016.

[76] S. Dama, T. V. Pasca, V. Sathya, and K. Kuchi, "A novel rach mechanism for dense cellular-iot deployments," in *2016 IEEE Wireless Commun. and Networking Conf.*, April 2016, pp. 1–6.

[77] M. Vilgelm, H. M. Grsu, W. Kellerer, and M. Reisslein, "Latmapa: Load-adaptive throughput- maximizing preamble allocation for prioritization in 5g random access," *IEEE Access*, vol. 5, pp. 1103–1116, 2017.

[78] D. Flore. (2015, Feb) Evolution of LTE in Release 13. [Online]. Available: http://www.3gpp.org/news-events/3gpp-news/1628-rel13

[79] J. Gozalvez, "New 3GPP Standard for IoT [Mobile Radio]," *IEEE Veh. Technol. Mag.*, vol. 11, no. 1, pp. 14–20, March 2016.

[80] Ericsson, "Introduction of NB-IoT," 3GPP TSG RAN WG1 Meeting-85, Tech. Rep. R1-165971, May 2016.

[81] Huawei and HiSilicon, "Introduction of Rel-13 feature of NB-IoT in 36.212," 3GPP TSG RAN WG1 Meeting-85, Tech. Rep. R1-166045, May 2016.

[82] M. Hua, M. Wang, K. W. Yang, and K. J. Zou, "Analysis of the frequency offset effect on zadoff-chu sequence timing performance," *IEEE Trans. Commun.*, vol. 62, no. 11, pp. 4024–4039, Nov 2014.

[83] J. Hu, M. Wang, K. J. Zou, K. W. Yang, M. Hua, and J. Zhang, "Enhanced lte physical downlink control channel design for machine-type communications," in *2015 7th Int. Conf. on New Technologies, Mobility and Security (NTMS)*, July 2015, pp. 1–5.

[84] M. Wang, W. Yang, J. Zou, B. Ren, M. Hua, J. Zhang, and X. You, "Cellular machine-type communications: physical challenges and solutions," *IEEE Wireless Commun. Mag.*, vol. 23, no. 2, pp. 126–135, April 2016.

[85] Y. E. Wang *et al.*, "A Primer on 3GPP Narrowband Internet of Things (NB-IoT)," *CoRR*, vol. abs/1606.04171, 2016.

[86] Motorola Mobility, "Introduction of NB-IoT," 3GPP TSG RAN WG1 Meeting-85, Tech. Rep. R1-165111, May 2016.

[87] J.-J. van de Beek, M. Sandell, and P. Borjesson, "ML estimation of time and frequency offset in OFDM systems," *IEEE Trans. Signal Process.*, vol. 45, no. 7, pp. 1800–1805, 1997.

[88] S. Ma, X. Pan, G.-H. Yang, and T.-S. Ng, "Blind Symbol Synchronization Based on Cyclic Prefix for OFDM Systems," *IEEE Trans. Veh. Technol.*, vol. 58, no. 4, pp. 1746–1751, 2009.

[89] I. Kim, Y. Han, and H. K. Chung, "An efficient synchronization signal structure for OFDM-based cellular systems," *IEEE Trans. Wireless Commun.*, vol. 9, no. 1, pp. 99–105, 2010.

[90] Y. Tsai, G. Zhang, D. Grieco, and F. Ozluturk, "Cell search in 3GPP long term evolution systems," *IEEE Veh. Technol. Mag.*, vol. 2, no. 2, pp. 23–29, 2007.

[91] K. Manolakis, D. Gutierrez Estevez, V. Jungnickel, W. Xu, and C. Drewes, "A Closed Concept for Synchronization and Cell Search in 3GPP LTE Systems," in *IEEE Wireless Commun. and Networking Conf.*, 2009, pp. 1–6.

[92] H. Setiawan and H. Ochi, "A low complexity physical-layer identity detection for 3GPP Long Term Evolution," in *Int. Conf. on Advanced Communication Technology*, vol. 1, 2010, pp. 8–13.

[93] C.-C. Liao, P.-Y. Tsai, and T.-D. Chiueh, "Low-Complexity Cell Search Algorithm for Interleaved Concatenation ML-Sequences in 3GPP-LTE Systems," *IEEE Trans. Wireless Commun. Lett.*, vol. 1, no. 4, pp. 280–283, 2012.

[94] A. Ali and W. Hamouda, "Cell search evaluation: A step towards the next generation LTE-MTC systems," in *2016 IEEE Wireless Commun. and Networking Conf.*, April 2016, pp. 1–6.

[95] J. J. van de Beek, O. Edfors, M. Sandell, S. K. Wilson, and P. O. Borjesson, "On channel estimation in OFDM systems," in *IEEE Veh. Tech. conf.*, vol. 2, Jul 1995, pp. 815–819.

[96] G. Auer and E. Karipidis, "Pilot aided channel estimation for OFDM: a separated approach for smoothing and interpolation," in *IEEE Int. Conf. on Commun.,*, vol. 4, May 2005, pp. 2173–2178.

[97] Y. Li, L. J. Cimini, and N. R. Sollenberger, "Robust channel estimation for OFDM systems with rapid dispersive fading channels," *IEEE Trans. Commun.*, vol. 46, no. 7, pp. 902–915, Jul 1998.

[98] E. A. Ahmed and M. M. Khairy, "Semi-adaptive channel estimation technique for LTE systems," in *IEEE Symp. on Computers and Commun.*, June 2011, pp. 457–482.

[99] C. Y. Hsieh, D. W. Lin, and C. Ma, "LMMSE-Based Channel Estimation for LTE-Advanced MIMO Downlink Employing UE-Specific Reference Signals," in *IEEE Veh. Tech. conf.*, May 2015, pp. 1–5.

[100] W. J. Hwang, J. H. Jang, and H. J. Choi, "An enhanced channel estimation with partial interference cancelation for MU-MIMO system," *IEEE Commun. Lett.*, vol. 16, no. 8, pp. 1232–1235, August 2012.

[101] T. Kamenosono, M. Kaneko, K. Hayashi, and M. Sakai, "Compressed sensing-based channel estimation methods for LTE-Advanced multi-user downlink MIMO system," in *IEEE Veh. Tech. conf.*, May 2015, pp. 1–5.

[102] MCC Support, "Final Report of 3GPP TSG RAN WG1-85 v1.0.0," 3GPP TSG RAN WG1 Meeting-85, Tech. Rep. R1-166056, Aug 2016.

[103] Nokia. (2015) Optimizing LTE for the internet of things. [Online]. Available: http://networks.nokia.com/file/34496/lte-m-optimizing-lte-for-the-internet-of-things

[104] J. Mitola and G. Maguire Jr., "Cognitive radio: making software radios more personal," *IEEE Personal Commun. Mag.*, vol. 6, no. 4, pp. 13–18, 1999.

[105] A. Ibrahim, A. Sadek, W. Su, and K. Liu, "Cooperative communications with relay-selection: when to cooperate and whom to cooperate with?" *IEEE Trans. Wireless Commun.*, vol. 7, no. 7, pp. 2814–2827, 2008.

[106] Y. Jing and H. Jafarkhani, "Single and multiple relay selection schemes and their achievable diversity orders," *IEEE Trans. Wireless Commun.*, vol. 8, no. 3, pp. 1414–1423, 2009.

[107] P. J. Kolodzy, "Interference temperature: a metric for dynamic spectrum utilization," *Inter. J. of Network Manage.*, vol. 16, no. 2, pp. 103–113, Mar. 2006.

[108] A. Tajer and X. Wang, "Multiuser diversity gain in cognitive networks," *IEEE/ACM Trans. Netw.*, vol. 18, no. 6, pp. 1766–1779, 2010.

[109] R. Horn and C. Johnson, *Matrix Analysis.* Cambridge Univ. Press, 1990.

[110] S. Haykin, *Adaptive Filter Theory, 3rd ed.* Prentice-Hall, Inc., 1996.

[111] I. Gradshteyn and I. Ryzhik, *Table of Integrals, Series, and Products*, 7th ed. San Diego, CA: Academic, 2007.

[112] A. Talbot, "The accurate numerical inversion of laplace transforms," *IMA J. of Appl. Math.*, vol. 23, pp. 97–120, 1979.

[113] Y. Hao, Y. Jing, and S. ShahbazPanahi, "Energy efficient network beamforming design using power-normalized snr," *Wireless Communications, IEEE Transactions on*, vol. 13, no. 5, pp. 2756–2769, May 2014.

[114] R. Vahidnia and S. Shahbazpanahi, "Multi-carrier asynchronous bi-directional relay networks: Joint subcarrier power allocation and network beamforming," *Wireless Communications, IEEE Transactions on*, vol. 12, no. 8, pp. 3796–3812, August 2013.

[115] M. Elsaadany, "Optimal power allocation in cognitive networks using non-orthogonal af relays," in *Local Computer Networks (LCN), 2014 IEEE 39th Conference on*, Sept 2014, pp. 410–413.

[116] A. Khabbazibasmenj, F. Roemer, S. Vorobyov, and M. Haardt, "Sum-rate maximization in two-way AF MIMO relaying: Polynomial time solutions to a class of dc programming problems," *IEEE Trans. Signal Process.*, vol. 60, no. 10, pp. 5478–5493, 2012.

[117] K. Lee, C.-B. Chae, R. Heath, and J. Kang, "Mimo transceiver designs for spatial sensing in cognitive radio networks," *IEEE Trans. Wireless Commun.*, vol. 10, no. 11, pp. 3570–3576, Nov. 2011.

[118] R. Manna, R. H. Y. Louie, Y. Li, and B. Vucetic, "Cooperative Spectrum Sharing in Cognitive Radio Networks With Multiple Antennas," *IEEE Transactions on Signal Processing*, vol. 59, no. 11, pp. 5509–5522, Nov 2011.

[119] K. Jitvanichphaibool, Y.-C. Liang, and R. Zhang, "Beamforming and power control for multi-antenna cognitive two-way relaying," in *Proc. IEEE Wireless Commun. and Networking Conf. (WCNC)*, Apr. 2009, pp. 1–6.

[120] Y. Li and A. Nosratinia, "Spectrum sharing with distributed relay selection and clustering," *IEEE Trans. Commun.*, vol. 61, no. 1, pp. 53–62, Jan. 2013.

[121] D. Li, "Performance analysis of MRC diversity for cognitive radio systems," *IEEE Trans. on Veh. Technol.*, vol. 61, no. 2, pp. 849–853, Feb. 2012.

[122] R. Duan, R. Jantti, M. Elmusrati, and R. Virrankoski, "Capacity for Spectrum Sharing Cognitive Radios with MRC Diversity and Imperfect Channel Information from Primary User," in *Proc. IEEE Global Telecomm. Conf. (GLOBECOM)*, Dec. 2010, pp. 1–5.

[123] S. Thoen, L. V. der Perre, B. Gyselinckx, and M. Engels, "Performance analysis of combined transmit-SC/receive-MRC," *IEEE Trans. Commun.*, vol. 49, no. 1, pp. 5–8, Jan 2001.

[124] X. Cai and G. B. Giannakis, "Performance analysis of combined transmit selection diversity and receive generalized selection combining in rayleigh fading channels," *IEEE Trans. Wireless Commun.*, vol. 3, no. 6, pp. 1980–1983, Nov 2004.

[125] Y. Deng, M. Elkashlan, P. L. Yeoh, N. Yang, and R. Mallik, "Cognitive MIMO relay networks with generalized selection combining," *IEEE Trans. Wireless Commun.*, vol. 13, no. 9, pp. 4911–4922, Sept. 2014.

[126] P. L. Yeoh, M. Elkashlan, K. J. Kim, T. Q. Duong, and G. K. Karagiannidis, "Transmit Antenna Selection in Cognitive MIMO Relaying With Multiple Primary Transceivers," *IEEE Trans. Veh. Technol.*, vol. 65, no. 1, pp. 483–489, Jan 2016.

[127] P. Osti, P. Lassila, S. Aalto, A. Larmo, and T. Tirronen, "Analysis of PDCCH Performance for M2M Traffic in LTE," *IEEE Veh. Technol. Mag.*, vol. 63, no. 9, pp. 4357–4371, Nov 2014.

[128] M. Elsaadany, A. Ali, and W. Hamouda, "Cellular LTE-A Technologies for the Future Internet-of-Things: Physical Layer Features and Challenges," *IEEE Communications Surveys Tutorials*, vol. 19, no. 4, pp. 2544–2572, 2017.

[129] Y. Qi, A. Ijaz, A. Quddus, M. Imran, P. Navaratnam, M. Webb, Y. Morioka, Y. Ma, and R. Tafazolli, "On the physical layer design for low cost machine type communication in 3GPP LTE," in *2014 IEEE 80th Vehicular Technology Conference (VTC2014-Fall)*, Sept 2014, pp. 1–5.

[130] O. Arouk, A. Ksentini, and T. Taleb, "Group Paging-Based Energy Saving for Massive MTC Accesses in LTE and Beyond Networks," *IEEE Journal on Selected Areas in Communications*, vol. 34, no. 5, pp. 1086–1102, May 2016.

[131] A. Talukdar, "Performance evaluation of the Enhanced Physical Downlink Control Channel in a LTE network," in *IEEE Sym. on Personal Indoor and Mobile Radio Comm.*, Sept 2013, pp. 987–991.

[132] M. Wang, W. Yang, J. Zou, B. Ren, M. Hua, J. Zhang, and X. You, "Cellular machine-type comm unications: physical challenges and solutions," *IEEE Wireless Communications*, vol. 23, no. 2, pp. 126–135, April 2016.

[133] Ericsson, "Further LTE Physical Layer Enhancements for MTC," Tech. Rep. RP-152259, Dec 2015, 3GPP TSG RAN Meeting-70. [Online]. Available: http://www.3gpp.org/DynaReport/TDocExMtg--RP-70--31199.htm

[134] T. P. C. de Andrade, C. A. Astudillo, and N. L. S. da Fonseca, "Allocation of Control Resources for Machine-to-Machine and human-to-human Communications Over LTE/LTE-A Networks," *IEEE Internet of Things Journal*, vol. 3, no. 3, pp. 366–377, June 2016.

[135] Ericsson, "RAN1 agreements for Rel-13 eMTC sorted and edited by topic," Tech. Rep. R1-157733, Nov 2015, 3GPP TSG RAN WG1 Meeting-83. [Online]. Available: http://www.3gpp.org/DynaReport/TDocExMtg--R1-83--31259.htm

[136] M. Patzold, *Mobile Radio Channels*, 2nd ed. John Wiley & Sons, England, 2011.

[137] F. Sanzi and J. Speidel, "An adaptive two-dimensional channel estimator for wireless OFDM with application to mobile DVB-T," *IEEE Transactions on Broadcasting*, vol. 46, no. 2, pp. 128–133, Jun 2000.

[138] G. Auer and E. Karipidis, "Pilot aided channel estimation for OFDM: a separated approach for smoothing and interpolation," in *IEEE International Conference on Communications, 2005. ICC 2005. 2005*, vol. 4, May 2005, pp. 2173–2178 Vol. 4.

[139] Y. Li, "Pilot-symbol-aided channel estimation for ofdm in wireless systems," *IEEE Transactions on Vehicular Technology*, vol. 49, no. 4, pp. 1207–1215, Jul 2000.

[140] P. Hoeher, S. Kaiser, and P. Robertson, "Two-dimensional pilot-symbol-aided channel estimation by wiener filtering," in *1997 IEEE International Conference on Acoustics, Speech, and Signal Processing*, vol. 3, Apr 1997, pp. 1845–1848 vol.3.

[141] K. C. Hung and D. W. Lin, "Pilot-based lmmse channel estimation for ofdm systems with power delay profile approximation," *IEEE Transactions on Vehicular Technology*, vol. 59, no. 1, pp. 150–159, Jan 2010.

[142] L. Xiao, X. Dong, and A. C. K. Soong, "On the design of sinc interpolator for pilot symbol assisted modulation systems," *IEEE Transactions on Wireless Communications*, vol. 5, no. 9, pp. 2578–2585, September 2006.

[143] Y. Zhao and A. Huang, "A novel channel estimation method for OFDM mobile communication systems based on pilot signals and transform-domain processing," in *1997 IEEE 47th Vehicular Technology Conference. Technology in Motion*, vol. 3, May 1997, pp. 2089–2093 vol.3.

[144] X. Dong, W. s. Lu, and A. C. K. Soong, "Linear Interpolation in Pilot Symbol Assisted Channel Estimation for OFDM," *IEEE Transactions on Wireless Communications*, vol. 6, no. 5, pp. 1910–1920, May 2007.

[145] J. w. Seo, J. w. Wee, W. g. Jeon, J. h. Paik, and D. k. Kim, "An Enhanced DFT-Based Channel Estimation Using Virtual Interpolation with Guard Bands Prediction for OFDM," in *2006 IEEE 17th International Symposium on Personal, Indoor and Mobile Radio Communications*, Sept 2006, pp. 1–5.

[146] J. Lorca, "Increasing coverage and maximum CFO in DFT-s-OFDM for Machine-Type Communications," in *Int. Conf. on Commun.*, 2015, pp. 982–987.

Appendix:
List of Publications

Journal Articles:

- **M. Elsaadany**, A. Ali, and W. Hamouda, "Cellular-Enabled Technologies for the Future Internet-of-Things: Physical Layer Features and Challenges", IEEE Communications Surveys and Tutorials, vol. 19, no. 4, pp. 2544-2572, Fourth quarter 2017.

- **M. Elsaadany** and W. Hamouda, "Antenna Selection for Dual-hop Cognitive Radio Networks: A Multiple-Relay Scenario", IEEE Transactions on Vehicular Technology, vol. 66, no. 8, pp. 6754-6763, Aug. 2017.

- **M. Elsaadany** and W. Hamouda, "Performance Analysis of Non-Orthogonal AF Relaying in Cognitive Radio Networks", IEEE Wireless Communications Letters, vol.4, no.4, pp.373-376, 2015.

- **M. Elsaadany**, A. Ali, and W. Hamouda, "Low-Complexity Channel Estimation Technique for Machine Type Communications in 3GPP LTE-A", in preparation, 2018.

Conference Proceedings:

- **M. Elsaadany** and W. Hamouda, "The New Enhancements in LTE-A Rel-13 for Reliable Machine Type Communications", IEEE International Symposium on Personal, Indoor and Mobile Radio Communications (IEEE PIMRC 2017).

- **M. Elsaadany** and W. Hamouda, "Energy Efficient Design for Non-Orthogonal AF Relaying in Underlay Spectrum Sharing Networks", IEEE International Conference on Communications (ICC), 2016.

- **M. Elsaadany** and W. Hamouda, "Enhancing the Performance of Amplify-and-Forward Cognitive Relay Networks: A Multiple-Relay Scenario", IEEE Global Communications Conference (GLOBECOM), 2015.

- **M. Elsaadany**, A. Ali, and W. Hamouda, "Fast-Decoding Channel Estimation Technique for Downlink Control Channel in LTE-MTC Systems", accepted, IWCMC 2018.